Studies on Sponge-like Cryogel Particles Modified with Phospholipid Membrane toward Design of Sophisticated Bioseparation

Hayato TAKASE

March 2023

Studies on Sponge-like Cryogel Particles Modified with Phospholipid Membrane toward Design of Sophisticated Bioseparation

A dissertation submitted to

THE GRADUATE SCHOOL OF ENGINEERING SCIENCE

OSAKA UNIVERSITY

in partial fulfillment of the requirements for the degree of

DOCTOR OF PHILOSOPHY IN ENGINEERING

BY

Hayato TAKASE

March 2023

Abstract

In the design and development of the chemical process, it is important to improve the efficiency and selectivity of the separation process. In order to keep high separation efficiency and selectivity, it is essential to optimize the separation process at the *macroscopic* scale and, furthermore, to control the physicochemical properties of the core materials for separation at the *meso*/*micro* scale and. It is therefore important to focus on the utilization of "self-organized system of the molecules"; for example, it can be achieved via the integration of the ordered phospholipid membranes and cryogels with large porosity and sponge-like elasticity. The purpose of this study is to separate cryogel particles modified with phospholipid membranes by using mechanical stimuli as a driving force. A method for preparing polymer particle carriers with elasticity that is easy to process and manipulate is established in this thesis. Furthermore, the method of modifying the polymer surface with phospholipid membranes is systematically discussed. Based on these findings, a method of modification of polymer surfaces by phospholipid membranes was established. The possibility of using the modified phospholipid membranes as advanced separation materials is demonstrated by controlling the properties of the membranes via mechanical stimulation

In Chapter 2, cryogel particles, which are porous polymer particles, were synthesized via a two-step preparation process combining the reverse Leidenfrost effect and cryopolymerization. The reverse Leidenfrost effect was utilized to prepare frozen particles by dropping the polymer precursor onto liquid nitrogen (-196 oC). Cryogel particles were then prepared by cryopolymerization of the recovered particles under freezing (-15 oC). The cryogel particles prepared by this method were evaluated in terms of pore structure, swelling property, and mechanical properties.

In Chapter 3, the versatility of the method for preparing surfactant-free cryogel particles was demonstrated by preparing cryogel particles using five different precursors (hydrophilic monomer, hydrophobic monomer, and natural polymer). The basic properties of the obtained particles were systematically evaluated and compared in terms of i) appearance, ii) porous structure, and iii) mechanical properties, respectively. Different precursors used in the preparation enabled the preparation of particles with different physical and chemical properties.

In Chapter 4, hierarchical porous structures were designed by controlling the pore properties (i.e., pore orientation, bimodal pores, and porosity) of cryogel particles. Cryogel particles with supermacropores (10-200 μm) and macropores (>50 nm) were prepared by controlling the formation of directional pores from the particle surface to the interior and the phase separation during the cryopolymerization process by utilizing the temperature gradient during the preparation.

In Chapter 5, a method of the modification of the prepared cryogel particles by phospholipid membrane was established and was shown as a qualitative scheme. The advantages and disadvantages of the various methods were systematically compared by classifying the phospholipids into colloidal dispersion systems (i) vesicle, (ii) oil-in-water, and (iii) molecular dispersion systems (solution), respectively, and the most suitable modification method was proposed for the modification purpose and the characteristics of the material carriers. Especially focusing on (iii), the usefulness of surface modification of polymer particles by the impregnation-support method was clarified through the characterization using energy-dispersive X-ray and fluorescence spectroscopy.

In Chapter 6, the phospholipid membrane-modified particles prepared by the impregnation-support method were utilized for the chiral separation of the amino acids as a case study of the cryogel modified with phospholipid membrane. L-tryptophan was found to be preferentially adsorbed on the phospholipid membrane modified on the cryogel particles similarly in the case do the chiral adsorption properties of liposome membranes.

In Chapter 7, the possibility of controlling the membrane properties of phospholipid membrane-modified cryogel particles via mechanical stimuli was investigated. The surface-modified cryogel particles were characterized using the membrane-environment sensitive fluorescent probe Laurdan. The results of time-resolved fluorescence analysis indicated that the membrane properties could be controlled by two states of the carrier particles, i.e., compressed and swollen states. This indicates the possibility of controlling the adsorption properties by changing the membrane properties of the lipid membrane coated on the cryogel particles by mechanical stimuli.

In Chapter 8, for the purpose of establishing a bioseparation design that maintains high efficiency and selectivity, a method for the preparation of particle carrier materials with sponge-like elasticity that is versatile in preparation method and easy to control various properties was established. A method to modify the surface of the carrier materials with phospholipid membranes was then established. The effectiveness of the method was confirmed through two case studies of potent sophisticated bioseparaiton. The results and methodology presented in this study are expected to be applicable to advanced bioseparations with high efficiency and selectivity.

PREFACE

This dissertation work was conducted under the supervision of Professor Hiroshi Umakoshi at Division of Chemical Engineering, Graduate School of Engineering Science, Osaka University from 2020 to 2023.

In this study, the method of preparation surfactant-free cryogel particles were developed and were applicated for sophisticated bio-separation by using them as core materials after the modification of the particle surface with lipid membrane. The cryogel particles were comprehensively characterized, focusing on the macroscopic properties, internal porous properties, and their physicochemical properties. The surface properties of the lipid membrane modified on the cryogel particles were further characterized and utilized for the mechano-chemical control of the target adsorption, that can be performed by inducing changes in their membrane properties via mechanical stimulation.

The author hopes that this research would contribute to the design of the porous polymer particles modified with lipid membrane, that can be used as functionalized materials with high efficiency and high selectivity. Furtherly, the insight obtained in this study is also expected to cause a breakthrough in the field of chemical engineering.

Hayato Takase

Division of Chemical Engineering
Graduate School of Engineering Science
Osaka University
Toyonaka, Osaka, 560-8531, Japan

Contents

Chapter 1

General Introduction

In the field of chemical engineering, the separation technique is important for the improvement of the process efficiency and selectivity, followed by the deeper understanding of several phenomena (phase equilibrium and transport phenomena). To achieve sophisticated separation with high-performance and high-efficiency, it is necessary to design the optimized method systematically and strategically after looking at the whole process from the bird's eye viewpoint.

1. Separation Techniques

In general, there are several kinds of separation methodologies, such as distillation, adsorption, chromatography and they are applied depending on the type of target molecules (i.e. rare metal, wastewater, amino acids) as shown in **Table 1-1**. As for the principle of separation, equilibrium separation and rate-governed separation are commonly adopted (**Fig.1-1**). In equilibrium separation, the process design is based on the equilibrium of the system, caused by the difference of chemical potentials between two phases (i.e, liquid-liquid, solid-liquid, gas-liquid), together with that at the interface of the phases. Whereas, in rate-governed separation, the process design is based on the difference in transport phenomena through a given media by gradients in driving force such as concentration, temperature, pressure and electric field. All separation techniques can here be classified by Gidding's proposal (1990) in relation to the phase equilibrium and transport phenomena (**Fig.1-1**). Although these methodologies are widely spread and utilized in modern industries, the separation method still have reminded problems to realize both high selectivity and high purity, and high efficiency such as high yield and large-scale separation. For breakthrough in the conventional separation method, it is essential to control the properties at molecular level on the micro/meso scale and to optimize separation operations on the macro scale. In order to complete it, it is necessary to design and development of the "*core materials for the sophisticated separation*", that (i) could have recognitive nature for target material on the surface (*micro*-scale), (ii) could be controlled easily by using the external intensive forces (e.g. temperature, pH, physical stress, and so on) (*meso*-scale), and (iii) could be utilized as the bulk materials themselves or filling materials in the column type devices (*macro*-scale).

Table 1-1. List of separation methodologies

Method	Example of target	Principle	Ref
Distillation	Petroleum	Equilibrium separation	E. Anderson *et al.,* 2018
Coagulation	Colloid particles		M. Lu *et al.,* 2018
Adsorption	Amino acids		T. Ishigami *et al.,* 2015
Crystallization	Oligomer		S. Xu *et al.,* 2021
Solvent extraction	Fuel		M. Sharma *et al.,* 2013
Centrifugation	Protein	Rate-governed Separation	N. Milkovic *et al.,* 2020
Chromatography	RNA, DNA		O. Coskun *et al.,* 2016
Membrane separation	Wastewater		S. Rajendran *et al.,* 2021

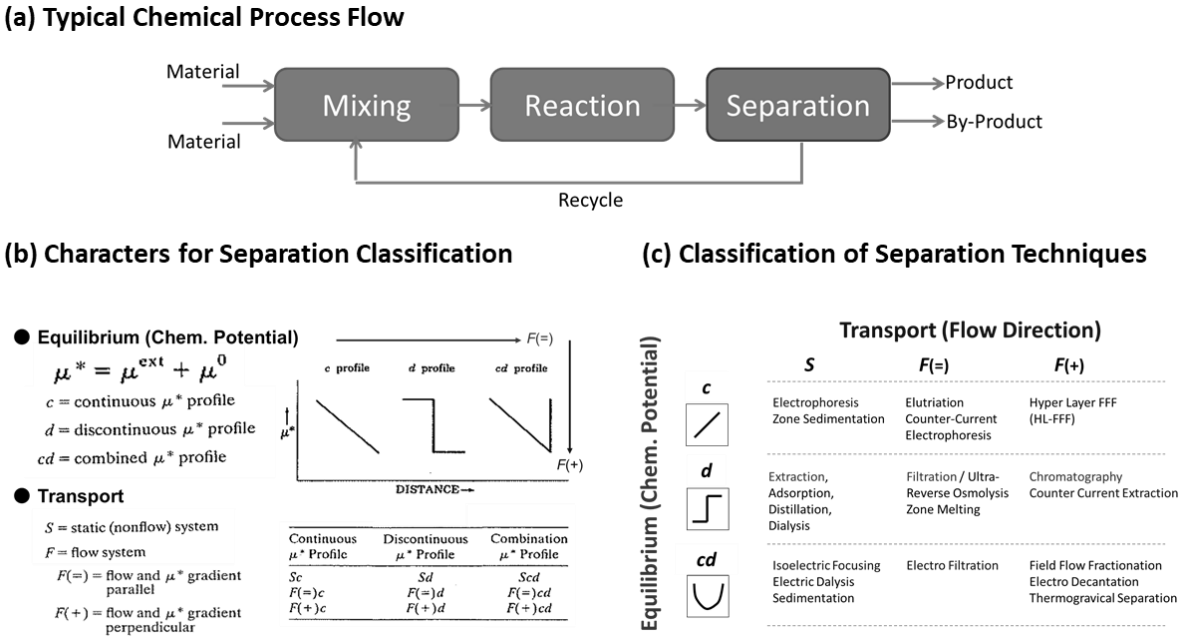

Figure 1-1. Classification of separation technologies. (a) Typical chemical process flow, where the separation techniques consume much energy (around 70% for all). (b) and (c) shows the scientific classification of all the separation techniques proposed by Giddings ("Unified Separation Science", J. C. Giddings, Wiley (1991)) in relation to the equilibrium and transport phenomena.

2. Design of Porous Polymer Materials for Carriers

Porous polymer materials are represented as separation materials, encapsulation agents for controlled release of drugs, sensors, supports for catalysts by modification properties via immobilization, composite, coating techniques. Among the possible polymer materials, "*porous*" polymer materials play an important role in stabilizing physically and chemically modified molecules as a substrate. The macroscopic shape of porous polymer materials can be designed to optimize for separation method. As shown in **Fig.1-2**, various macroscopic shape of porous materials (a1) sheet, (b1) particle, (c1) cylinder, and (d1) disk and separation devices (a2) hollow fiber, (b2) particles packed column, (c2) monolithic column, and (d2) semipermeable membrane are categorized. Various macroscopic shape of polymer materials can be conventionally prepared by using mold vessel. In contrast, preparation of spherical shape may necessitate a technique. For example, polymer particles were synthesized by adopting the emulsion polymerization method. Since the progression of porous polymer particles research has accelerated, various preparation methodologies and polymer components have been developed by combination techniques.

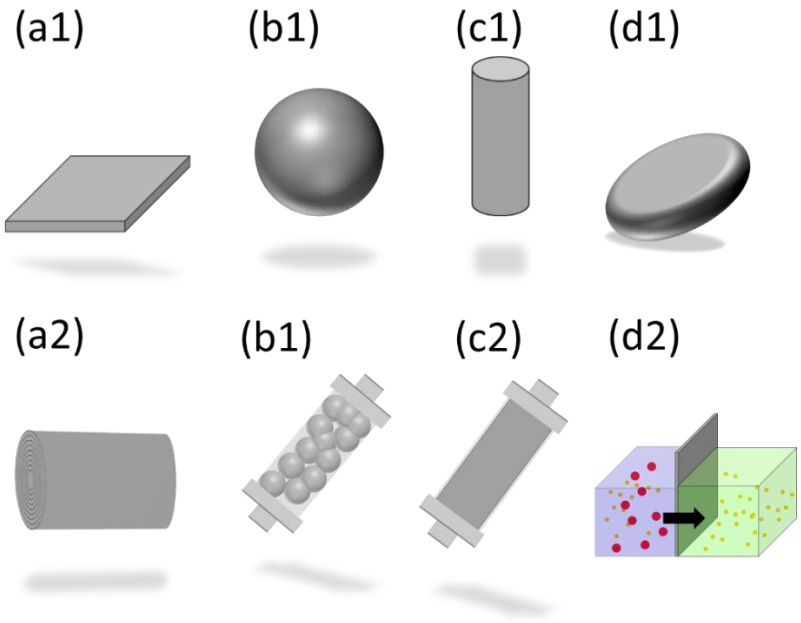

Figure 1-2. Macroscopic shape of porous polymer materials (a1) sheet and (a2) hollow fiber membrane, (b1) particle and (b2) particles packed column, (c1) cylinder and (c2) monolithic column, and (d1) disk and (d2) semipermeable membrane.

Table 1-2. Classified pore size of polymer particles

Porous	Size	Example of porogen	Composition
Micropore	2 nm <	Microemulsion	pMEK
Mesopore	2-50 nm	Emulsion	Silica
Macropore	< 50 nm	Polymer particles	p(St-*co*-DVB)
Supermacropore	10-200 μm	Ice crystals	p(HEMA-*co*-MBA)

Here, porous properties also play important roles for separation. Regarding a characteristic of porous structure, the pore size is defined as microporous with smaller than 2 nm in diameter, mesoporous with 2-50 nm, and macroporous with larger than 50 nm. In addition, supermacroporous with 10-200 μm is named (**Table 1-2**). The porous structure is also necessary to design for application purpose. It has possibility that the overall efficiency become rate-limiting because the pore size is too small, a large specific area can be available, however the diffusion kinetic is decreased for mass transfer within the pores. In contrast, the too large pore size promotes rapid mass transfer within the pores although the efficiency is decreased due to the specific surface area is small. Regarding a characteristic of porous structure, the pore size is defined as microporous with smaller than 2 nm in diameter, mesoporous with 2-50 nm, and macroporous with larger than 50 nm. In addition, supermacroporous with 10-200 μm is named (**Table 1-2**).

3. Cryogel Materials

Cryogel have attracted attention in many fields such as separation, biochemistry, biomedical fields. With their highly interconnected and open super-macroporous structure, cryogel have quickly proven to be essential for application. A set of unique cryogel properties, (i) including large water content, (ii) substantial pore size, (iii) high porosity (iv) high pore connectivity, (v) high pore connectivity, and (vi) shape memory. In the cryogelation process, solvent crystals (i.e. water, acetic acid, DMSO) are used as porogens. Defrosting solvent crystals leave behind large and interconnected pores (**Fig.1-3**). When compared to other techniques used to generate macroporous structure, cryogelation tends to be a time and resource efficient method. Furthermore, various parameters can be easily fine-tuned to customize cryogels for their intended use. Other

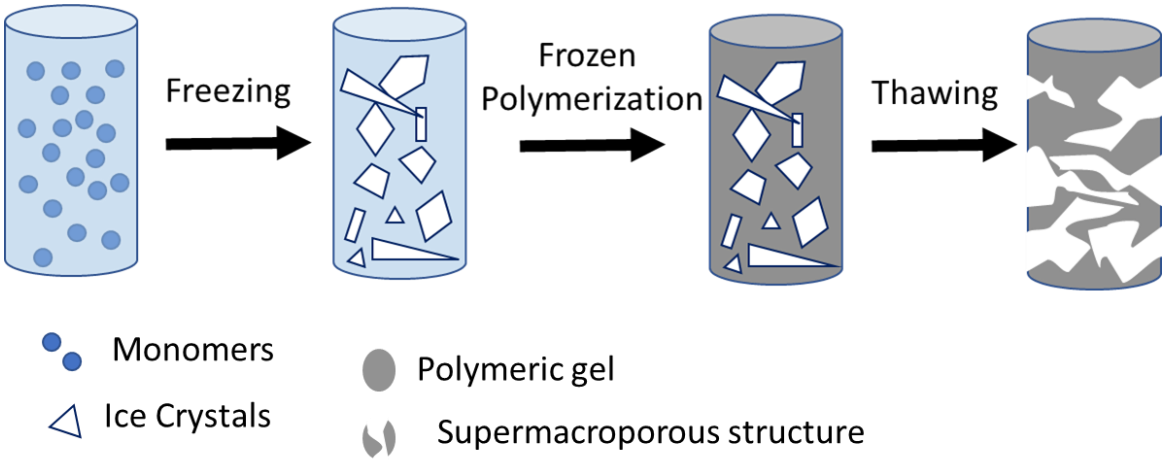

Figure 1-3. Mechanism of preparation of cryogel.

advantages of cryogels include the flexibility of their preparation and operating mostly with water as a solvent, making this type of biomaterials more economical and environmentally friendly. Focusing on mechanical properties of cryogel materials for separation carrier, cryogel is suitable for application to chromatography. Their high elasticity and compressibility, which allow for lab operation at high velocities with low backpressure, decreasing processing time. Under high compression the cryogel pores remain open, preventing backpressure forming. Furthermore, cryogels are chemically stable due to the hydrophobic nature of their polymers, leading to minimal nonspecific interactions, Additionally, cryogel have high mechanical strength due to the high polymer concentration at the pore walls. During cryogelation, freezing of porogen displaces polymer from the pore to the pore wall, increasing concentration and thus strength. Due to these properties, cryogels can withstand numerous cleaning and regeneration cycles. In addition, because cryogels can be dried and re-swollen quickly without their structure being affected, they can be stored for long periods of time in their dried state.

4. Self-assembly Phospholipid Membrane

Recently, self-assembled materials have attracted many interests of researchers in various research fields. As shown in **Fig. 1-4**, amphiphilic molecule such as phospholipid form self-assemble system (i.e, micelle, bicelle, liposome). Depending on the property derived from chemical structure and/or surrounding environment, some kinds of amphiphilic molecules can be automatically assembled to form the supramolecular

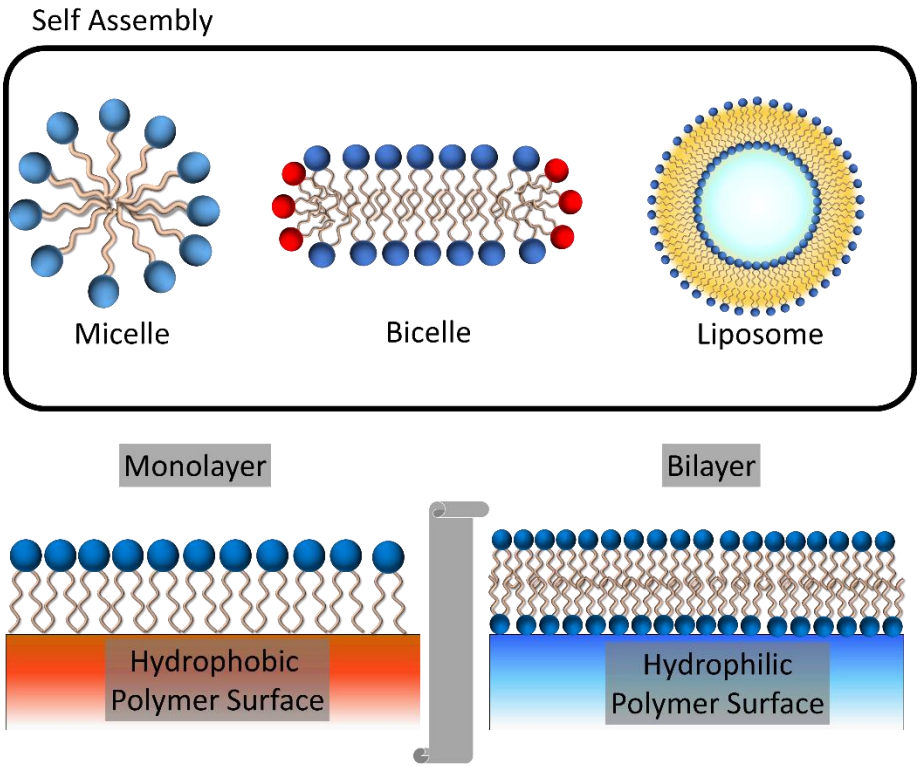

Figure 1-4. Polymer material modified with self-assembly.

structures. Amphiphilic molecules, for example, can form the self-assembly by several driving forces, such as electrostatic interactions and van der Waals interactions in hydrophobic regions. Thus, it can be possible that the self-assemble system modify the polymer surface according to thermodynamically stable state. When the substrate is hydrophobic, a monolayer form on the polymer surface, while a bilayer forms when the substrate is hydrophobic.

Apart from the typical polymers formed by covalent bonds, such self-assembly structures can show dynamic property despite of the increment of entropy, which is regarded as fluctuation in non-equilibrium state. These phenomena are described as the theory of dissipative systems (Prigogine *et al.,* 1967). According to the biomolecules, various organisms such as cells is formed by the assemblies, called as “self-organization” system. For example, cell membranes, which exist in the boundary of cells, are composed by amphiphilic phospholipids. The dynamic changes of cell membranes such as endocytosis are induced by the rearrangement of phospholipid components of outer or inner membranes (Farge *et al.,* 1995). It is possible to design new core materials for the

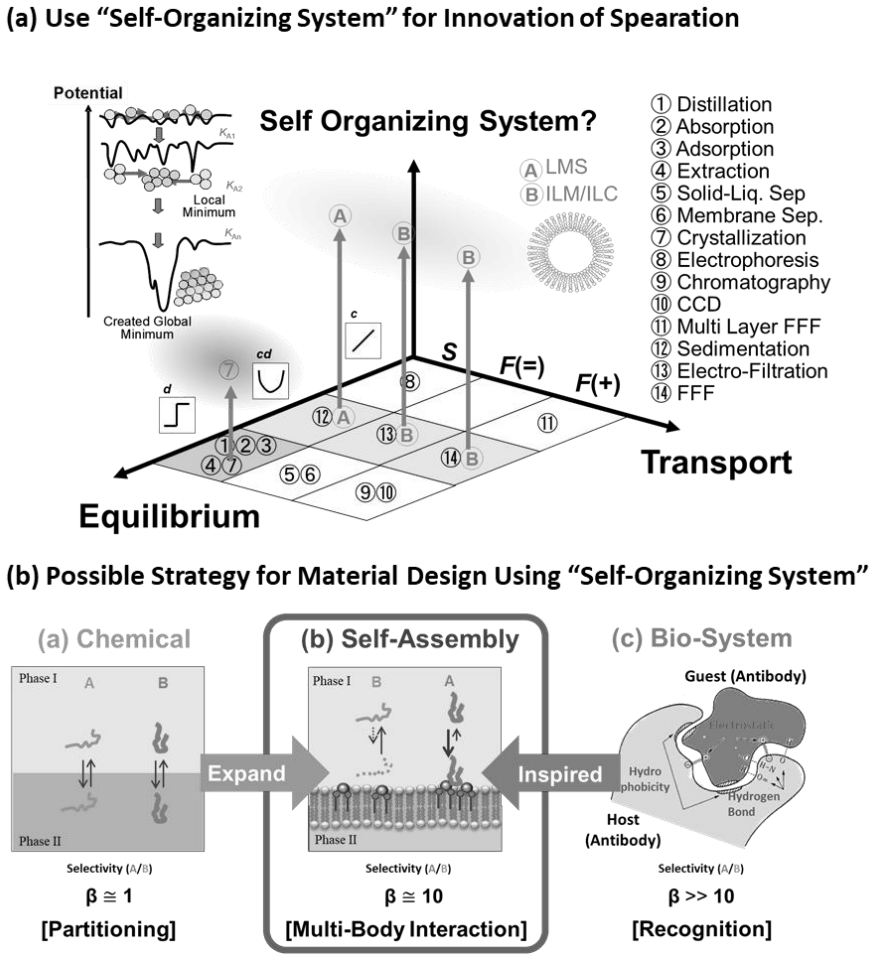

Figure 1-5. Plausible direction for new separation techniques and their materials

sophisticated separation by utilizing and integrating this "self-organizing system" (**Fig.1-5(a)**). These dynamic regulations of assembled states may possibly play important role for the flexible recognition of target materials similarly in the case of the biomacromolecules (i.e. enzyme, antibody, etc). The molecular recognition system using self-assembly system has been recently developed for efficient processes, such as separation. Some studies revealed the high performance in the separation of chiral molecules by means of chiral monomers (Ishigami *et al.,* 2015). Since self-assembly system can easily form the interactions with foreign molecules with "low energy consumption", In addition, it is expected that the formation of highly-ordered structure required for asymmetric recognition is automatically induced in the self-assembly

systems (Lee *et al.,* 2002; Mohanty *et al.,* 2005; Kamata *et al.,* 2015). These membranes have the ordered alignment of phospholipids, inducing the increasing anisotropy of several steroid molecules. This feature is expected to contribute to the formation of stereospecific interactions. This finding means that phospholipids can form the specific materials that can include the hierarchical assembly in their material structure. The several findings about the phospholipid assemblies indicate the emergence of functions and materials with varying systems dynamically (Walde *et al.,* 2014). It is therefore promising to design and develop the polymer materials modified with the phospholipid membranes as the recognitive and switchable surface (**Fig.1-5(b)**).

5. Overview of This Study

The final purpose of this thesis is to establish the design method of core materials for sophisticated bio-separation with high-performance and high-efficiency. To achieve this goal, it is required to design entire the material for controlling of physicochemical properties at the *meso*/*micro* scale by considering "*molecular alignment*" for the optimization of carrier materials for application to separation. The framework and flow chart of the present study are schematically shown in **Fig.1-6** and **Fig.1-7,** respectively.

In chapter 2, the preparation process for surfactant-free cryogel particles were developed. The preparation process was included in the two steps: preparation of frozen droplets using the inverse Leidenfrost effect, followed by cryo-polymerization by frozen polymerization. Fist, a polymer precursor was dropwise added into bulk liquid nitrogen (-196 ºC). Then, frozen droplets were created by the inverse Leidenfrost effect, that was subsequently polymerized in liquid paraffine (-15 ºC). After thawing and drying, the cryogel particles were obtained. The monolithic super-macroporous structure was observed by scanning electron microscopy (SEM). The mechanical properties of the cryogel particles were studied via compression-swelling tests. At maximum compression, the particles achieved a 94.3% degree of deformation; remarkably, they returned to their original shape under the swelling state. The strategy proposed herein, which combines the inverse Leidenfrost effect with a cryo-polymerization technique, could be applied to prepare various polymer particles without employing surfactants.

In chapter 3, the versatility of a two-step preparation method, without surfactant,

was investigated that combines both inverse Leidenfrost effect and cryogelation technique by using the macroporous particles of different kinds of monomers (four vinyl monomers) or natural polymers (agarose). First, the precursor of polymers was dropped into liquid nitrogen to prepare the spherical frozen droplet by inverse Leidenfrost effect. Secondly, the frozen droplets were cryo-polymerized under frozen temperature; then cryogel particles were prepared after thawing. Subsequently, the basic characteristics of the macroporous polymer particles obtained above were compared; focusing on the appearances, porous morphologies, and mechanical properties.

In chapter 4, the porous structure of cryogel particles was design with directional and bimodal porous structure by controlling phase separation in microphase and generation of porogen during cryo-polymerization process. The formed pores, supermacroporous structure, have monolithic directional porous structure through surface to interior of the particles and macroporous structure was formed on the polymer wall whose contributed as framework of supermacropores. Furthermore, the porous properties were observed by SEM and evaluated by mercury intrusion porosimeter (MIP). The porous designed cryogel particles can be expected to utilize for separation material.

In Chapter 5, a method of the modification of the prepared cryogel particles by phospholipid membrane was established and was shown as a qualitative scheme. The advantages and disadvantages of the various methods were systematically compared by classifying the phospholipids into colloidal dispersion systems (i) vesicle, (ii) oil-in-water, and (iii) molecular dispersion systems (solution), respectively, and the most suitable modification method was proposed for the modification purpose and the characteristics of the material carriers. Especially focusing on (iii), the usefulness of surface modification of polymer particles by the impregnation-support method was clarified through the characterization using energy-dispersive X-ray and fluorescence spectroscopy.

In Chapter 6, the phospholipid membrane-modified particles prepared by the impregnation-support method were utilized for the chiral separation of the amino acids as a case study of the cryogel modified with phospholipid membrane. L-tryptophan was found to be preferentially adsorbed on the phospholipid membrane modified on the cryogel particles similarly in the case do the chiral adsorption properties of liposome membranes.

In chapter 7, the possibility to control the membrane properties on the surface of the cryogel particles was studied by applying them to the mechanical stimulation. The lipid membrane coated cryogel particles was characterized by fluorescence probe Laurdan. Through the analysis by using the time-resolved emission spectroscopy, the membrane properties were found to be controlled between two states; the compression state and the swelling state. Consequently, the adsorption properties could be controlled by changing the lipid membrane properties coated on cryogel particles via mechanical stimulation.

The results obtained in this work are summarized in the chapter 8 as the General Conclusions section. Suggestions for Future Woks are described as extension of the present thesis.

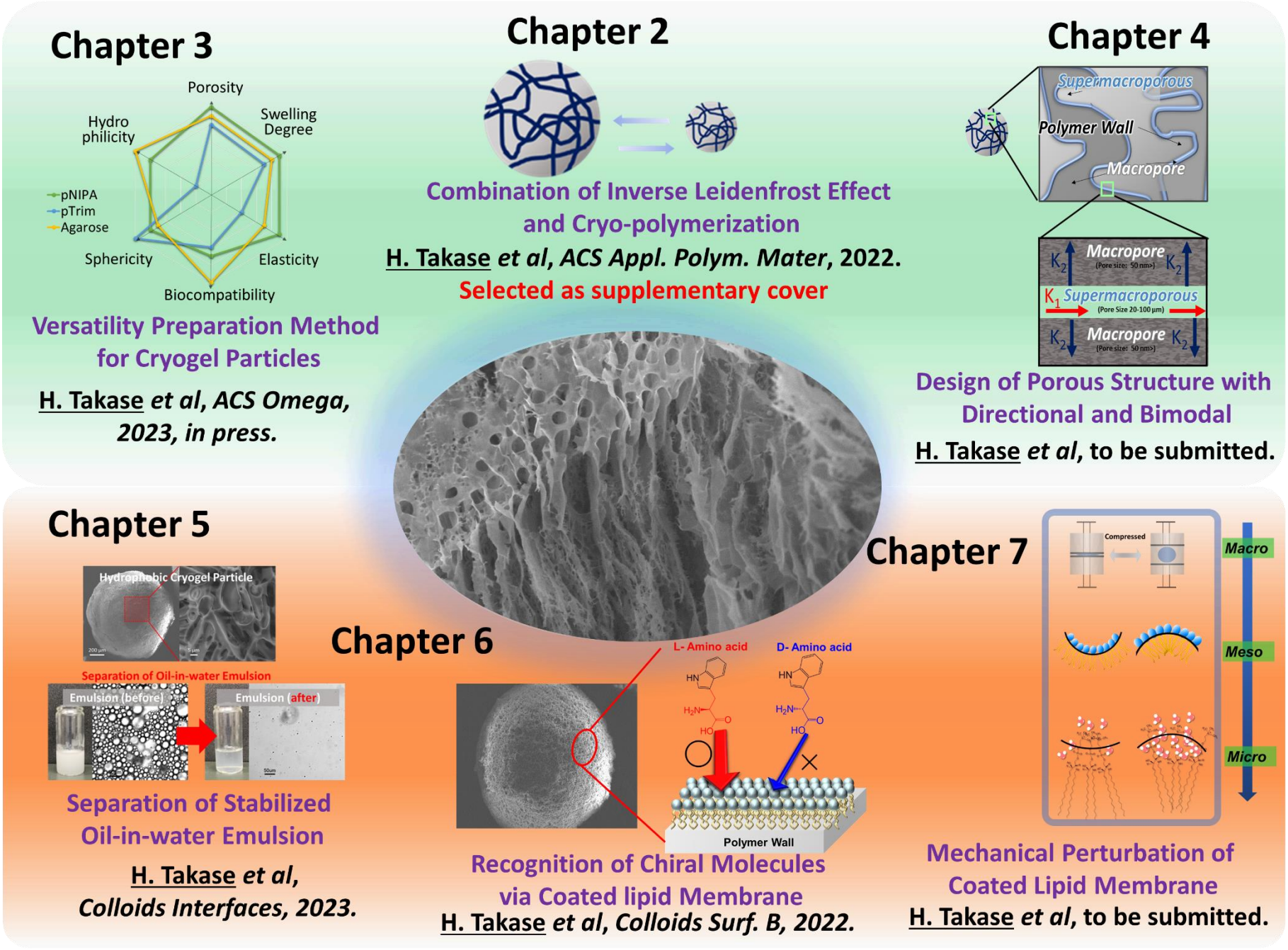

Fig. 1-6. Concept of this study.

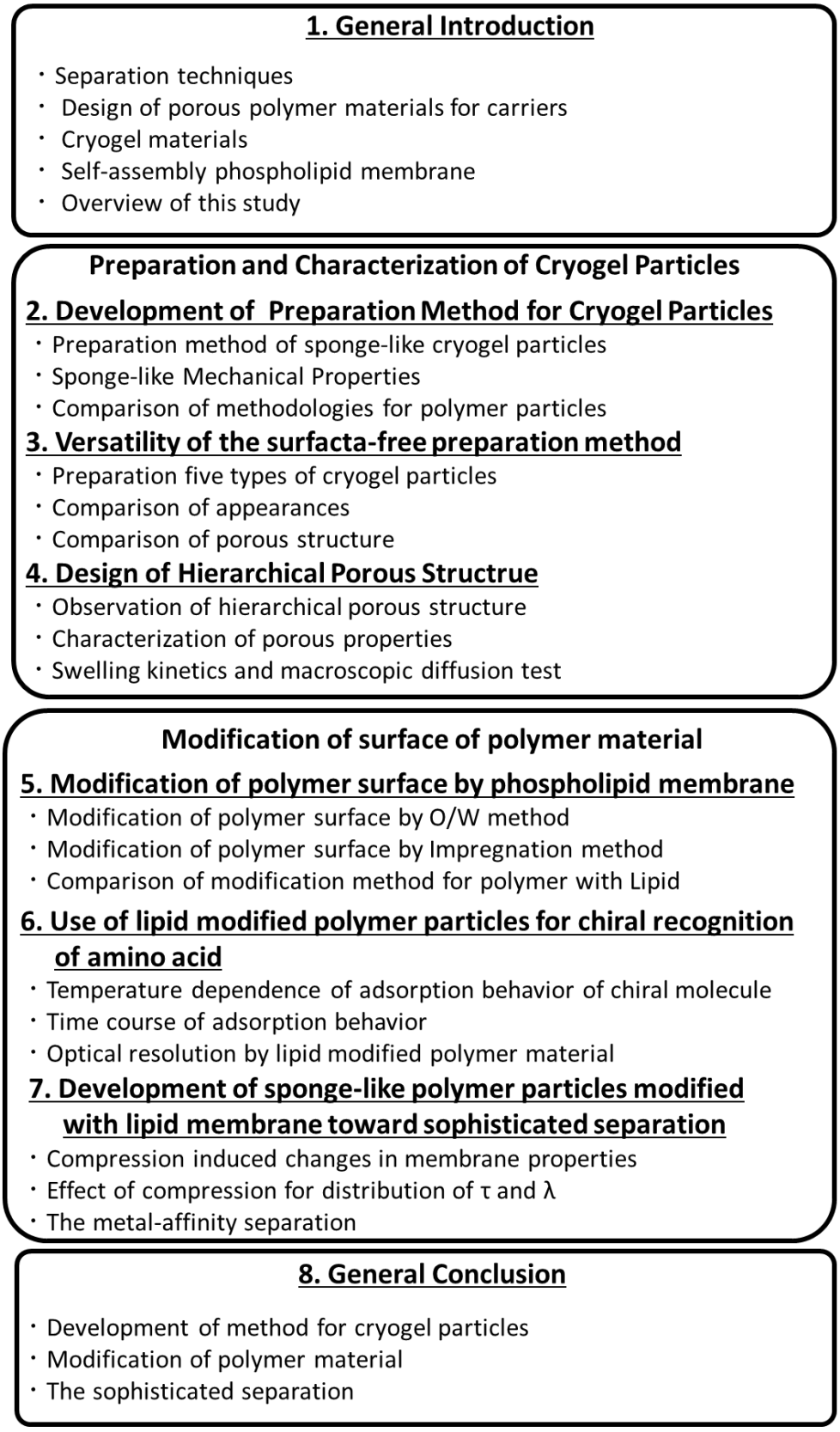

Fig. 1-7. Flow chart of the present study.

Chapter 2

Preparation and Characterization of

Sponge-like Cryogel Particles

1. Introduction

Polymer particles have attracted notable scientific interest and possess great application potential in various fields, such as biology, sensors, and support materials in manufacturing processes. Polymer particles are often processed by coating their surface, mixing different monomers to prepare composite materials, and/or enclosing the beneficial materials (i.e., catalysts and bioagents) inside, depending on the intended applications. In general, polymer particles can be prepared by several methods including: (i) inverse emulsion polymerization (Bao *et al.,* 2015), (ii) Pickering emulsion polymerization (Lotierzo *et al.,* 2017; Shen *et al,* 2011), (iii) solvent evaporation polymerization (Takei *et al.,* 2008), and (iv) mechanical stirring in a multi-phase system (Luo *et al.,* 2015). A common feature of the above methods is the requirement of a surfactant/detergent substance to stabilize the multi-phase interface, where the preparation conditions must be optimized for each polymer material; however, to maintain both the stability of the dispersed phase and a good reactivity at the interface, the applied surfactant/detergent must remain in the obtained polymer particles. Therefore, surfactant-free methods are necessary for the versatile design of functional polymer particles.

Controlling the droplet stability during the internal polymerization process is crucial for preparing functional polymer particles. A viable method that enables the preparation of such particles without the use of surfactants/detergents is through the inverse Leidenfrost effect (Gauthier *et al.,* 2019; Arrieta *et al.,* 2020; Kumar *et al.,* 2022). The inverse Leidenfrost effect is a phenomenon in which the droplets (i.e., aqueous solution) are coated by a boiling-film and become spherical when they approach the substrate under a temperature difference that significantly exceeds the boiling point (i.e.,

−196 °C for liquified N_2). Although this phenomenon has shown good application potential in many fields, such as cryogenics (Gauthier *et al.,* 2019) aerospace (Wells *et al.,* 2015), green chemistry (Abdelaziz *et al.,* 2013) and surface science (Pacheco *et al.,* 2021), its main mechanism remains largely unexplored. This is primarily attributed to the boiling-film's presence on the droplet surface, which apart from restricting their contact with the reaction substrate, also inhibits their dynamic behaviors, like self-propulsion, gliding, spinning, bobbing, and bouncing (Matumoto *et al.,* 2021; Shi *et al.,* 2021; Gauthier *et al.,* 2020). The use of the inverse Leidenfrost effect for the preparation of polymer particles could enable us to achieve a surfactant-free strategy, to alleviate these complications.

Porosity is one of the most prominent characteristics of polymer particles. In general, porous materials are known to exhibit high porosities (Wu *et al.,* 2012) and large specific surface areas (Mohamed *et al.,* 2022; Wang *et al.,* 2012). Porous structures are usually classified as follows: (a) super-macropores are up to 100 μm in diameter; (b) macropores are larger than 50 nm in diameter; (c) mesopores are in the range of 2–50 nm in diameter; and (d) micropores are smaller than 2 nm in diameter, where the pore size is engineered according to the application. Porous materials can be applied for the preparation of various functional polymers, such as scaffolds (Trimpathi *et al.,* 2009), catalyst carriers (Han *et al.,* 2015), and separation and reaction media (Kartal *et al.,* 2020; Takase *et al.,* 2020; Hiramure *et al*; 2018; Inda *et al*; 2018). Although several techniques have been devised to control the porosity of polymer materials, the most commonly employed one relies on the use of porogens during polymerization, that serve as a template for the evolution of the porous region (Wu *et al.,* 2012). Examples of commonly used porogens are micelles (Tan *et al.,* 2007), organic solvents (Batchuluun *et al.,* 2021), organic metals (Luz *et al.,* 2019), and ice crystals (Memic *et al.,* 2019). Completely removing these templating substances after polymerization is a difficult task, however, because they are deeply embedded within the polymer region during the polymerization process.

Ice crystals are considered highly auspicious porogen material candidates and are thus prominently used in cryo-polymerization methods (Savina *et al.,* 2005; Sahiner *et al.,* 2018). Generally, cryogel exhibits numerous advantageous properties, such as

biodegradability (i.e., in natural polymers) (Chen *et al.,* 2016; Guastaferro *et al.,* 2021), sponge-like mechanical durability (Zhao *et al.,* 2018), shape-memory deformation (Bencherif *et al.,* 2012), and super macroporous structure (Sahiner *et al.,* 2018). Cryogels are typically obtained when the polymer precursors are polymerized at temperatures below the freezing point of the solvent. During the polymerization process, phase separation occurs in the solution containing the concentrated polymer precursor (liquid phase) and the ice crystals (solid phase), where the latter are utilized as porogens (Kumar *et al.,* 2010). Eventually, the porous cryogel is obtained by thawing, and the porogens (ice crystals) can be easily removed from the polymer materials (Memic *et al.,* 2019). Despite the lower reactivity of the polymer precursor owing to the freezing temperature conditions, this method could be beneficially combined with the above-mentioned inverse Leidenfrost effect, prior to cryo-polymerization, to achieve efficient droplet formation.

In this chapter, it was explored a method to prepare cryogel particles with sponge-like mechanical properties, along with high porosity and high elasticity, by combining a cryo-polymerization technique with the inverse Leidenfrost effect. The preparation of the cryogel particles was achieved through the following two steps: (1) preparation of frozen droplets by the inverse Leidenfrost effect and (2) cryo-gelation by frozen polymerization. The obtained cryogel particles with sponge-like structures were studied by scanning electron microscopy (SEM) and compression-swelling experiments.

2. Materials and Methods

2.1. Materials

2-Hydroxyethylmethacrylate (HEMA), *N,N′*-methylenebisacrylamide (MBA), ammonium persulfate (APS), *N,N,N′,N′*-tetramethylethylenediamine (TEMED), liquid paraffine, *n*-hexane, and ethanol were purchased from Wako Pure Chemical Industry Ltd. (Osaka, Japan). Ultra-pure water (conductivity 18.2 MΩ cm) was prepared with Direct-Q UV 3 (Merck, Osaka, Japan). All materials were used as received without further treatment.

2.2. Preparation of Cryogel Particles

The cryogel particles were prepared by polymerization under freezing conditions,

according to our previous method (Hiramure *et al.,* 2018). In the polymerization process, ice crystals were templated in a polymer precursor and utilized as porogens. Therefore, the thawed cryogel was a porous material with monolithic pores. Herein, the cryogel particles were prepared by the droplet method using the inverse Leidenfrost effect. HEMA and MBA were used as a monomer and crosslinker, respectively. Both substances were dissolved in 15 mL of ultra-pure water, cooled with ice, and purged with N_2 for 5 min to remove the oxygen traces. Subsequently, 0.57 mmol APS and 0.22 mmol TEMED were added to the solution and quickly transferred to a syringe. Next, the polymer precursor was dropped into liquid nitrogen from the syringe, using a 16 gauge needle. Then, the completely frozen droplets were transferred to liquid paraffin at −15 °C and underwent polymerization for 24 h. The polymerization reaction for preparation cryogel particles is shown in supporting information (**Fig.2-1**). On the other hand, the gel particles were prepared at 5 °C using the same procedure as with the cryogel particles. The polymerized particles were thawed at 25–28 °C, and the residual monomers and paraffine were removed using *n*-hexane, ethanol, and ultra-pure water.

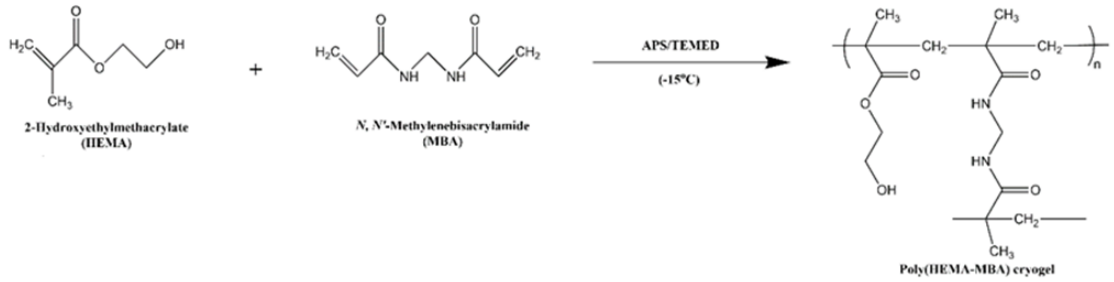

Figure 2-1 Chemical structure of polymerization reaction for cryogel particles.

2.3. Observation of Cryogel Particle Morphologies

Generally, the cryogel particles exhibited a monolithic structure comprising super macropores at the inner section. Here, the morphologies of the cryogel particles prepared via the droplet method were observed by a charge-coupled device (CCD, iPhone 12 MJNJ3J/A) camera, and a scanning electron microscope (SEM, JEOL JCM-6000PLUS). As a pretreatment step, the cryogel particles were lyophilized and cut into half with a cutter to observe their surface and cross sections via SEM.

2.4. Characterization of Swelling Behavior of Cryogel Particles

The swelling behavior of the cryogel particles was primarily characterized by their swelling ratio. To evaluate the swelling ratio, the weights of the dried cryogel particles were measured. Initially, the dried cryogel particles were immersed in ultra-pure water until reaching equilibrium at 25–28 °C; then, they were removed, the ultra-pure water on their surface was wiped off using filter paper, and their weight was measured. The swelling degrees (SDs) of the particles were calculated according to Eq. 2-1.

$$SD = \frac{(W_{eq} - W_d)}{W_d} \qquad \text{(Eq. 2-1)}$$

where W_{eq} and W_d are the weights of the equilibrium and dried cryogel particles, respectively.

The porosity (φ) was calculated by Eq. 2-2.

$$\varphi = \frac{(W_{eq} - W_s)}{W_{eq}} \qquad \text{(Eq. 2-2)}$$

where W_s is the weight of the squeezed cryogel particles

2.5. Characterization of Mechanical Properties of Cryogel Particles

Cryogel particles are known to have different mechanical properties from gels. In general, cryogel particles exhibit sponge-like elasticity and can withstand large compressive deformation. Furthermore, cryogel particles have a shape-memory functionality, which allows them to recover their original shape after the external compression force is removed. Here, the mechanical properties of our prepared cryogel particles were investigated by performing compression and swelling testing cycles. Initially, a cryogel particle was inserted into a microsyringe (Hamilton, 500 μL); then, it was mechanically compressed, and its changing shape was observed by an optical microscope with a ×4 objective lens (the experimental setup is shown in **Fig.2-5a**). Parallelly, its behavior and motion were video recorded. The deformation and recovery behavior of both the cryogel and gel particles during consecutive compression and release

cycles were determined from the optical microscope images and calculated according to Eq. 2-3.

$$Ratio\ of\ Shape\ Deformation = \frac{(A_0 - A)}{A_0} \times 100 \qquad \text{(Eq. 2-3)}$$

where A_0 and A are the areas of the particle before and after compression, respectively. The area of the particle was measured by using the software Image J.

2.6. Raman Spectroscopic Analysis

The chemical structure of poly(Trim-*co*-MBA) cryogel particles was characterized by using a LaBRAM HR-800 confocal Raman microscope (Horiba, Ltd., Kyoto, Japan). As the pretreatment, cryogel particles were lyophilized. The measurement was performed with a 100mW YAG laser operated with an excitation wavelength of 532 nm and an x20 objective lens focused the laser beam.

3. Results and Discussion

3.1. The Preparation Method of Sponge-like Cryogel Particles

The cryogel particles were prepared as follows: (i) the polymer precursor solution was added dropwise into liquid nitrogen; (ii) the frozen droplets were polymerized at freezing temperature; and (iii) the ice crystals were thawed inside the polymerized particles. Step (i) plays a key role in this method: directly after the dropwise addition of the polymer precursor solution into the bulk liquid nitrogen, the droplets start to float because of the inverse Leidenfrost effect, caused by the extreme temperature difference between the solution droplets [room temperature (around 20 °C)] and the bulk liquid nitrogen (−196 °C). By abruptly placing the droplets on the extremely cold liquid nitrogen interface, the inverse Leidenfrost effect causes their surfaces to be immediately coated with a gas film of evaporated nitrogen. The actual preparation process of cryogel particles employed here is schematically illustrated in **Fig.2-2**. This preparation process comprises two steps: in the first step, the frozen droplets were prepared via the inverse Leidenfrost effect. As a precursor solution, 2-hydroxyethylmethacrylate (HEMA), *N, N′*-

methylenebisacrylamide (MBA), and a mixed initiator (APS and TEMED) were dissolved in water (see the Materials and Methods section for the detailed condition); then, the solution was inserted into a microsyringe and dropwise added into liquid nitrogen (**Fig.2-2a**). The self-propulsion behavior of the droplets in bulk liquid nitrogen was video recorded as movie. After the addition of the precursor solution, the droplets were hovering and hopping for approximately 12 s on the bulk liquid nitrogen surface, until they finally sank inside. As illustrated in **Fig.2-2b**, the liquid nitrogen was rapidly evaporated, causing N_2 gas to flow on the droplet surfaces and coat them with a boiling-film, which in turn induced the droplets' self-propulsion and rotation. When the droplets were completely frozen and the system temperature reached thermal equilibrium (after ~12 s), the boiling-film disappeared, and the frozen droplets were completely sunk into the bulk liquid nitrogen (**Fig.2-2c**). In the second step, the frozen droplets were cryo-gelated by frozen polymerization. The completely frozen droplets were transferred from liquid nitrogen to liquid paraffine (−15 °C) and allowed to stand overnight, where frozen polymerization was initiated (**Fig.2-2d**). During the frozen polymerization process, the frozen droplets composed of the polymer precursor underwent phase separation via spinodal-decomposition (Tedeschi *et al.,* 2006). At −15 °C, the polymer precursor solution trapped inside the frozen droplets melted and seeped out, until it was concentrated around the ice crystals. Thus, the separated phases comprised a non-frozen region of the concentrated polymer precursor and a frozen region of ice crystals (**Fig.2-2e**). The sponge-like mechanical properties of the finally-obtained polymer particles were strongly affected by the polymerization conditions described above (e.g*.,* freezing temperature), which starkly influenced the concentrated polymer precursor behavior and the ice crystal formation process. As shown in **Fig.2-2f**, after the thawing of the frozen polymer particles, the ice crystals in the frozen region melted, while in the non-frozen region, a monolithic super macroporous structure was formed (Kumar *et al.,* 2010). The main advantage of this two-step preparation method resides in its non-necessity to use surfactants to form a particle template microemulsion; cargo, it can be applied for the preparation of various kinds of polymer particles (data not shown). Furthermore, the cryogel particles obtained through this method are expected to show superior mechanical properties (i.e*.,* elasticity and/or stimuli-responsive features).

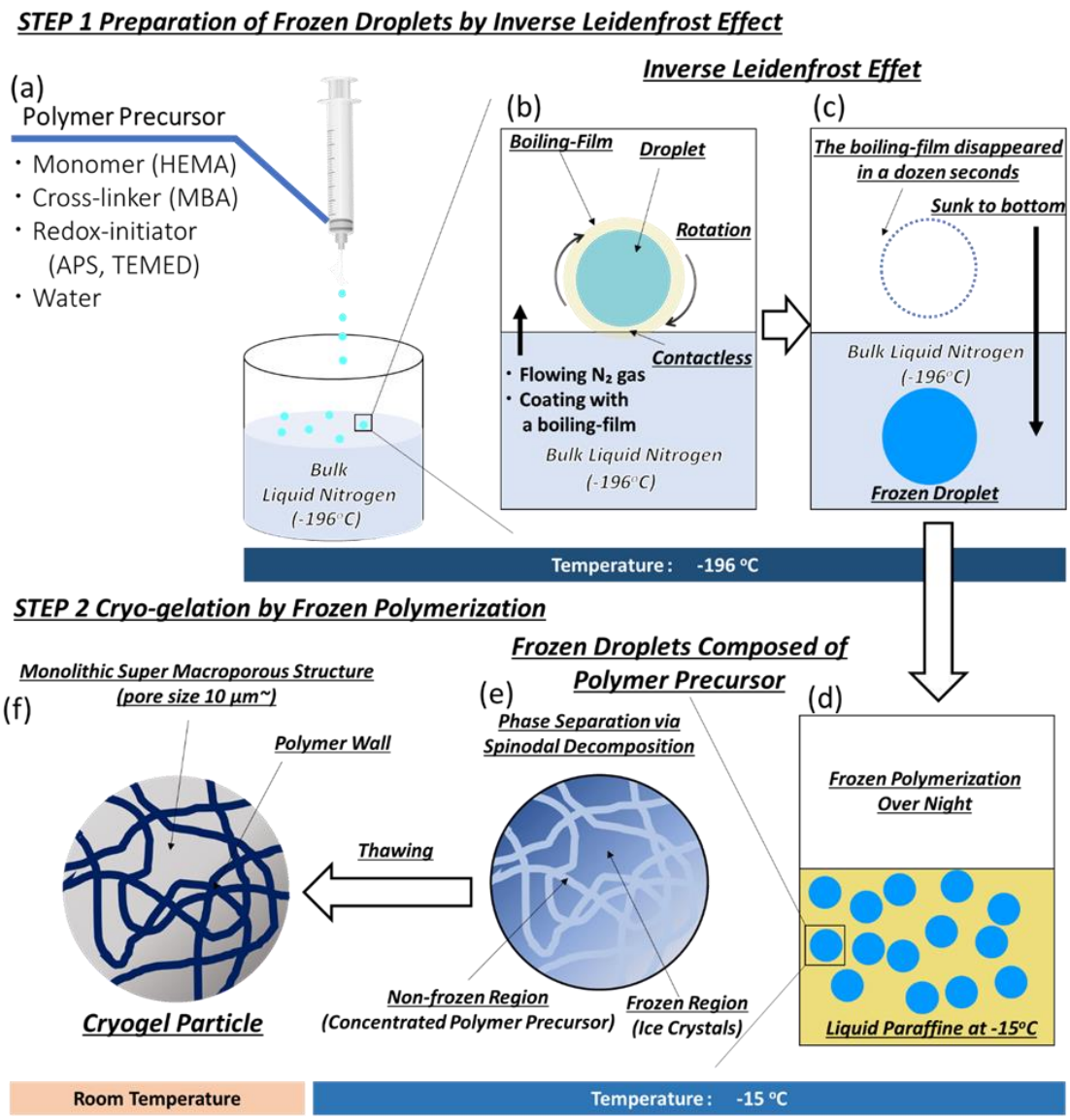

Figure 2-2. Schematic illustration of cryogel particles preparation process. **(a)** Polymer precursor dropped in bulk liquid nitrogen (-196 °C). **(b)** A droplet is coated, floated and rotated by boiling-film. **(c)** After disappearance of boiling-film (12 s), the droplet sinks to bottom of flask and becomes frozen. **(d)** Frozen droplets composed of polymer precursor are transferred to liquid paraffine at -15 °C and polymerized. **(e)** Frozen droplets undergo phase separation during frozen polymerization, where non-frozen and frozen regions occur via spinodal-decomposition. **(f)** Cryogel particles are prepared by thawing and removing the ice crystals. The monolithic super macroporous structure of the cryogel particles is due to the ice crystals acting as porogens.

3.2. Observation Macroscopic Structure and Porous Morphologies

The cryogel particle preparation process through the above two-step method was recorded by a CCD camera (**Fig.2-3a**) and analyzed by SEM (**Figs.2-3(c)** and (**d)**). As shown in **Fig.2-3a**, the appearance of cryogel particles in ultra-pure water, which were prepared by this method, had a spherical shape because of the polymerization in the frozen droplet. As the cryogel particles swelled, they retained the thawed water in their interiors; further, their appearance was white and opaque owing to light diffraction caused from their porous structure (Kisebom *et al.,* 2010). After pretreating the cryogel particles with lyophilization, their surface and cross sections were observed by SEM. **Figure 2-3(b)** schematically illustrates the surface and cross sections of the cryogel particles. According to the corresponding SEM images (**Figs.2-3 (c)** and **(d)**), both the surfaces and interiors of the cryogel particles were revealed to exhibit a characteristic "monolithic porous" morphology. These results implied that a phase separation, followed by spinodal-decomposition, occurred during the polymerization process in the frozen droplets containing the polymer precursor (Tedeschi *et al.,* 2006).

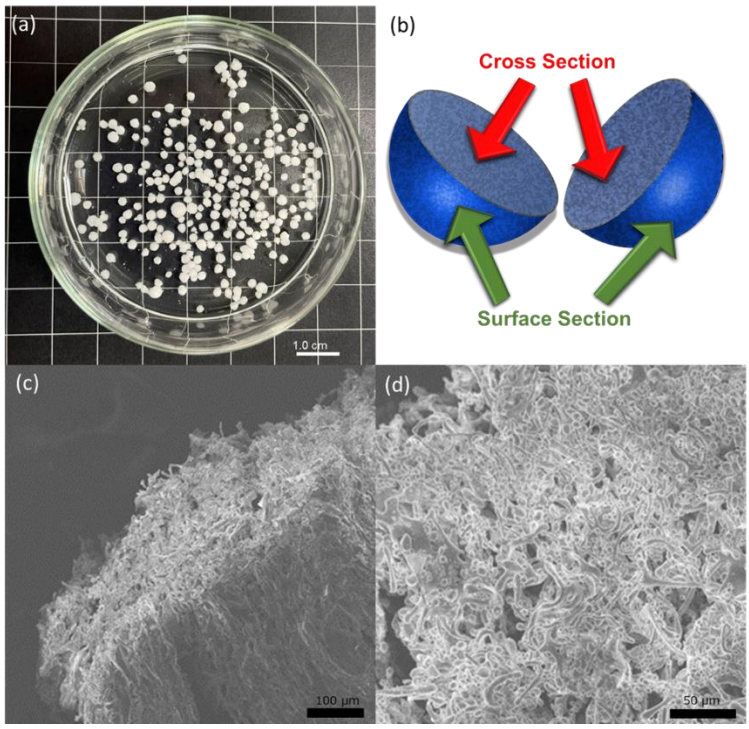

Figure 2-3. Observation of cryogel particles: **(a)** whole image of cryogel particles; **(b)** Schematic illustration of surface section and cross section of cryogel particles; SEM images of **(c)** surface section and **(d)** cross section.

Here, the separated phases in the frozen droplets were denoted as the non-frozen and frozen regions (**Fig.2-2(e)**); specifically, the polymer precursor formed the former, and the ice crystals formed the latter. Thus, after polymerization, the ice crystals used as porogens were removed by thawing, resulting in the formation of the monolithic pores. Additionally, sizes of the monolithic pores both at the surfaces and cross sections of the cryogel particles were evaluated according to the SEM images (**Figs.2-3 (c)** and **(d)**); the size of the pores was revealed to be approximately 10 μm. Pores with such large sizes in polymeric matrices are called "super macropores" (Kumar *et al.,* 2010). In summary, it has been demonstrated that the preparation method can enable the preparation of cryogel particles with characteristic monolithic structures and super-macropores, which bear resemblance to previously reported cryogel matrices (Hiramure *et al.,* 2018).

3.3. Characterization of High Swelling Degree and Porosity

The physical properties of cryogel particles are an important factor to consider when developing functional materials to accommodate a variety of applications (Hixon *et al.,* 2017). Hence, the physical properties of our cryogel particles were characterized with regard to their swelling degree and porosity. **Figure 2-4** illustrates the swelling degree (left axis) and porosity (right axis) of various cryogel particles as a function of the relative molar concentration of the cross-linker (MBA) to the monomer (HEMA).

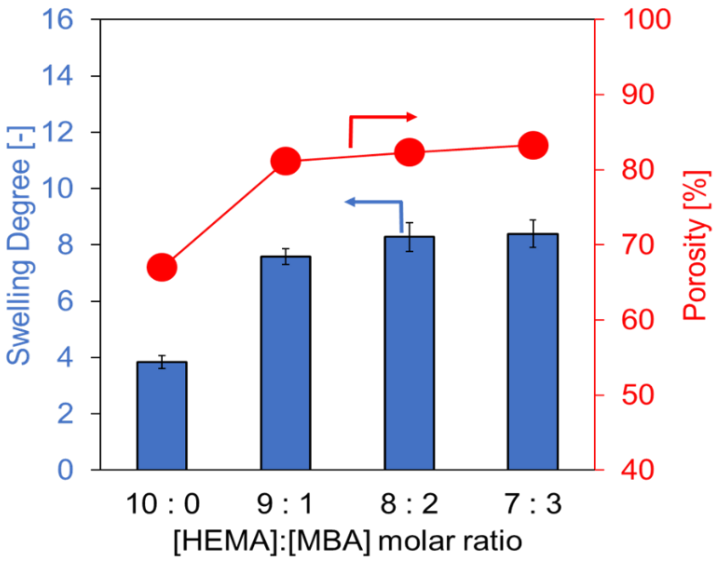

Figure 2-4. Swelling degree and porosity of poly-HEMA cryogel particles.

The formation of poly(HEMA-*co*-MBA) was confirmed based on the Raman shifts of HEMA, MBA, and poly(HEMA-*co*-MBA) (**Figure 2-5**). From the pectrum of cryogel particles, the peaks derived from HEMA and MBA were detected. Under all HEMA/MBA molar ratios (except for that without MBA), the obtained cryogel particles exhibited higher swelling degrees, as indicated by the ~8 times higher weight of the water-swollen cryogel particles compared to that of their lyophilized equivalents. Moreover, our obtained cryogel particles demonstrated a significant porosity approaching 85%. Furthermore, with the increase of the crosslinker (MBA) ratio, both the swelling degree and porosity of the poly(HEMA-*co*-MBA) cryogel particles became higher. This was theoretically inferred to have been caused by the polarity (hydrophilicity) of the polymer backbone inside the cryogel by considering the dielectric constants of HEMA and MBA; this highlights the significance of the hydrogen bonds between the water and polymer molecules, which can be related to the water retention mechanism on the polymer surface. Since the crosslinker (MBA) has a higher dielectric constant than the monomer (HEMA), the average dielectric constant of the poly(HEMA-*co*-MBA) cryogel particles was increased at higher molar ratios, thereby enhancing hydrophilicity. The obtained results (high swelling degree and large porosity of the poly(HEMA-*co*-MBA) cryogel particles) closely resembled those of the conventional hydrogel particles (poly(HEMA-*co*-MBA)), verifying that the obtained cryogel particles prepared by our method possess quite similar physical properties as typical hydrogel polymers.

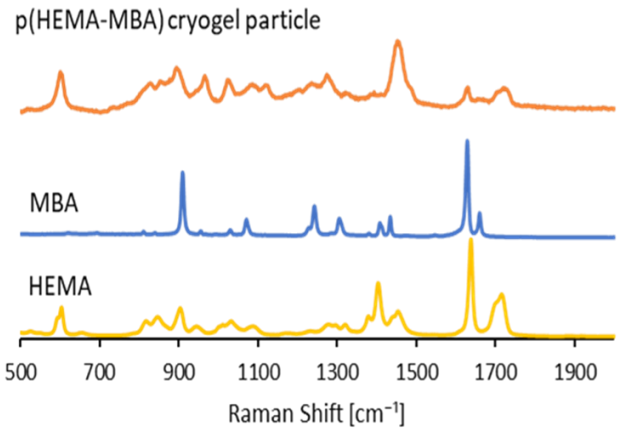

Figure 2-5. Raman spectroscopic analysis of cryogel particles

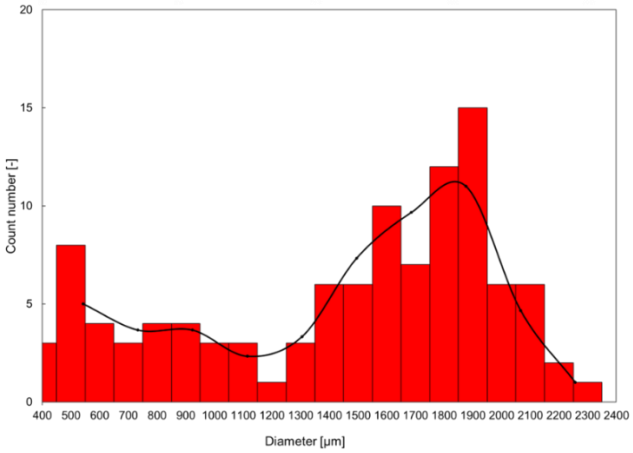

Figure 2-6. Size distribution of cryogel particles

3.4. Mechanical Properties of Cryogel Particles

The prepared cryogel particles were measured their diameter by using optical microscope and the size distribution was calculated as shown in **Figure 2-6**. Large number of the cryogel particles were distributed around 1800 µm.

Subsequently, Cryogel is an attractive porous polymer material with good structural stability and mechanical durability (Zhao *et al.,* 2018). The mechanical properties of the polymer particles (cryogel particles and conventional hydrogel particles) obtained here were investigated by mechanical compression-release tests in a microsyringe, as illustrated in **Fig.2-7**.

Polymer particles were confined to a microsyringe and then compressed and released repeatedly (**Fig.2-7(a)**). Although the shape of the cryogel particles was significantly deformed under mechanical compression, it returned to its original shape upon the release of the mechanical force (**Figs.2-7(b)–(d)**). The mechanical compression-release experiments of the cryogel particles were repeated for several cycles, and their deformation behavior was video recorded as movie. The observation that the compressed cryogel particles reversibly returned to their swollen shape with a rather fast restoration rate when the plunger of the microsyringe was pulled, confirmed their sponge-like reversibility properties. On the other hand, once the conventional hydrogel particles were compressed, they never returned to their original shape after the release of mechanical force (**Figs.2-7(e)–(g)**). Furthermore, the shape deformation ratios of the particles between their compressed and released states were monitored by microscopically observing the cross-sectional areas of the particles at each state (**Fig.2-7(h)**). The shape

deformation ratios of the cryogel particles at the compressed and released states were 93.4 and 3.9%, respectively; notably, the corresponding values of the conventional hydrogel particles were 91.4 and 65.7%, respectively. These results indicated a significant disparity in the mechanical properties of the cryogel and conventional hydrogel particles, despite their identical chemical compositions. Their different polymerization temperatures were considered to have played a role in this outcome.

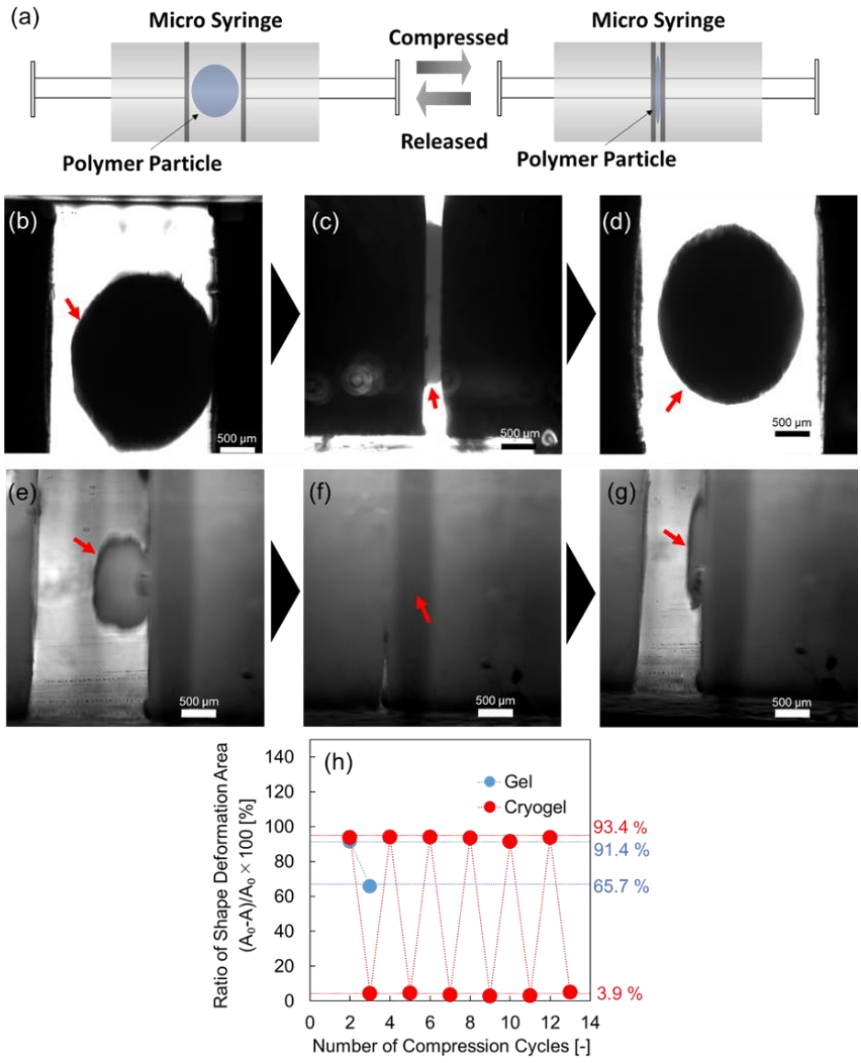

Figure 2-7. Properties of cryogel particles. **(a)** Schematic illustration of compression and release of polymer particles in microsyringe. Optical microscope images of cryogel particles: **(b)** before compression, **(c)** during compression, and **(d)** after compression. Optical microscope images of gel particles: **(e)** before compression, **(f)** during compression, and **(g)** after compression. Red arrows indicate the polymer particle. **(h)** Reversibility of shape deformation of polymer particles.

3.5. A Sophisticated Protocol for Preparation of Cryogel Particles

A new protocol to prepare the micro sponge ball, a polymer particle, has been proposed, where the obtained polymer particle was found to show some beneficial characteristics. Various prominent methodologies for the preparation of polymer particles and cryogels are summarized and compared in **Table 2-1**, with regard to the type of monomer (cross-linker), methodology used during particle formation and polymerization, and characteristics of the obtained materials (i.e., porosity, swelling behavior, and shape memory function). Our sophisticated preparation method offers the substantial benefit of feasibly and accurately controlling the design process and properties of the prepared cryogel particles. This is the first report to describe the preparation of sponge-like polymer particles by combining the cryo-gelation method and the inverse Leidenfrost effect. The core preparation strategy is feasible and straightforward: the ice droplets of the polymer precursor only need to be dropwise added to liquified nitrogen, prior to the polymerization process inside the droplets. As a result, the preparation of the polymer particles can be achieved without any surfactants/detergents. Also, such an extremely-cold environment is beneficial for the cryo-gelation process that employs ice crystals as porogens. Overall, using the strategy discussed above, it can be obtained polymer particles with: (i) high swelling capacity, (ii) high porosity, (iii) high elasticity, and (iv) memory-shape sponge-like capabilities. Our method can be effectively applied for the preparation of various kinds of polymer particles, regardless of the physicochemical characteristics of the monomers/polymers (this aspect will be further discussed in the forthcoming paper).

Table 2-1. Preparation of polymer particles and cryogel methodologies.

[This Study] Monomers (Cross-linker)	Pore Size[a]	Particle Size	Elasticity	Methodologies	Polymerization	Shape	Porosity[b]	Swelling degree[c]	Shape memory[d]	Temperature[e]
HEMA (*N, N'*-methylenebisacrylamide)	10-200 μm	n.d.	High	Cryo-gelation	Radical polymerization	Particles	High	High	Positive	-196/-20
[Comparison Study] Monomers (Cross-linker)	Pore Size	Particle Size	Elasticity	Methodologies	Polymerization	Shape	Porosity	Swelling degree	Shape memory	Temperature
Agarose	10-400 μm	(Bulk Gel)	n.d.	Cryo-gelation	Physical Crosslinking	(Bulk Gel)	n.d.	n.d.	n.d.	n.d.
Agarose-gelatin	76-187 μm	(Bulk Gel)	High	Cryo-gelation	Physical Crosslinking	(Bulk Gel)	n.d.	High	Positive	-12
HEMA-agarose	10-100 μm	(Bulk Gel)	High	Cryo-gelation	Physical Crosslinking	(Bulk Gel)	n.d.	High	Positive	-12
Acrylamide-co-MBA (*N,N'*-methylenbisacrylamide)	n.d.	(Bulk Gel)	High	Cryo-gelation	Graft Polymerization	n.d.	n.d.	n.d.	n.d.	-12
Acrylamide (*N,N'*-methylenbisacrylamide)	3-90 μm	240-330 μm	High	Inverse emulsion polymerization	Radical Polymerization	Particle	High	n.d.	n.d.	-12 or -18
Acrylamide (*N,N'*-methylenbisacrylamide)	n.d.	500-2000 μm	n.d.	Micro flow Channel with Inverse Emulsion Polymerization	Radical Polymerization	particle	95.70%	n.d.	n.d.	-20 to -23
Methacrylate gelatin	15.6 μm	100-200 μm	High	Inverse Emulsion Polymerization	Radical Polymerization (photo initiator)	Particle	n.d.	n.d.	Positive	-20
Quarternized chitosan	100-200 μm	(Bulk Gel)	High	Cryo-gelation	Radical polymerization	Cylindrical Shape	n.d.	High	Positive	-20
Alginate (MA-alginate)	10-600 μm	(Bulk Gel).	High	Cryo-gelation	Radical polymerization	n.d.	n.d.	High	Positive	-20
Alginate	200-500 μm	(Bulk Gel)	High	Cryo-gelation	Radical Polymerization	n.d.	n.d.	n.d.	n.d.	-20
Collagen (Dialdehyde starch)	20-200 μm	(Bulk Gel).	High	Cryo-gelation	Physical Crosslinking	n.d.	High	High	Positive	-15
Acrylamide (*N,N'*-methylenbisacrylamide)	n.d.	n.d.	High	Cryo-gelation	Radical Polymerization	n.d.	n.d.	High	n.d.	-16
HEMA (*N,N'*-methylenbisacrylamide)	10-100 μm	n.d.	n.d.	Cryo-gelation	Radical Polymerization	n.d.	High	High	Positive	-12
HEMA (*N,N'*-methylenbisacrylamide)	10-100 μm	n.d.	n.d.	Cryo-gelation	Radical Polymerization	n.d.	High	High	n.d.	-12
HEMA (*N,N'*-methylenbisacrylamide)	10-200 μm	n.d.	n.d.	Cryo-gelation	Radical Polymerization	n.d.	n.d.	High	n.d.	-16
HEMA (Polyethylene glycol diacrylate)	10-100 μm	n.d.	High	Cryo-gelation	Radical Polymerization	n.d.	High	High	Positive	-16
NIPAm (*N,N'*-methylenbisacrylamide)	10-200 μm	n.d.	n.d.	Cryo-gelation	Radical Polymerization	Cylindrical Shape	High	High	n.d.	-18
Lauryl methacrylate (Divinylbenzene)	3-20 μm 10-20 μm	n.d.	n.d.	Cryo-gelation	Radical Polymerization	n.d.	High	High	n.d.	-18
Methacrylic acid (Ethyleneglycol dimethacrylate)	10-330 nm	80-240 μm	n.d.	Pickering Emulsion Polymerization	Radical Polymerization	Particle	n.d.	n.d.	n.d.	60
Stylene (Divinylbenzene)	20 nm	8-22 μm	n.d.	Emulsion Polymerization	Radical Polymerization	Particle	n.d.	n.d.	n.d.	75

"n.d." shows "no data". [a]The pore size was determined based on SEM images of the particles. [b]The porosity of cryogel particles was observed by SEM. [c]The swelling degree was characterized from the weight of the cryo-gel particles at dried and swollen state. [d]The shape memory function of cryogel particle was characterized by cycle of compression-swelling test. [e]Polymerization temperature.

4. Summary

Here, a sophisticated strategy is demonstrated by combining a cryo-polymerization technique with the inverse Leidenfrost effect that is aimed at preparing cryogel particles with several beneficial properties. The cryogel particles were prepared via two steps: first, polymer precursor-containing droplets were added to bulk liquid nitrogen (−196 °C) to prepare frozen droplets by exploiting the inverse Leidenfrost effect. In the second step, the frozen droplets were removed from the bulk liquid nitrogen and added to liquid paraffine (−15 °C) to realize frozen polymerization (cryo-gelation). After the polymerization, the monolithic super macroporous structure was formed by melting and drying the templated ice crystals. The swelling degree and the porosity of the cryogel particles prepared with HEMA and MBA (cross-linker) were significantly enhanced. The obtained cryogel particles were confirmed to possess elasticity and shape-memory functions, resembling those of a sponge. Notably, the shape deformation ratio of the cryogel particles reached as high as 93.4%, while exhibiting good reversibility features. Overall, the method proposed herein is prospected to provide an auspicious platform for the design and preparation of various polymer materials with sponge-like mechanical properties. In particular, the cryogel particles obtained here are attractive for the design of mechanical stimuli-responsive materials, such as biosensors with added bio-separation/purification functionalities.

Chapter 3

Versatility of Preparation Method for Cryogel Particles

1. Introduction

Porous polymer particles are useful materials to apply for various fields, such as sensor materials, basal particular materials for separation and purification, culture matrixes for tissue engineering, and so on (Dhamecha *et al*, 2022; Shiomori *et al.,* 2021; Cheng *et al.,* 2021; Pandey *et al.,* 2022, Saeed *et al et al.,* 2014). The porous polymer particles have a large specific surface area due to porous morphologies (i.e. macro-; > 50 nm / meso-; 2-50 nm / micro-porous structures; < 2 nm) which could contribute to the efficient diffusion of the target molecules in the case of separation and purification process. Furthermore, it is known that the porous polymer particles possess some superior physical properties, for instance, durability, stretchability, and elasticity (Mi *et al.,* 2019; Hashmi *et al.,* 2009; Do *et al.,* 2017). In addition, the porous polymer particles could also be utilized for the immobilization of self-assemblies which usually exist as a "dispersed" state in water, such as liposomes/vesicles (Watanabe *et al.,* 2019; Izza *et al.,* 2022), colloids (Grundy *et al.,* 2018) and supermolecules (Qian *et al.,* 2008), resulting in the utilization of the specific functions of their self-assemblies in a separation process design. From another point of view, the macro-/micro-porous polymer particles are expected to be applied as functional supports for various kinds of separation by modifying their surface by active and functional molecules (Takase *et al.,* 2022). In general, an emulsion polymerization method is commonly adopted for the preparation strategy of porous polymer particles (Gokmen *et al.,* 2012). In general, during the polymerization process, detergents were required for stabilization of emulsion in order to use them as a mold of the particle shape; the detergent molecules were adsorbed at the interface between continuous phase and dispersed phase, the emulsion therefore exists stably in the bulk phase during the polymerization process (Mcchlements *et al.,* 2018). However, there is a concern that detergents themselves may affect the performance of porous polymer particles. Remained detergents retained on the particle may negatively interfere the

characteristics of polymer surface modified with the foreign molecules.

In order to overcome the above-mentioned problem, it is important to establish a "Detergent-free" method for the preparation of porous polymer particles, which enable us to prepare a variety of polymer particles regardless of the polymer characters. Cryogels are a unique porous material that are known to have monolithic supermacroporous (10-100 μm) (Kumari *et al.,* 2017). They are generally produced by polymerization of polymer precursor solution under frozen temperature point of the solvent (i.e. water) (Milakin *et al.,* 2020). During the cryo-polymerization step, a phase separation occurs between solvent crystals and concentrated polymer precursor (i.e. frozen phase and unfrozen liquid micro phase) (Kisebom *et al.,* 2009). As a result, the crystals are deposited as porogen and cryogel forms large porous structures after polymerized and thawing (Kumar *et al.,* 2010). Here, the properties of cryogel can be easily controlled by polymerization condition (e.g. monomer / polymer component, polymerization temperature, amount ratio of monomer and solvent). In addition to the beneficial aspect that various properties of the cryogels are flexibly designed, the shape of cryogel particles are difficult to be controlled without the use of detergent, where the emulsion without any detergent for the cryo-polymerization under frozen temperature becomes unstable, therefore the colloidal coalescence occurs (Xu *et al.,* 2019). There have recently reported the novel preparation method via two-step process for cryogel particle without any detergent, where (1) inverse-Leidenfrost effect and (2) cryo-polymerization method were adopted stepwisely (Takase *et al.,* 2022). The polymer particles at spherical shapes can be easily formed on the liquid nitrogen because the boiling-film coats the surface of the water droplet including polymer precursors and included water droplets contribute to the formation of macro-porous structure in the polymer particle via cryo-polymerization.

In this Chapter, it was investigated the versatility of the two-step preparation method, without detergent, that combines both inverse-Leidenfrost effect and cryo-gelation technique by preparing the macro-porous particles of different kinds of monomers (four vinyl monomers that differ in the structure and physicochemical character) or natural polymer (agarose). Subsequently, the prepared cryogel particles were systematically characterized, focusing on the (i) macroscopic structures (particle shape and size by using CCD camera optical microscope), (ii) microscopic structures (porous

and monolithic structures by using scanning electronic microscope (SEM)), and (iii) mechanical properties (elasticity and shape memory by using the CCD and a piston device). The results obtained were finally compared to discuss the versatility of the proposed methodology.

2. Materials and Methods

2.1. Materials

Acrylamide (AAm), *N,N'*-methylenebisacrylamide (MBA), *N*-isopropylacrylamide (NIPA), ammonium persulfate (APS), *N,N,N',N'*-tetramethlethylenediamine (TEMED), glutaraldehyde solution (25%), gelatin, agarose XP (low melting point ≦ 65 ºC, gelling temperature ≦ 30 ºC), liquid paraffine, acetic acid, ethanol were purchased from Wako Pure Chemical Industry Ltd. (Osaka, Japan) Ultra-pure water (conductivity 18.2MΩcm) was prepared with Direct-Q UV 3 (Merch, Osaka, Japan). Trimethylolpropane trimethacrylate (Trim), benzoyl peroxide (BPO), and ethyl-4-dimethylaminobenzoate (EDMAB) were purchased from Tokyo Chemical Industry Ltd. All materials were used as received without further treatment.

2.2. Protocol of Preparation Method

Briefly, cryogel particles were prepared harnessing the technique reported in our previous research. Cryogel particles were synthesized via a two-step process: (1) preparation of frozen droplets by inverse Leidenfrost effect, (2) cryo-gelation by frozen polymerization. The spherical shape of cryogel particles were formed by inverse Leidenfrost effect. When droplets approached to extremely cold substrate such as liquid nitrogen (-196 ºC), they were coated by boiling-films and formed into the spherical shape frozen droplets.

2.3. Preparation of Cryogel Particles

Our method for the preparation of cryogel particles enables easy design / control of their properties. By combining different types of monomers and cross-linkers, different kinds of monomer or natural polymer (agarose) based cryogel particles were prepared; (a) Acrylamide (AAm), (b) *N*-isopropylacrylamide (NIPA), (c) 2-hydroxyethylmethacrylate (HEMA), (d) trimethylolpropane trimethacrylate (Trim), (e)

agarose. The AAm based cryogel particles were prepared via the process: 20 mmol of AAm and 3.2 mmol *N,N'*-metheylebisacrylamide (MBA) were dissolved in 40 mL of ultra-pure water and degassed with N_2 gas for 15 min. After that, 1 mM of APS and 60 µl of TEMED were added into the solution. Then, the obtained solution was dropped into liquid nitrogen from syringe and prepared frozen droplets contained polymer precursor. With the same operations, the NIPAm based cryogel particles were prepared. 20mmol of NIPAm, 3.2 mmol MBA, 1mM of APS, and 60 µl of TEMED were used. Next, the Trim based cryogel particles were prepared. 29 mmol Trim and 2.4 mmol of MBA were dissolved in 25 mL of acetic acid. After that, 3 mmol of BPO and 2.9 mmol of EDMAB were added into the solution. Then, the obtained solution was dropped into liquid nitrogen from syringe. All different type of frozen droplets were transferred to liquid paraffine (-15 ^{o}C) and started cryo-polymerization overnight.

2.4. Shape of Cryogel Particles

All the different based cryogel particles were observed by optical microscope (BX53, Olympus, Tokyo, Japan); ×4 objective lens and CCD camera. The particles sizes and sphericities were measured from optical microscope images. The sphericity of cryogel particles (S) was defined as following Eq. 3-1.

$$S\,[\%] = r/R \times 100 \qquad \text{Eq. 3-1}$$

where, R and r is represented maximum and minimum diameters of cryogel particles, respectively. The particles sizes are measured from *r*.

2.5. Morphology of Cryogel Particles

The porous structure of cryogel particles was observed by scanning electronic microscope (SEM), operated 20 keV. As pretreatment, all cryogel particles were dried by lyophilization and coated with gold for 30 second by spattering. The surface section and cross section of cryogel particles were observed according to **Fig.3-1**. The porosity of section of the cryogel particle. cryogel particles were calculated from SEM images by using Image J software.

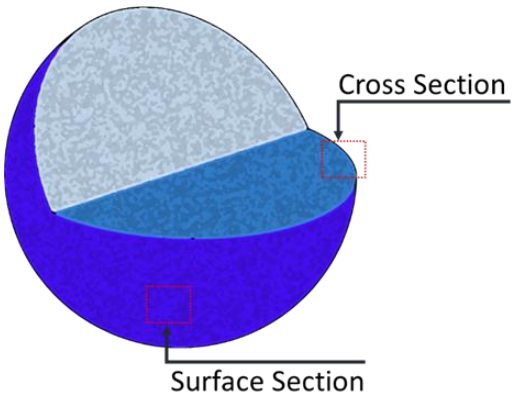

Figure 3-1. Schematic illustration of SEM observation position for surface and cross section

2.6. Mechanical Compression Test

Mechanical properties of cryogel particles were confirmed by mechanical compression-released cycle. As shown in **Fig.3-2**, the experimental setup was setup was performed. The obtained cryogel particle was inserted into a microsyringe (Hamilton, 500μl). Subsequently, the shape of particle in microsyringe was observed by optical microscope with a ×4 objective lens. While the particle in **Fig.3-2** image shows an elliptical shape due to the refraction on the surface of cylindrical shaper of the microsyringe, it is confirmed that the shape of particle is spherical before and after the place the particles in the syringe without compression.

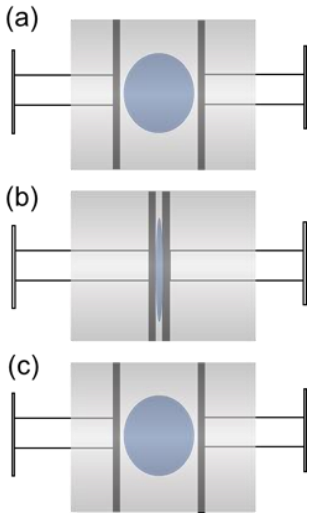

Figure 3-2. Schematic illustration of mechanical compression test for cryogel particles in microsyringe. (a) State of before compression, (b) state of during compression, and (c) state of after compression.

3. Results and Discussion

3.1. Versatility of the Cryogel Particles

The properties of polymer materials are known to be dependent on the type of physicochemical natures of their building block. Hence, the choice of the monomers for the synthetic polymer and cross-linker and natural polymer itself is a key factor to obtain the appropriate materials for their specific application. It was prepared five kinds of cryogel particles by selecting four synthetic polymers with different monomers and a natural polymer as case studies in order to prove versatility of our previous method including the two-step preparation process (Takase *et al.,* 2022). All the experimental conditions and results for the polymer particles were summarized in **Table 3-1**, **Fig.3-3**, and **Figs.3-4**.

3.2. Characterization of Macroscopic Shape and Porous Morphologies

The chemical structures and natures of the monomers and polymers used here were summarized in the top lines (1st to 3rd lines) of **Table 3-1** and **Figs.3-1(a1) - (a5)**. In relation to the synthetic polymers, hydrophilic monomers, such as (a) acrylamide (AAm) and (b) *N*-isopropylacrylamide (NIPA) are used for the polymer particle preparation, where AAm has a primary amide group (-$COONH_2$) and NIPA has an amide group (-CO-NH-) as their branched group. NIPA also has an isopropyl group (-$CH(CH_3)_2$). (c) 2-Hydroxyethylmethacrylate (HEMA) monomer is also selected as a "hydrophilic" monomer that possesses a hydroxyethyl functional group (-CH_2-CH_2-OH), an ester group (-COO-), and an acrylic functional group. (d) Trimethylolpropane trimethacrylate (Trim) is selected because of its "hydrophobic" nature. There are only a few reports on the preparation of hydrophobic cryogels (Chen *et al.,* 2016). Trim has three hydrophobic methacrylic groups that are conjugated with "hydrophobic" and "branched" trimethyl propanyl group in its monomer structure and mechanically tough polymer materials are known to be obtained after its polymerization. (e) Agarose is known as a natural polymer. The chemical structure of a minimal unit of agarose is disaccharide and the unit of alternating 1-4 linked 3,6-anhydro-α-L-galactropyranose and 1,3-linked β-D-galactropyranose is repeated in a polymer (Tripathi *et al.,* 2009). The properties of polymer materials are also varied depending on the type of cross-linking (i.e. chemical

and physical cross-linking). The synthesized polymer of cryogel particles based on AAm, NIPA, HEMA, and Trim were crosslinked with *N,N'*-methylenebisacrylamide (MBA) via chemical crosslinking whereas the cryogel particles of natural polymer, agarose, was crosslinked with gelatin via physical crosslinking. The role of porogen is important to prepare porous materials. During the cryo-polymerization, the frozen region (solvent crystals) and the non-frozen region (concentrated precursor) are formed as a result of the phase separation. The type of the porogen is shown in the 4th line of **Table 3-1**. The solvent such as water and acetic acid used for resolving monomers / natural polymers in an aqueous solution becomes solvent crystals under the frozen condition and act as porogen. Hence, the ice crystals were the porogen of hydrophilic cryogel particles, whereby the acetic acid crystals were one for the preparation of "hydrophobic" cryogel particles.

Physical characters of the polymer particles obtained above were summarized in **Figs.3-3(b1) - (b5)** and **(c1) - (c5)**. The appearance of cryogel particles prepared via our preparation method were observed by using CCD camera as shown in the images (**Figs.3-3 (c1) - (c5)**). All the particles based on different monomer were opaque, implying that cryogel particles have porous structure and the light was scattered (Kisebom *et al.,* 2010). The pAAm, pNIPA, pHEMA, and pTrim cryogel particles were white in color whereas agarose cryogel particles were yellow. Subsequently, the shapes and sizes of cryogel particle was observed by using optical microscope as shown in the images (the 6th line, **Table 3-1**). Average diameters of the particle were around 1600-1800 μm with high sphericities (93.4-96.0 %)(the 7th line, **Table 3-1**). Herewith, only agarose cryogel particles have a relatively large diameter. In this preparation process, the diameter of the particles was dependent on droplets volume (V) and it was calculated from Eq. 3-2.

$$V = \frac{d_0 \pi \sigma}{\rho g} \qquad \text{Eq.3-2}$$

where d_0 is the needle's interior diameter, σ and ρ are represented surface tension and the density of the solution, g is the gravitational force, respectively. Herein, agarose solution during preparation process has high viscosity as compared to other type of monomer solution. As a result, the σ value increases and the V becomes large, resulting in the diameter of the agarose cryogel becoming larger. Moreover, from Eq.3-2,

the diameter of particles is possibly controlled by the needle's interior diameter (data not shown).

Cryogel is known to have a unique porous structure called as "supermacroporous structure" in the range of 10-200 μm pore size. The morphologies were observed by using SEM on surfaces and cross sections of cryogel particles. The obtained images of surface of the polymer particles were summarized in **Figs.3-3 (d1) - (d5)**. It was found that the large pores were distributed on surface section of almost all cryogel particles, except for agarose cryogel particles (**Fig.3-3 (d5)**). Subsequently, the cross section of cryogel particles were also observed by SEM **(Figs.3-3 (e1) - (e5)**), resulting that all the cryogel particles have a supermacroporous structure with high porosity. Interestingly, the porous structure of agarose cryogel particle was found to be different between on its surface and cross section; the surface is smooth with less pores, on the other hand, the porous structure is remained at the interior. The formation of this different porous morphology between surface and internal was due to the high viscosity of the precursor (Tripathi *et al.,* 2009). A shear stress work at the fluid interface (Pourali *et al.,* 2021). During the preparation process, when the polymer precursor droplet was coated with boiling-film of liquid nitrogen by inverse Leidenfrost effect, the shear stress would work at the interface between the droplet and nitrogen gas. As a result, agarose cryogel particles have specific surface texture with smooth appearance. However, there is a limitation for shear stress to reach deep inside of particles due to the high viscosity of the precursor, and the macroporous structure could be maintained at interior. In contrast, the solution of other polymer precursors (i.e. AAm, NIPA, HEMA, Trim) has low viscosity as compared with agarose precursor solution, therefore, these systems would not experience shear stress on the surface of droplet which results in the porous structure to be uniformed throughout the particle.

3.3. Shape-memory Function of Cryogel Particles

The mechanical properties of materials are important factor for application such as separation and purification technologies. Herein, the mechanical property of cryogel particles was investigated with compression and release operation in a microsyringe. The images of "before compression" "during compression", and "after compression" could be

used to discuss the shape-memory properties. The obtained results were summarized in **Fig.3-4**. The cryogel particles of pAAm, pNIPA, and pHEMA were confirmed to show sponge-like elasticity (8^{th} line in **Table 3-1**). After the shape of these particles was deformed during compression, it was restored rapidly after released mechanical force (from **(a)** to **(c)** for each polymer particle in **Fig.3-3**). On the contrary, the hydrophobic cryogel particle of pTrim indicated different mechanical behavior: mechanical compression was not reversible (13^{th} lines). The pTrim cryogel particle was cracked and, after released mechanical force, it was not restored to the original shape. This is possibly because the part of three acrylic groups of Trim could work as cross-linker and, then, high-density polymer wall could be formed, resulting in the mechanical property of the polymer being kept tough. Hence, the decrease of entropic elasticity probably caused by the side groups of the polymer backbone, showing that the particle is revealed to be tough and does not have sponge-like elasticity. This is the first report on the preparation of hydrophobic cryogel particles of pTrim. As shown in **(a5)**, **(b5)** and **(c5)** in **Fig.3-4**, the agarose cryogel particle was found to show an interesting mechanical behavior. Although agarose cryogel particles had elastic property, their mechanical property was different from that of other hydrophilic cryogel particles. The particle was slightly hard as compared with synthetic polymers and, after the release of mechanical compression, it took several minutes to restore the shape (data not shown). Furthermore, the particle was cracked with strong mechanical impact. This property is considered to be caused by the gradient porosity of agarose cryogel particles. Since the surface of agarose cryogel particles does not have well-distributed pores, water diffusion into the inside of the particles is low. Hence, it takes a relatively longer time for the particles to restore their shape after compression. The structure of agarose cryogel particles can be expected to be applicable as functional particles that enable us to control sustain-released materials.

Table 3-1. Summary of experimental conditions of preparation of different polymer particles and their physical characteristics.

Monomer (Cross-linker)	(a) AAm (MBA)	(b) NIPA (MBA)	(c) HEMA (MBA)	(d) Trim (MBA)	(e) Agarose (Gelatin)
1. Name	Acrylamide	*N*-isopropylacrylamide	2-Hydroxyethyl-methacrylate	Trimethylolpropane-trimethacrylate	Agarose
2. Cross-linking	Chemical cross-linking	Chemical cross-linking	Chemical cross-linking	Chemical cross-linking	Physical cross-linking
3. Hydrophilicity	Hydrophilic	Hydrophilic	Hydrophilic	Hydrophobic	Hydrophilic
4. Porogen	Ice crystals	Ice crystals	Ice crystals	Acetic acid crystals	Ice crystals / acetic acid
5. Particle size [μm]	1807.3	1682.8	1490.4	1599.5	2721.5
6. Sphericity [%]	95.2	96.0	92.9	93.4	96.5
7. Porosity [%]	88.4	79.2	82.3	74.3	81.0
8. Elasticity	Positive	Positive	Positive	Negative	Positive

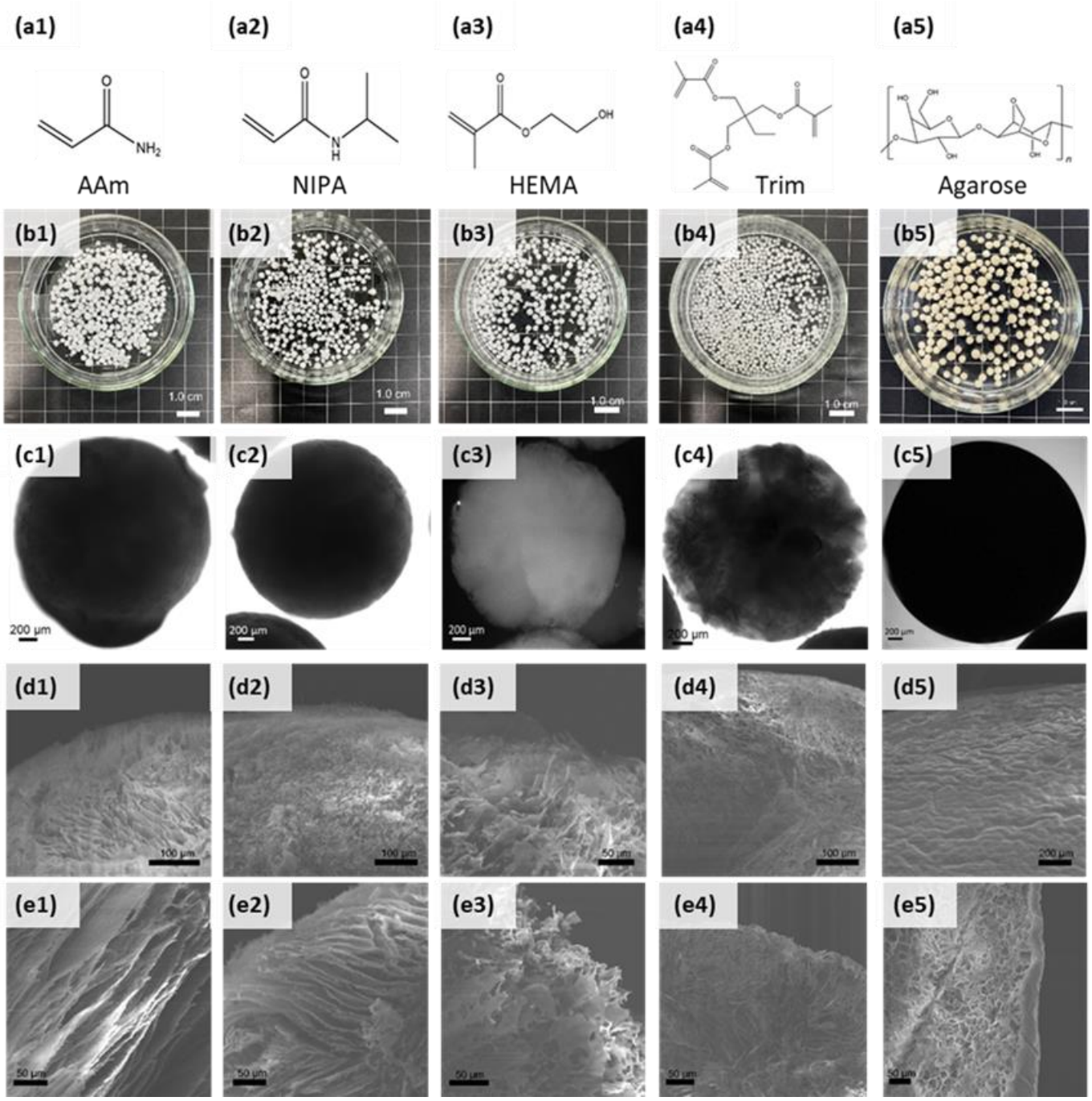

Figure 3-4. Structures of polymer particles obtained by cryo-polymerization combined with inverse-Leidenfrost effect. **(a1)-(a4)**: Chemical Structure of different monomers and **(a5)**: Basal unit structure of Agarose. **(b1)-(b5)**: CCD images of obtained polymers particles. **(c1)-(c5)**: Microscopic images of obtained polymers particles. **(d1)-(d5)**: SEM images of surface section of the polymer particles. **(e1)-(e5)**: SEM images of cross-section of the polymer particles.

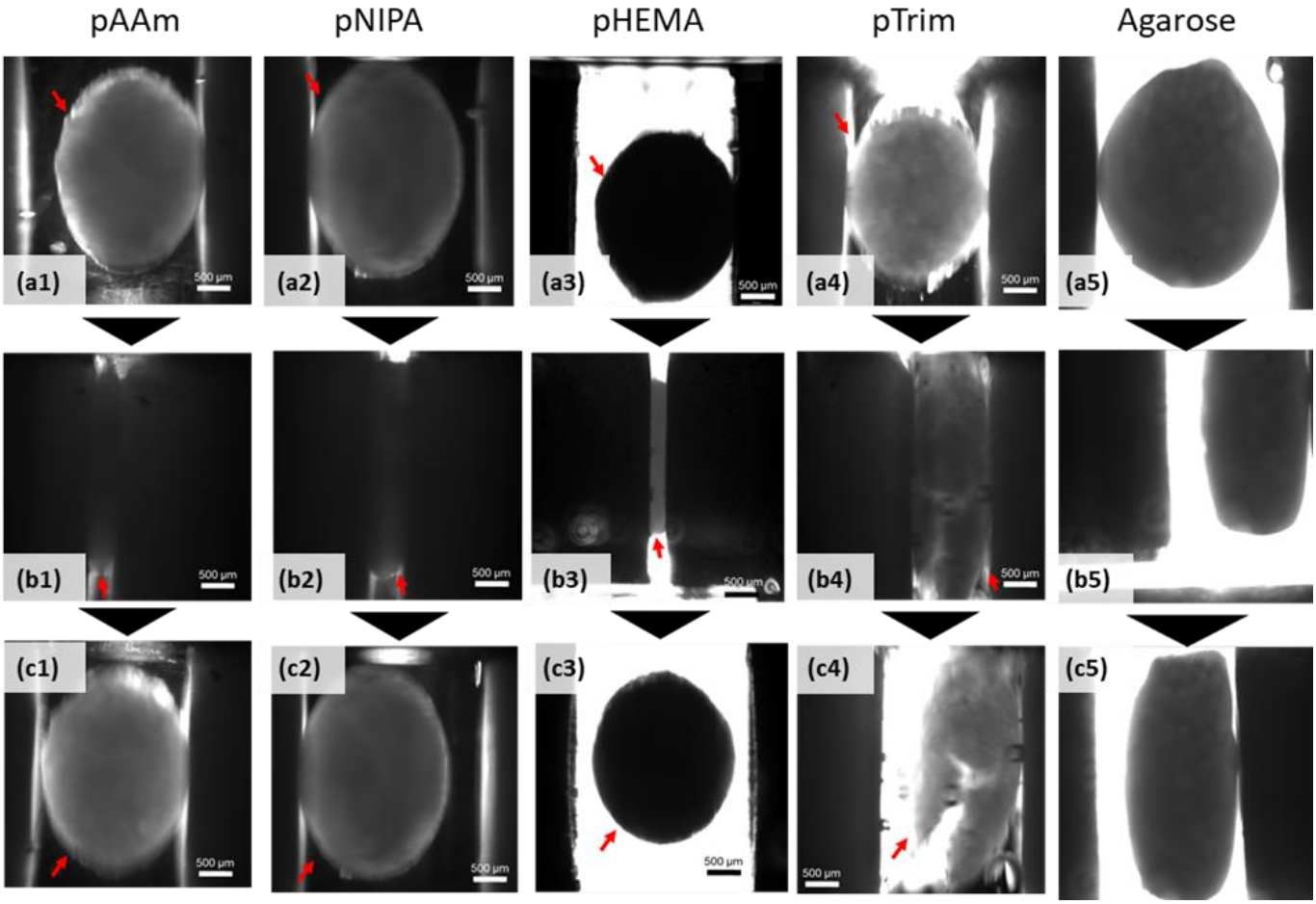

Figure 3-5. Mechanical properties of cryogel particles under compression and release of the polymer particles in microsyringe. Optical microscope images of cryogel particles: before compression **(a1)-(a5)**, during compression **(b1)-(b5)**, and after compression**(c1)-(c5)**.

4. Summary

Five types of cryogel particles, which differ in physicochemical properties of polymers, were successfully prepared by using our previous method, without the use of detergent, that combines the i) inverse Leidenfrost effect method for the preparation of frozen droplets containing precursor and ii) cryo-polymerization method for polymerization under frozen temperature. In all cases of hydrophilic and hydrophobic polymers, spherical polymer particles with macroporous structures were found to be successfully prepared, while there are some slight differences in the detailed characters. The hydrophilic polymer particles prepared, such as pAAm, pNIPA, pHEMA, and agarose, show shape-memory properties, while hydrophobic polymer particles of pTrim does not. As a whole, this method was found to be versatile and could possibly be beneficial for the "*tailor-made*" preparation of porous polymer particles because of no limitation caused by detergents for emulsion formation and could also be applied in chemical engineering (i.e. separation materials) and biomedical engineering (i.e. tissue engineering matrix).

Chapter 4

Characterization of Directional and Bimodal Porous Structural Cryogel Particles

1. Introduction

Polymer particles have attracted notable scientific interest and possess great application (Wu *et al.,* 2022). The development of such as a virtually infinite number of combinations that will play an important role in many application fields such as separation (Yusof *et al.,* 2013), catalysis (Eivgi *et al.,* 2022), sensor (Xu *et al.,* 2013), controlled release carriers (Hussain *et al.,* 2013). In recent years, preparation methodologies of polymer particles are developed in huge number of research. At the design of development for polymer particles, the synthesis of polymer particles process is essential factor with strategy. Here, the synthesis method for polymer particles such as solvent-evaporation method (Kizilbey *et al.,* 2019), emulsion polymerization method (Han *et al.,* 2018), in situ polymerization with Pickering emulsion method (Guan *et al.,* 2020). These methodologies are useful for synthesis of particles with stably produce. Nevertheless, the general methodologies are remained as an inevitable problem in term of versatility with improvement of the method and friendly with environment. Thus, the new preparation method for polymer particles were developed with high versatility by combining inverse Leidenfrost effect and cryo-polymerization technique (iLF Cryo-method). It can be expected that is easy to design and extend the method by controlling and changing synthesis conditions. Therefore, the properties of polymer particles can be design for purpose to application. For examples of the factor of controlling conditions; based monomers and cross-linkers, amounts, polymerization systems, blending, mixing ternary substance, and so on. Consequently, the physicochemical properties and responsive functions are modified to the polymer particles.

The next generation of advanced materials for carrier requires the materials with

unique properties. Cryogel have unique properties such as (a) large pores, (b) high capacity, (c) shape-memory, (d) high swelling degree, and (e) ultrafast swelling. Hence, cryogel is widely utilized in many fields such as bio-separation (Wang *et al.,* 2022), tissue engineering (Shiekh *et al.,* 2018), and delivery of therapeutics (Jensen *et al.,* 2016). Cryogel is synthesized by polymerization under frozen temperature of the solvent. For causing polymerization under frozen temperature (cryo-polymerization), the polymerization systems are required the redox-initiator (APS/TEMD, KPS/TEMED). The polymer precursor including redox-initiator as homogenous system become heterogenous system by temperature being driven force during cryo-polymerization. Because the phase separation cause between concentrated polymer precursor and ice crystals. Thus, the ice crystals are adopted as porogen, cryogel have unique porous structure (i.e. monolithic supermacroporous) by thawing ice crystals after the polymerization (Memic *et al.,* 2019). Therefore, it can be expected that the design of porous properties for cryogel by modification the phase separation process and the generation ice crystals.

Designing hierarchical architectures porous materials is attracting great interest in a variety of technology (Yang *et al.,* 2017). The formation of porous structure can be dependent on porogen species and process of phase separation such as the sol-gel process accompanied by the phase separation (spinodal decomposition) (Rui *et al.,* 2022), temperature induced phase separation (TIPS) (Wang *et al.,* 2021), and polymerization induced phase separation (PIPS) (Li *et al.,* 2000). Various kinds of hierarchical porous structure have been developed by changing process of formation of porogen. Various properties, such as pore size (i.e. micropore, mesopore, macropore, supermicropore), pore shape (i.e. monothic, open-pore, close-pore), and pore type (i.e. monomodal, bimodal, multimodal) are required to be optimized for the suitable material for the application. When the porous particles can be utilized for separation media, these porous properties are directly affected their efficiency in relation to the diffusion kinetics and the specific surface area (Correa *et al.,* 2020; Nguyen *et al.,* 2022).

In this chapter, the hierarchical porous structure with directional and bimodal was designed in the cryogel particles and was characterized in relation to their porous morphologies by using scanning electronic microscope and mercury intrusion

porosimeter. The cryogel particles, which possess unique porous structure with bimodal porous structure consisted of macroporous open-pores and directional monolithic supermacroporous structure, were synthesized by using the expanded iLF cryo-method. The performance as separation carrier was confirmed from macroscopic diffusion test and kinetics of swelling degree.

2. Materials and Methods

2.1 Materials

N-Isopropylacrylamide (NIPA). 2-hydroxyethylmethacrylate (MBA), ammonium persulfate (APS), *N,N,N′,N′*-tetramethylethylenediamine (TEMED), liquid paraffine, *n*-hexane, ethanol, and acetone were purchased from Wako Pure Chemical Industry Ltd. (Osaka, Japan). Ultra-pure water (conductivity 18.2 MΩ cm) was prepared with Direct-Q UV 3 (Merck, Osaka, Japan). All materials were used as received without further treatment.

2.2. Preparation of Hierarchical Porous Cryogel Particles

Briefly, the cryogel particles were prepared by adopting our preparation method (Takase *et al.,* 2022; Takase *et al.,* 2022). At first, the polymer precursor was obtained by mixing monomer and cross-linker, redox-initiator and solvent (i.e. water and acetone) in the flask under ice bath (4 ºC). the polymer precursor was dropped into liquid nitrogen (-196 ºC) to form spherical frozen droplets via inverse Leidenfrost effect. Subsequently, the frozen droplets were transferred to vessel at -15 ºC and keep overnight. During keeping the droplets under -15 ºC, the cryo-polymerization occurs inside the droplets. After that, the cryogel particles were obtained by thawing at room temperature.

2.3. Observation Porous Morphologies

The porous structure of cryogel particles was dependent on the shape and size of the porogen in the preparation steps. Here, the morphologies of the cryogel particles prepared via the iLF Cryo-method (described in chapter 2) were observed by using scanning electronic microscope (SEM, HITACHI). The surface section and cross-section

were characterized from SEM images. As a sample pretreatment, all the cryogel particles were dried with lyophilization and were then coated with gold for 30 seconds by spattering for inhibiting a charge-up the sample from electronic beam. The samples were prepared by using monomodal porous cryogel particles for (1) surface section and (2) cross section and by using bimodal porous cryogel particles for (3) surface section and (4) cross section. For the cross-section image, the particle was cut along the center of gravity of the particles by using a sharp cutter in the preparation of hemisphere samples. For the analysis of porous properties, the porous structure and diameter of cryogel particles were measured by using image J software.

2.4. Macroscopic Observation of Cryogel Particles

The lyophilized both monomodal porous cryogel particle and bimodal one was observed by using optical microscope. At the observation position, the particle image of top view and cross-section was recorded. All the position of cryogel particle was observed by ×4 objective lens.

2.5. Characterization of Porous Properties by using MIP

Mercury intrusion porosimeter (MIP) could evaluate the porous properties of the particles through the analyzed relationship between pressure and intrusion of mercury in the pores. The cryogel particles were outgassed at 80 ºC in a vacuum oven prior to measurements. The pore diameter D of the porous polymer particles was calculated by the Washburn equation (Backer *et al.,* 2016). The D was following Eq. 4-1.

$$D = -\frac{4\gamma cos\Theta}{P} \qquad \text{Eq. 4-1.}$$

where γ represents the surface tension of mercury (0.485 Nm^{-1}), θ represents the contact angle the liquid mercury makes with the solid surface (130 ºC in this study), and P represents the mercury pressure applied, respectively.

2.6. Swelling Ratio of the Cryogel Particles

The prepared cryogel particles via iLF cryo-method were lyophilized for 24h until constant weight was reached. The weight of the dried cryogel particles (W_d) at room

temperature was recorded. The dried cryogel particles were immersed in ultra-pure water at room temperature for a period of the time and taken out. Then, measured the weight of swelling cryogel particles at room temperature. The swelling degree (*SW*) was calculated as shown in Eq. 4-2.

$$SD = \frac{(W_t - W_d)}{W_d} \qquad \text{Eq. 4-2. (Shirbin } et\ al.,\ 2016)$$

where the W_t was represented the swelling weight of cryogel particles at a given time.

2.7. Macroscopic Diffusion Test

The diffusion behavior of water in the directional cryogel particle was confirmed. The dyed ultra-pure water was prepared with dissolving CCB in ultra-pure water as blue color. The 2 μl of dyed ultra-pure water was dropped on upper surface of both the monomodal porous cryogel particle and the bimodal porous cryogel particle. After 1 minute, the particle was cut for half and record as photographic images to observe the diffusion behavior in the pores of cryogel particles.

3. Results and discussion

3.1. Porous Structure of Cryogel Particle

In general, SEM was used to accurately observe the porous structure of cryogel. The morphologies of cryogel particles prepared via iLF cryo-method were observed by using SEM. From the SEM images, some characteristics, such as porous structure, shape and size, were characterized and determined. **Figure 4-1** shows the top view and cross section of the obtained cryogel particles, showing that both monomodal porous cryogel particle and bimodal one was observed. From the overall image of cryogel particle **(Fig.4-1, (a)** and **(e))**, the macroscopic shape of cryogel particles was found to be observed as spherical shape. In addition, the numerous pores were found to be distributed on surface section of cryogel particles **(Fig.4-1, (b)** and **(f))**. The monomodal and bimodal porous particles were observed from the top view of SEM image with high magnification as shown in **Fig.4-1, (b)** and **(f)**. The monolithic porous structure was herewith distributed on the surface without directional. Furthermore, the polymer wall framework that forms the supermacroporous structure was carefully observed, resulting that the porous

structures have different morphologies on the polymer wall between surface section of monomodal porous structure and bimodal one. As shown in **Fig.4-1, (b)**, the polymer wall on its surface was found to show smooth morphologies. Whereas, the macroporous structure in the range of 1-10 μm were distributed in the polymer wall of bimodal porous cryogel particles **(Fig.4-1, (f))**. In addition, the porous shape of macroporous structure on the polymer wall was open-pore morphology. Subsequently, the interior structure of the particle was characterized based on the SEM image of the cross section by observing the cross section of cryogel cut in half. From SEM image of the cross section on the edge region of the particle with low magnification, the directional supermacroporous structures were distributed at the interior of both the monomodal porous cryogel particles and the bimodal one **(Fig.4-1, (c)** and **(g))**. Interestingly, the direction of the supermacroporous structure was formed from the surface to the interior of the particles. In comparison of cross section SEM images of monomodal porous cryogel particles and bimodal one, the directional pores in monomodal porous cryogel particle were more precisely arranged and formed. In the view from cross section with high magnification, the morphologies were different between monomodal porous cryogel particles and bimodal one **(Fig.4-1, (d)** and **(h))**. For bimodal porous cryogel particle, the distributed macropores on surface of polymer walls formed the open-pore shape despite of the surface polymer wall of monomodal porous cryogel particle same as top view SEM image cryogel particle with high magnification. It was thus found that cryogel particle had an anisotropic porous structure and different porous morphologies on the position of observation, such as top view and cross section. In conclusion, porous morphologies of monomodal porous cryogel particles have (i) monolithic supermacroporous structure on top view and (ii) directional porous structure was distributed from surface to interior of the particle. In addition, bimodal porous cryogel particles formed (iii) monolithic supermacroporous structure with macroporous structure as open-pore shape formed on the polymer wall and (iv) directional porous structure was also distributed with the macropores on the polymer wall.

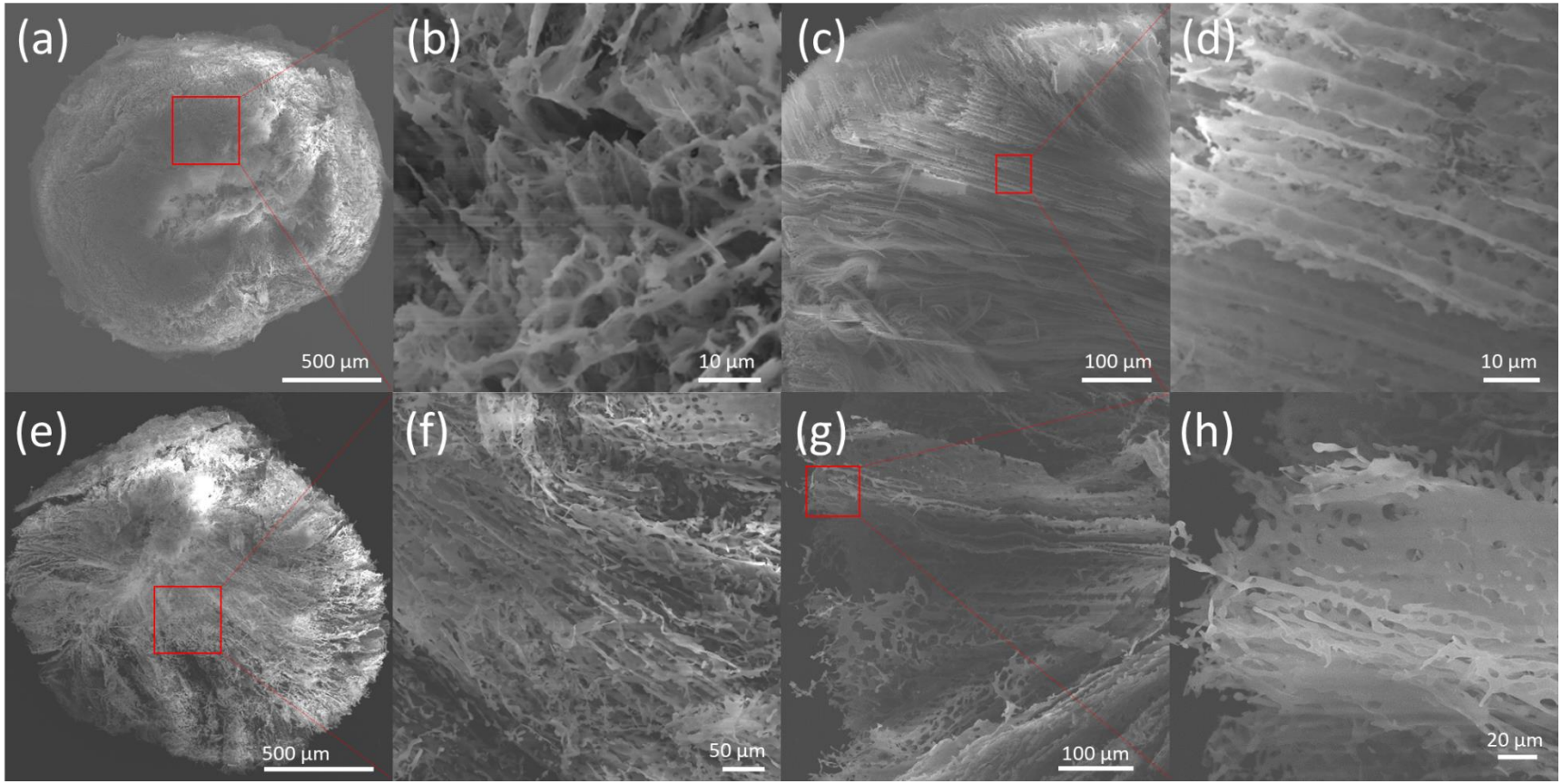

Figure 4-1. Porous structurer of cryogel particles. monomodal porous cryogel particle (a) overall surface section and (b) high magnification, and (c) overall cross-section and (d) high magnification. Bimodal porous cryogel particle (e) overall surface section and (f) high magnification, and (g) overall cross- section and (h) high magnification.

3.2. Characterization of Porous Structure by MIP

Cryogel particles of porous properties were furthermore characterized by using MIP. By adopting the MIP, the porous properties of porous materials can be determined from the relationship between the relative pressure and the amounts of mercury intrusion. **Figure 4-2** shows the MIP-analyzed results on the porous properties of cryogel particles. The cumulative intrusion values to the cryogel particles increased with the increase of the relative pressure around 10 psia **(Fig.4-2, (a))**. In addition, the bimodal porous cryogel particles of cumulative intrusion value was higher than monomodal one. It was shown that the supermacroporous capacity for bimodal cryogel particles was larger than that for monomodal one. Subsequently, the relative pressure curves become to reach a plateau, where mercury could not be intruded into the pores even when the relative pressure was increased. After that, the bimodal porous cryogel particles of the relative pressure was drastically increased and, then, became to reach a plateau, whereas that value for the monomodal porous cryogel particles were kept constant. As the results, the porous structures with different type were formed after the comparison of these particles. Finally, both curves of relative pressure became to reach a plateau and the cumulative intrusion value in the bimodal porous cryogel became twice in contrast to that in the monomodal porous cryogel. As shown in **Fig.4-2, (b)**, the distribution of pore sizes was characterized. For the monomodal porous cryogel particles have pores in the range of 20-100 μm. In the case of bimodal porous cryogel particles, the distribution of pore was splitting to two types in the range of 1-10 μm and 20-100 μm. These results are well corresponding with the results on pore sizes observed from SEM images.

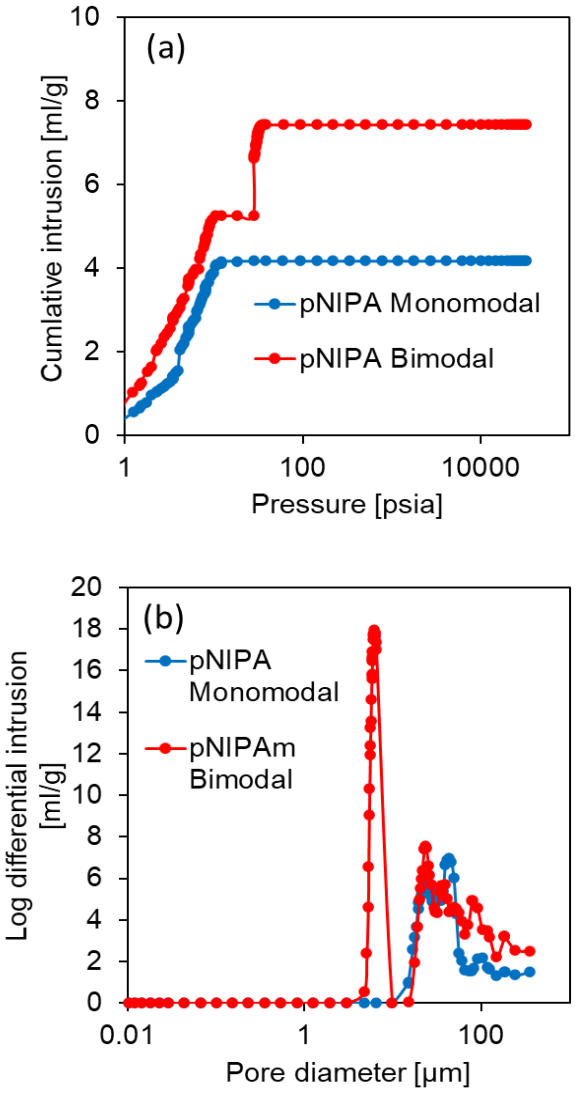

Figure 4-2. Characterization of cryogel particles by mercury intrusion porosimeter (a) mercury intrusion curves and (b) size distribution of porous structure.

3.3. Swelling Kinetics of Cryogel Particles

The swelling kinetics of the cryogel particles, prepared as monomodal porous type and bimodal porous type, were characterized from the weight of dried particles and the swelling particles in given time. As shown in **Fig.4-3**, the swelling kinetic of both cryogel particles was found to elucidate ultrafast swelling behavior. All the dried cryogel particles reached to their equilibrium of swollen state within one minute. This ultrafast swelling behavior resulted from the directional porous structure from outside to interior side of the

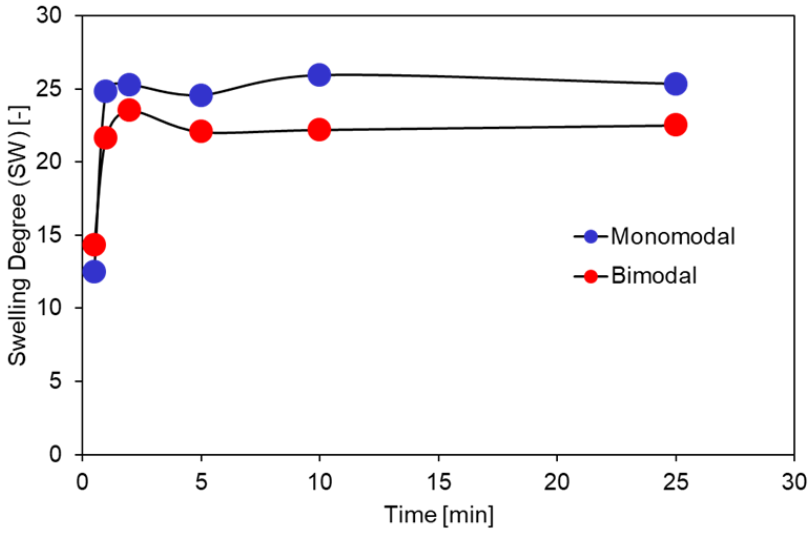

Figure 4-3. Kinetics of swelling degree for monomodal cryogel particles and bimodal cryogel particles. The experiment was measured at 30 ºC.

cryogel particles prepared by using iLF cryo-method. Hence, water molecules could easily diffuse into the interior of the cryogel particles. Here, the results can be emphasized that both monomodal cryogel particles and bimodal one show high swelling degree and ultrafast swelling performance. Because the supermacroporous structure of cryogel particles support high water retention capacity; in other words, high swelling degree and the directional porous structure from surface to interior of the particles improved mass transfer due to easy to diffuse for molecules into the interior from outside.

3.4. Comparison of Macroscopic Diffusion

The macroscopic porous structure and diffusion test was characterized as shown in **Fig.4-4**. The top view side and the interior side of overall cryogel particles was observed from optical microscope images **(Fig.4-4 (a)-(b),** and **(d)-(e))**. From the microscope images, it was obviously confirmed that there is a difference in the morphology of cryogel particles with both monomodal porosity and bimodal one between top view side and interior side. Subsequently, the diffusion behavior was investigated as shown in **Fig.4-4 (c)** and **(f)**. This diffusion test is a further proof of the monomodal and bimodal porous, and the directionality of the porous structure of the obtained cryogel particles. The stained water diffused by itself without any external impetus, so the distribution of the stained

water in the cryogel particles would reflect the pore structure of the samples conveniently. As shown in **Fig.4-4 (c)**, in the case of the monomodal porous cryogel particles, the pores formed parallel to the freezing direction, so the stained water diffused along the directional pores. One fact that should be mentioned is that water could diffuse both in the pores and through the pore walls. However, the diffusion rate in the pores would be much faster than that through the pore walls, especially in the case of cryogel particle with large-interconnected pores. The above phenomena are considered to result in a macroscopically one-dimensional diffusion phenomenon of the stained water in the aligned porous cryogel particle with monomodal porous structure. As shown in **Fig.4-4 (f)**, in the case of the bimodal porous cryogel particles, the stained water diffused in all directions to almost the same distance. As the diffusion steps, firstly the water molecules were diffused into the bimodal porous cryogel particles from bulk through the directional monolithic supermacropores. Then, secondly, the water molecules were diffused into the entire of the particle through the macropore with open-pore shape after diffusion of supermacropores.

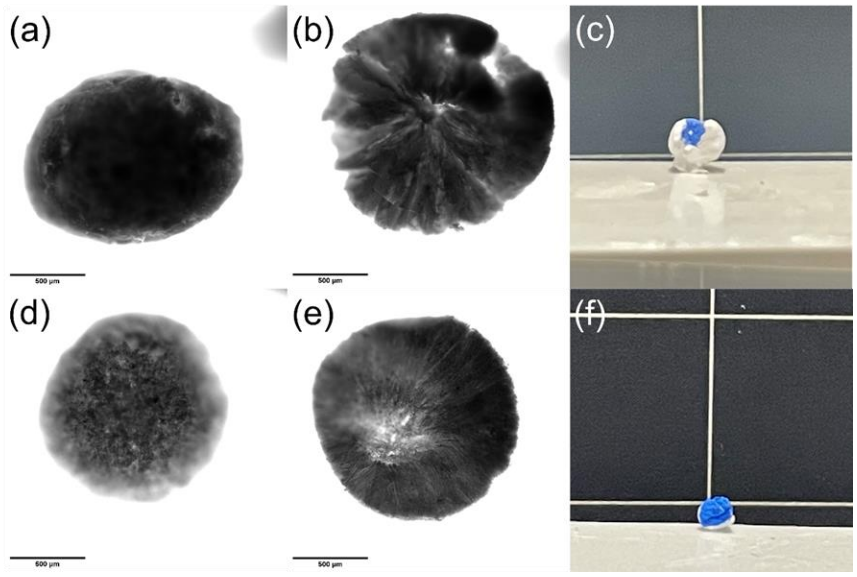

Figure 4-4. Monomodal porous cryogel particles. optical microscope image of (a) top view and (b) cross-section, (c) macroscopic diffusion test. Bimodal porous cryogel particles. optical microscope image of (d) top view and (e) cross-section, and macroscopic diffusion test.

3.5. Scheme of Characterization of Sponge-like Polymer Particles

The properties of polymer particles (i.e, particle size, porosity, porous structure; monomodal and bimodal, elasticity) are important for application of polymer particles. Here, the scheme for characterization of sponge-like polymer particles is described in **Scheme 4.1**. Firstly, since the component of polymer particles is required, the property of polymer is depended on the components. Hence, the polymer precursor such as AAm, HEMA, NIPA, Trim, Agarose is selected as the component. Regarding to the droplet method, the particle size is related with polymer precursor. The viscosity is different with each polymer precursor, therefore the droplet size is decided during dropping. Thus, the polymer particles of D_p is characterized from polymer precursor of droplet size and microscope image of polymer particles. Subsequently, the determination of porosity is required. They are categorized as monomodal and bimodal porous structure in this chapter. In general, the porosity is increased by bimodal porous structure. Subsequently, the shape-memory function is characterized by using mechanical force such as compression and releasing cycle. If the elasticity of polymer particles is low, the direction of scheme should be step-back to select polymer precursor. In contrast, the case of high elasticity, the characterization of sponge-like polymer particles is implemented.

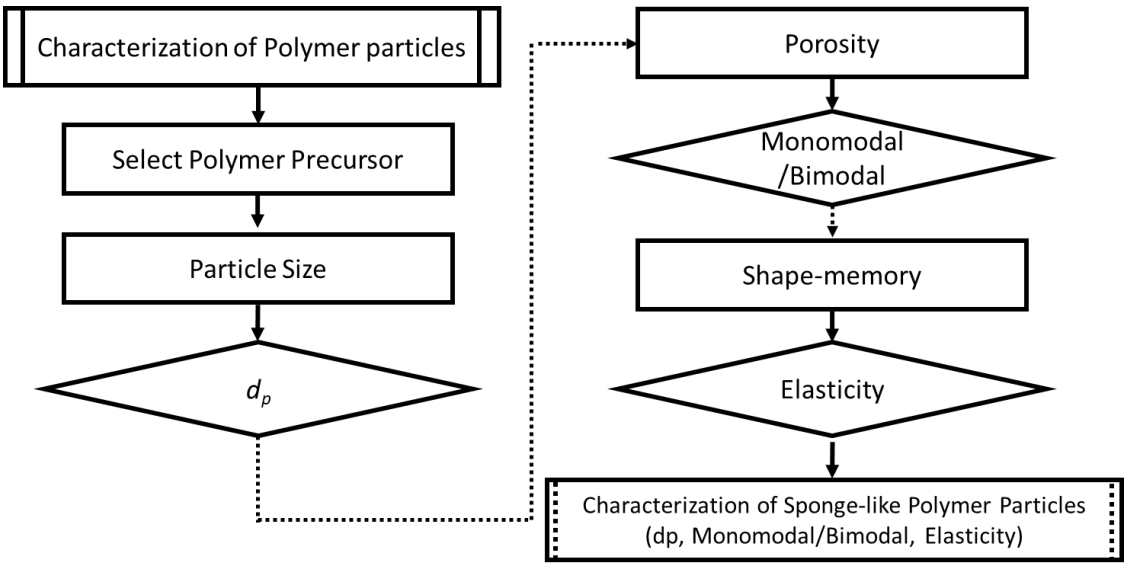

Scheme 4-1. Scheme for characterization of sponge-like polymer particles.

4. Summary

In this chapter, the porous properties relating to the hierarchical porous structure with directional and bimodal were characterized at the interior of the cryogel particles. The porous structures on cryogel particles were here shown to be classified in relation to (i) shape (i.e. monolithic, orientation, and open-pore), (ii) size (i.e. supermicropore and macropore), and (iii) place of distribution pores (i.e. surface side and interior side, polymer wall) and characterized by SEM and MIP. Here, the cryogel particles, which possess unique porous structure with bimodal porous structure consisted of microporous open-pores and directional monolithic supermacroporous structure, were prepared by expanded iLF cryo-method. Following the comparison of porous morphologies between monomodal and bimodal porous cryogel particles, it was revealed that the expanded iLF cryo-method was effectively utilized for designing hierarchical porous structure. In the case of monomodal porous cryogel particle, it has (i) monolithic supermacroporous structure on surface side and (ii) directional porous structure was distributed from surface to interior of the particle. In the case of bimodal porous cryogel particles, it was found that (iii) monolithic supermacroporous structure with microporous structure as open-pore shape formed on the polymer wall and (iv) directional porous structure was also distributed with the macropores on the polymer wall. Subsequently, the performance of cryogel particle was confirmed from macroscopic diffusion test and kinetics of swelling degree. It was found that bimodal porous cryogel particles could be beneficial for the efficient mass transfer to the entire the particle through the pores and could have ultrafast swelling ability. Therefore, the porous designed cryogel particles have potential to application to separation carrier with those porous properties.

Chapter 5

Application of Hydrophobic Cryogel Particles for Separation of O/W Emulsion

1. Introduction

Water pollution caused by oil spill accidents and leakage of industrial wastewater provokes serious environmental problems (Doshi *et al.,* 2018). Most waste oil is dispersed and exists as an emulsion in a heterogenous system due to the removal of the oil taking an effort compared to common immiscible oil solution (Tial *et al.,* 2022). Especially stabilized oil-in-water emulsion with surfactant can be regarded as a semi-equilibrium state with high durability. Thus, the oil-water separation process is important for treating oily wastewater contained in water. In the oil-water separation process, gravity-driven separation, centrifugal precipitation, coagulation, and chemical demulsification are represented (Yu *et al.,* 2016; Cambiella *et al.,* 2006; Kulkarni *et al.,* 2012; Abdularzaq *et al.,* 2022). However, these separation techniques can be restricted because of low-cost effectiveness by complex treatment and high energy consumption (Ammann *et al.,* 2018). Whereas the membrane separation method uses materials with hydrophobicity and physically adsorbs oil, it is a useful method in oil-removing strategies because of its low cost compared to conventional treatment (Goodarzi *et al.,* 2019).

In recent years, cryogel has been applied in a wide range of fields, such as separation, waste-water treatment, biotechnology, and tissue engineering (Baimenov *et al.,* 2022; Guo *et al.,* 2019; Juan *et al.,* 2022; Bencherif *et al.,* 2015). Cryogel is porous material obtained by polymerization of polymer precursor; solution containing monomers, cross-linker, and polymerization initiators, under frozen temperature (cryo-polymerization) (Kirsebom *et al.,* 2009; Memic *et al.,* 2019; Plieva *et al.,* 2008). In the process of cryo-polymerization, a phase separation occurs between the unfrozen region (concentrated monomers) and the frozen one (ice crystals), both inhabited by polymer

precursor (Kumar *et al.,* 2010). The porous structure that can be formed by melting and drying porogen (ice crystals) after cryo-polymerization is referred to as a "supermacroporous structure" in the range of μ-meter scale (Kumar *et al.,* 2010). It is necessary to consider the polymer composition, such as hydrophobic monomer and hydrophilic monomer, and the preparation method according to the purpose of application. Therefore, the hydrophobic cryogel, which prefer oil to water, is useful for the adsorption and separation of organic material from aqueous solutions (Chen *et al.,* 2016).

The monolithic porous structure has a large specific area and high porosity therefore they are applicable as chromatographic separations (Pfaunmiller *et al.,* 2013). Since the monolithic porous structure forms a hierarchically through porous structure with an interconnected network by the polymer wall, the structure supports efficient diffusive mass transfer. Herein, the properties of monolithic porous structure are classified into several parameters. To apply the optimized monolithic porous materials for a specific purpose, characterization of their properties is required. The parameters include: (i) size distribution of particle diameter, (ii) standard deviation of the particle diameter, (iii) coefficient of variation of particle, (iv) bulk density, and (v) size distribution of pore size. It can be attributed that the characterization of these material parameters helps improve and optimize their separation efficiency. Furthermore, the macroscopic shape of the cryogel; (a) cylinder, (b) sheet, (c) disk, and (d) particle is an essential factor in the design of separation devices such as particle packed column chromatography and monolithic column one. The various shape of cryogel (a) cylinder, (b) sheet, and (c) disk can be conventionally prepared by cryo-polymerization in the mold vessel. In contrast, preparation of cryogel for (iv) particle shape may necessitate a technique. By adopting the emulsion polymerization method, cryogel particles can be prepared in a heterogeneous system by cryo-polymerization in the phase which contains polymer precursor (Zhan *et al.,* 2013; Yun *et al.,* 2013). Since the progression of cryogel research has accelerated, various preparation methodologies and polymer components have been developed (Hiramure *et al.,* 2018; Plieva *et al.,* 2006). As a different preparation method, there is a combination technique we recently developed, inverse Leidenfrost effect and cryo-polymerization technique (iLF cryo-method) (Takase *et al.,* 2022; Takase *et al.,* 2022).

In this chapter, the iLF cryo-method was first adopted to create hydrophobic monolithic supermacroporous cryogel particles. The cryogel particles revealed a narrow size distribution of the diameter and numerous pores with monolithic supermacroporous structures. Furthermore, the physical properties, such as hydrophobicity, were characterized by using a dyed solvent. Unlike the aqueous droplet, which was kept on the cryogel particles with repelling properties, the organic droplet was immediately adsorbed into the particles in contact with each other. The cross section of the cryogel particle after adsorption of the organic droplet showed that the entire particle was stained, indicating that the oil diffused into the interior of the particle. For the separation of the oil-in-water emulsions stabilized with surfactants, the cryogel particles successfully removed emulsions from the system.

2. Polymer Surface Modification by Lipid Membrane

In the previous chapters, the method to prepare the polymer particles, focusing on the improvement of the porous characters. The functionalization of the polymer surface is important for the possible use of these polymer particles as "core materials" for the sophisticated bioseparation. Here, the porous polymer materials can be easily functionalized through the coating of their surface by the amphiphilic molecules by considering the method to "deliver" the amphiphiles onto the polymer surface with keeping the "membrane structure".

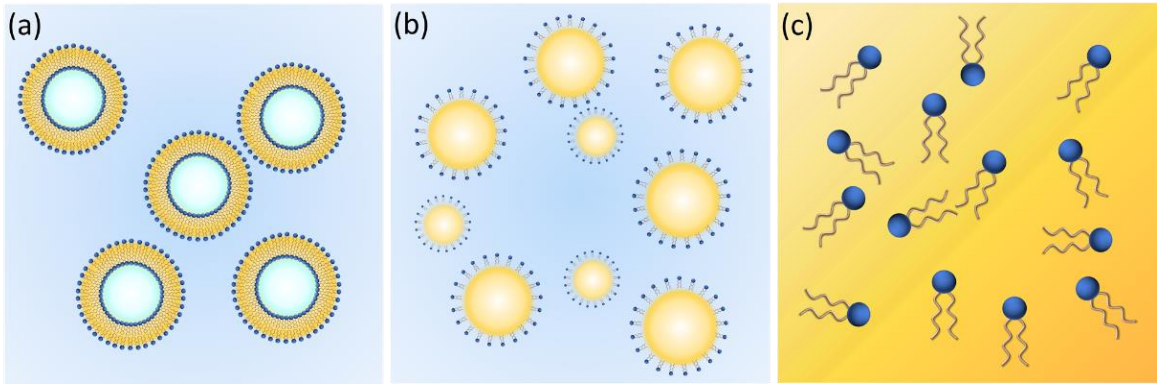

Figure 5-1. The status of lipid molecules for using coating on polymer surface (a) vesicles (b) O/W emulsions, and (c) dispersed molecules.

As shown in **Fig.5-1**, the modification methods for porous polymer particles by lipid membrane are summarized as a general classification of three categories: (1) vesicle fusion method (delivery of amphiphiles-on-vesicle), (2) O/W emulsion method (delivery of amphiphiles-on-emulsion), and (3) lipid impregnation method (delivery of amphiphiles-in-solvent and washout of the excess). In vesicle fusion method, the phospholipids or amphiphiles that formulate the bilayer membrane of vesicle are used for the coating after the vesicle delivery and then, the surface of polymer material can be modified after the vesicle fusion. As shown in **Fig.5-1(1-a)**, vesicles are first injected into an aqueous solution dispersing the polymer material, as shown in **Fig.5-1(1-b)**, the dispersed vesicles are approaching on polymer surface and, then, as shown in **Fig.5-1(1-c)**, the vesicles are ruptured their membrane onto surface of polymer, resulting that the lipid membrane are coated on the polymer surface. In O/W emulsion method, the surfactants or appropriate amphiphiles that are utilized for the stabilization of the emulsions are utilized for the modifiers of the polymer surface. Basic strategy of this method is similar with that of the above vesicle fusion method, where the lipid molecules or amphiphiles are accumulated on the interface of oil-(bulk)water phases when the emulsion dispersed in a bulk aqueous solution as shown in **Fig.5-1(2-a)**. The O/W emulsions dispersed in bulk aqueous solution are delivered and contacted with the surface of polymer materials to adsorb oil phase from the emulsion as shown in **Fig.5-1(2-b)**. During adsorption of the oil, the lipid molecules are transferred from the emulsion onto the polymer surface, resulting that the solid-liquid interface can be modified with lipid molecules and the lipid membrane of the accumulated lipids can be formulated as shown in **Fig.5-1(2-c)**. The final strategy can be called as “lipid impregnation method”, where the lipids are efficiently transferred into the internal parts of the materials because of the porosity (high diffusivity) of the polymer particles. As shown in **Fig.5-1(3-a)**, the porous polymer particles are prepared as carrier and substrate which the lipid molecules are delivered, and a lipid membrane are finally formed. As shown in **Fig.5-1(3-b)**, for the impregnation to the porous polymer particles, the particles are mixed with the solvent solubilizing the target lipid molecules. Subsequently, the solvent is removed and dried with rotary evaporator as shown in **Fig.5-1(1-c)**. The lipid molecules used for the impregnation are entirely transferred onto all the surface of the porous polymer particles

because of solvent. After the solvent evaporation, the lipid molecules are accumulated on the surface of the polymer wall. When the impregnated porous polymer particles are hydrated, the lipid membrane spontaneously form the membrane structure on the polymer wall. These methodologies for modification polymer surface with lipid membrane are useful technique for the functionalization of the polymer. Since each method has advantage/disadvantage, it is necessary to select the most appropriate method depending on the purpose and experiment condition, considering the characters of polymer materials and the amphiphilic molecules.

3. Materials and Methods [O/W Emulsion Method]

3.1. Materials

Trimethylolpropane trimethacrylate (Trim), benzoyl peroxide (BPO), etlyl-4-dimethylaminobenzoate (EDMAB), and nile red were purchased from Tokyo Chemical Industry Ltd. Acetic acid, toluene, n-hexane, *N,N'*-dimethylmethacrylate (MBA), liquid paraffine, sudan (IV), Coomassie brilliant blue G-250 (CBB), and polyoxyethylene sorbitan monooleate (Tween 80) were purchased from Wako Pure Chemical Industry Ltd. (Osaka, Japan). Ultra-pure water (conductive 18.2MΩ•cm) from a Merck Millipore. All materials were used as received without further treatment.

3.2. Preparation of Hydrophobic Cryogel Particles

The hydrophobic cryogel particles were prepared as described in previous works. Briefly, the cryogel particles were prepared via 2 step process: 1) preparation of frozen droplets by utilizing iLF effect and 2) cryo-polymerization under frozen temperature. Trim used as monomer and MBA used as cross-linker were dissolved in acetic acid. Then, BPO and EDMAB were added as initiators and obtained polymer precursor. Subsequently, the obtained polymer precursor was dropped onto liquid nitrogen and prepared frozen droplets. These droplets were transferred to liquid paraffine at -15 ^{o}C and polymerized overnight. After cryo-polymerization, hydrophobic cryogel particles were washed with n-hexane and lyophilized.

3.3. Observation of Macroscopic Shape

The overall cryogel particles in the bottle of glass were observed as photographic

images by a charge-coupled device (CCD, iPhone 12 MJNJ3J/A) camera. In order to evaluate the size distribution of particles, the diameter of particles was measured from optical microscope images. The mean diameter of the particles (D_v) and standard deviation (σ) were calculated from the optical microscope images by using image J software. Furthermore, the coefficient of variation (C_v) was calculated as according to Eq.5-1.

$$C_v = \frac{\sigma}{D_v} \times 100\ [\%] \qquad \text{Eq.5-1.}$$

Here, the tapped bulk density (ρ_{bulk}) was calculated according to Eq.5-2.

$$\rho_{bulk} = \frac{W_{particles}}{V_{cylinder}}\ [\text{g/ml}] \qquad \text{Eq.5-2}$$

The $W_{particles}$ and $V_{cylinder}$ were represented as the weight of the particles and the volume of the particles in the graduated cylinder, respectively. The scale of the graduated cylinder with particles was read after tapping 100 times (Nayk *et al.,* 2011).

3.4. Characterization of Porous Properties

The cryogel particle of porous structure on the surface was observed by scanning electronic microscope (Hitachi, SU3500, Japan, SEM), operated at 20 keV. As pretreatment, gold was coated on cryogel for 30 seconds by spattering. The pore diameters were measured according to **Fig.5-2** and the size distribution was analyzed by using image J software.

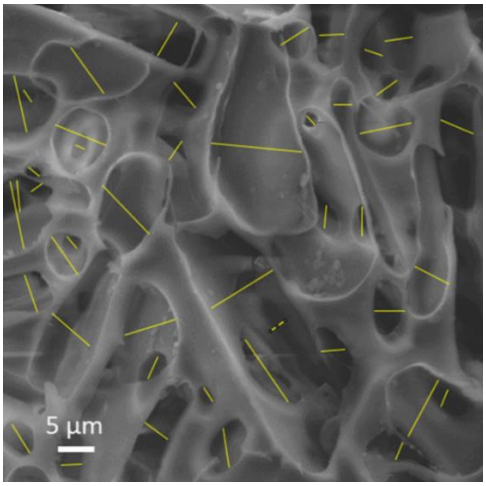

Figure 5-2. The analysis of pore diameters on the surface of cryogel particles.

3.5. Testing Hydrophobicity of Cryogel Particles

The hydrophobicity of cryogel particles was tested by using aqueous and organic droplets. The water was dyed with CBB as a blue-colored aqueous solution, and the toluene was dyed with Nile red as a red-colored organic solution, respectively. Then, the droplet placed on the cryogel particles was observed. Subsequently, the adsorption behavior of organic solvent by cryogel particles was investigated. The organic solution dyed as red was floated into the water and the cryogel particles were added to the water. A CCD camera was used to record the adsorption behavior over time three and ten seconds after the particle was added. Furthermore, the cryogel particle was cut in half after being adsorbed with the dyed organic solution and the cross-section was observed.

3.6. Separation of Stabilized Oil-in-Water Emulsion

The oil-in-water emulsion stabilized with surfactant was prepared by mixing 990 µL of n-hexane, 100 mg of Tween 80, and 99 mL of ultra-pure water under ultrasonication. The characterization of the emulsion after separation was recorded with photograph and the optical microscope image. To investigate the separation of stabilized oil-in-water emulsion by cryogel particles, the organic phase of the emulsion was dyed with Sudan IV during the preparation of oil-in-water emulsion (Wang *et al.,* 2015). Then, the emulsion was separated by mixing the emulsion and cryogel particles in the glass bottle and kept for 3h at room temperature. After that, the particles were removed from the solution by filter, and measured the UV-Vis spectra by spectrophotometer (Shimadzu UV-1800,

Kyoto, Japan).

3.7. Materials [Lipid-Impregnation Method]

DPPC was purchased from Avanti Polar Lipids, Inc. (Alabaster, AL, USA). Monomeric divinylbenzene (DVB) was purchased from Wako Pure Chemical Industries, Ltd. (Osaka, Japan). The DVB was washed with a 10 wt% NaOH aqueous solution to remove the polymerization inhibitor. 6-Lauroyl-2-dimethylaminonaphthalene (Laurdan) and other chemicals were also purchased from Wako Pure Chemical Industries, Ltd. (Osaka, Japan) and were used as received.

3.8. Preparation of PPP Coated with Phospholipid

Briefly, PPPs were prepared from a water-in-oil-in-water (W/O/W) emulsion by *in situ* polymerization (Inda *et al.,* 2017). The DVB monomer dissolved in the oil phase forms the polymer framework. The obtained PPPs and DPPC dissolved in chloroform and methanol solution (volume ratio of 2:1) were mixed in a round-bottom flask and dried using a rotary evaporator under vacuum to remove the solvent mixture. This procedure was repeated three times, and the phospholipid was impregnated in PPPs and kept under a high vacuum for at least 3 h to obtain DPPC-coated PPPs (DPPC-PPPs).

3.9. Characterization of PPPs Coated with Phospholipid

The surface and cross section of the DPPC-PPPs were observed using a scanning electron microscope (Hitachi, SU3500, Japan). The distribution of phosphorus atoms at the surface and cross section was confirmed by elemental mapping using EDX (AMETEK, USA). All samples were dried under vacuum prior to observation.

3.10. Evaluation of the Phospholipid Impregnated on the Particles

The DPPC-PPPs prepared with different amounts of phospholipids were evaluated by inductively coupled plasma (ICP) atomic emission spectroscopy (ICP-AES, Shimadzu ICPS-8100, Japan) to determine the amount of phospholipid deposited on the PPPs. The prepared DPPC-PPPs were decomposed using a digestion apparatus (Hack, Digesdahl Digestion Apparatus Models 23130-20, USA). To decompose DPPC-PPPs to a solution, they were mixed with concentrated sulfuric acid and hydrogen peroxide in a Digesdahl

digestion flask and heated to 440 °C. After complete decomposition of the particles in the flask, the solutions were cooled to room temperature and diluted with distilled water. In addition, the obtained solutions were analyzed using ICP-AES. The amount of phospholipids deposited on the PPP was determined according to the following Eq. 6-1.

$$E_{DPPC} = \frac{C_p}{Mw_P} \times \frac{V}{W_{PPP}} \quad \text{[mmol-lipids/g-PPP]} \qquad \text{Eq.6-1}$$

where E_{DPPC} is the entrapped amount of DPPC in PPP, C_P is the phosphorus concentration, V is the volume of the solution, $M\mathrm{w}_p$ is the molecular weight of phosphorus, and W_{PPP} is the weight of the porous polymer particles.

4. Results and Discussion

4.1. O/W Modification Method [Aqueous Solution]

4.1.1. Macroscopic Shape of pTrim Cryogel Particles

The pTrim cryogel particles were prepared by combining the inverse Leidenfrost effect and cryo-polymerization technique (iLF cryo-method) (Takase *et al.,* 2022; Takase *et al et al.,* 2022). By adding the water droplets containing polymer precursor into an extremely low temperature bath, inverse Leidenfrost phenomenon was induced and frozen droplets with spherical shape were formed on the liquid nitrogen. The frozen droplet was then polymerized under frozen temperature (-15°C). After cryo-polymerization, the pTrim cryogel particles were obtained by thawing and lyophilization. **Figure 5-3** shows the photo image of pTrim cryogel particles **(Fig.5-3 (a))** and the size distribution of the particles through the observation of optical microscope **(Fig.5-3(b))**. As shown in **Fig.5-3(a),** the pTrim cryogel particles had a spherical shape with white color. Subsequently, after the diameter of more than 200 individual particles was observed from the optical microscopic images, the size distribution was then determined. **Figure 5-3(b)** shows the size distribution of pTrim cryogel particles. As a result, the pTrim cryogel particle, prepared by our iLF-cryo method, was distributed in the range of 700-

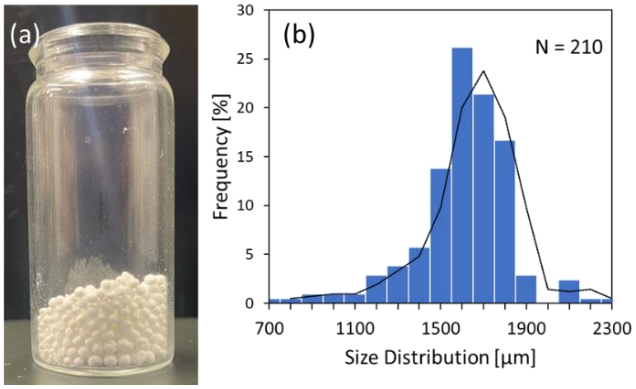

Figure 5-3. Macroscopic shape of pTrim cryogel particles (a) appearance and (b) size distribution of particle diameter.

2300 µm and have high frequency of around 1600 µm. Herein, the basic properties of pTrim cryogel particles were summarized in **Table 5-1**; the value of the mean diameter, D_v, and its standard deviation, σ, were 1654 µm and 220 µm, respectively. Furthermore, the variation coefficient, C_v, was shown to indicate a low value at 13 %. Hence, pTrim cryogel particles were found to exceed in relation to narrow size distribution and the high monodispersiblitiy in comparison with that of the conventional droplet (Merakchi *et al.,* 2019). The tapped bulk density, ρ_{bulk}, was calculated from bulk particle volume in a graduated cylinder and the weight of the particle, resulting that the ρ_{bulk} value was 0.3 g/ml. Comprehensively, macroscopic properties of pTrim cryogel particles adopted by the iLF cryo-method were characterized based on these factors D_v, σ, C_v, and ρ_{bulk}.

Table 5-1. Particle Properties of pTrim Cryogel Particles

D_V [a][µm]	σ^b [-]	C_v^c [%]	ρ_{bulk}^d [g/ml]
1654	220	13	0.3

[a] Mean diameter of the particles, [b] Stand deviation, [c] Coefficient of variation, and [d] bulk density.

4.1.2. Characterization of Porous Properties

In general, cryogel have monolithic porous structure with supermacropores in the range of µ-meter scale. During the cryo-polymerization process, the crystals supplied from the solvent (i.e. acetic acid) were employed as porogen; the porous structure was

therefore formed. As shown in **Fig.5-4**, the porous structure of the surface pTrim cryogel particle was observed via SEM analysis. The observations were performed for the surface section of pTrim cryogel particle as described in **Fig.5-4(a).** From the overall image, the particles were found to have a rough surface **(Fig.5-4(b))**. Subsequently, the surface section of the particle was observed from high magnification SEM image to characterize its porous structure **(Fig.5-4(c))**. It was found that the pTrim cryogel particle had a monolithic supermacroporous structure on its surface. Interestingly, the polymer wall of the porous structure appeared to have a smooth surface. The fine morphology of porous structure (i.e. surface roughness, undulation) is changed by employing different porogen (Kirsebom *et al.,* 2011).

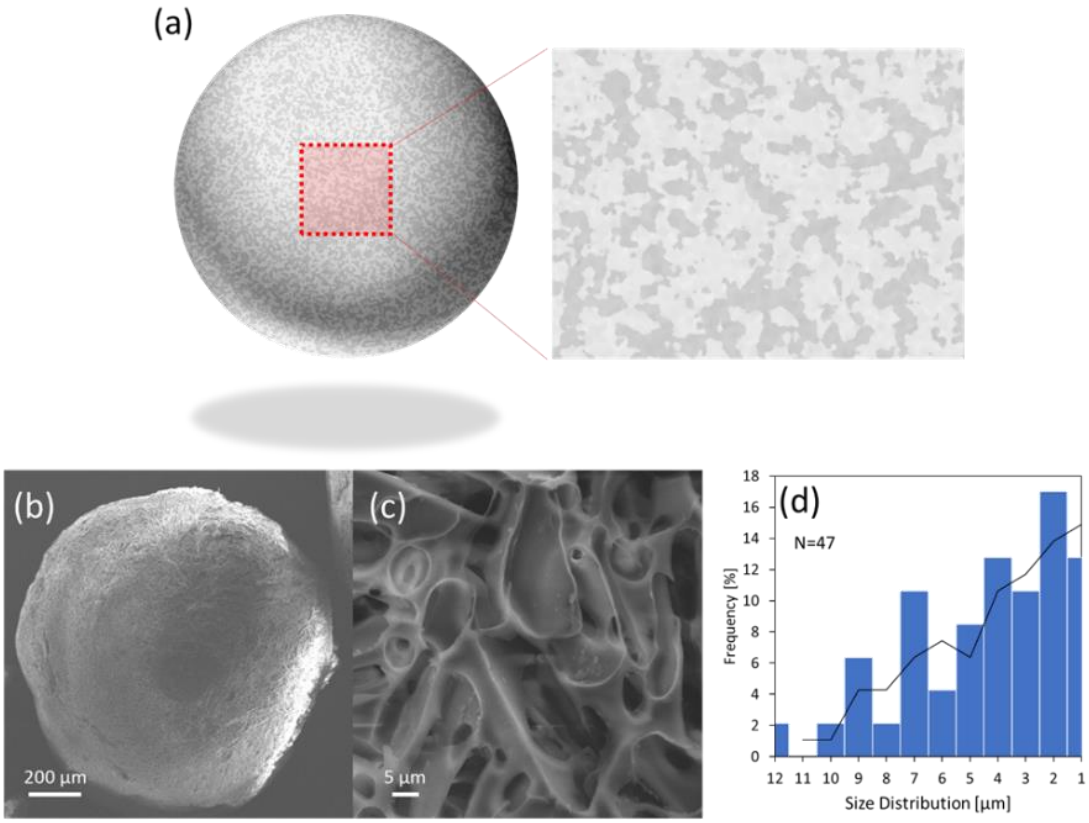

Figure 5-4. Characterization porous structure of pTrim cryogel particle. (a) schematic illustration of the morphological observation overall particle and a surface section of high magnification. (b) overall particle SEM image and (c) surface section at high magnification. (d) size distribution of pores diameter.

Herein, the pore diameter was measured from the number of 47 pore diameters by high magnification SEM image **(Fig.5-2)** to characterize the porous property. As shown in **Fig.5-4(d)**, the size distribution of porous diameter was evaluated. The porous diameters were distributed in the range of 1-12 μm, and the mean porous diameter d_p was 4.7 μm. The results suggest that pTrim cryogel particles have a unique porous structure on their surface which is monolithic with supermacroporous structure.

4.1.3. Hydrophobicity of pTrim Cryogel Particles

The hydrophobicity of polymer particles can be investigated by confirming the behavior of aqueous or organic droplets when they are contacting the polymer particles. When the aqueous droplet is placed on the hydrophilic polymer, the droplet penetrates the hydrophilic polymer, while the organic droplet is repelled. In the case of hydrophobic polymer, where the aqueous droplet is repelled, and the organic droplet is penetrating the hydrophobic polymer. As shown in **Fig.5-5**, the hydrophobicity of pTrim cryogel particles was investigated, where the behavior of droplets; aqueous solution (dyed as blue) and organic solvent (dyed as red) was placed on the pTrim cryogel particles **(Fig.5-5(a))**. As a result, the aqueous droplet was repelled onto the pTrim cryogel particles, whereas the organic droplet penetrated the particles. The cryogel particles herewith consist of pTrim and have a hydrophobic surface. Subsequently, the adsorption of organic solvent in the oil-water system by pTrim cryogel particles was examined in **Fig.5-5(b)** and **(c)**. The red dyed organic solvent was distributed in water in the beaker, and the cryogel particles were added. As shown in **Fig.5-5(b)**, three seconds after the addition of the particles, the particles were floated on the liquid surface, resulting in aggregate formation. Furthermore, the particles rapidly started to adsorb the dyed organic solvent. Eventually, the particles were found to adsorb all organic solvents in the beaker after only 10 sec **(Fig.5-5(c))**. After the adsorption of organic solvent, pTrim cryogel particle was cut in half, and the appearance of cross section was observed **(Fig.5-4(d))**. It was confirmed that the pTrim cryogel particle was colored red including the interior side from the image of the cross section. Hence, the adsorbed organic solvent was diffused till the interior of the particle. It is expected that the porous structure of pTrim cryogel particle has internal through porous and monolithic structure. These results are supported by the evidence that the monolithic porous structure was formed in pTrim cryogel particle (**Fig.5-4)**. The pTrim

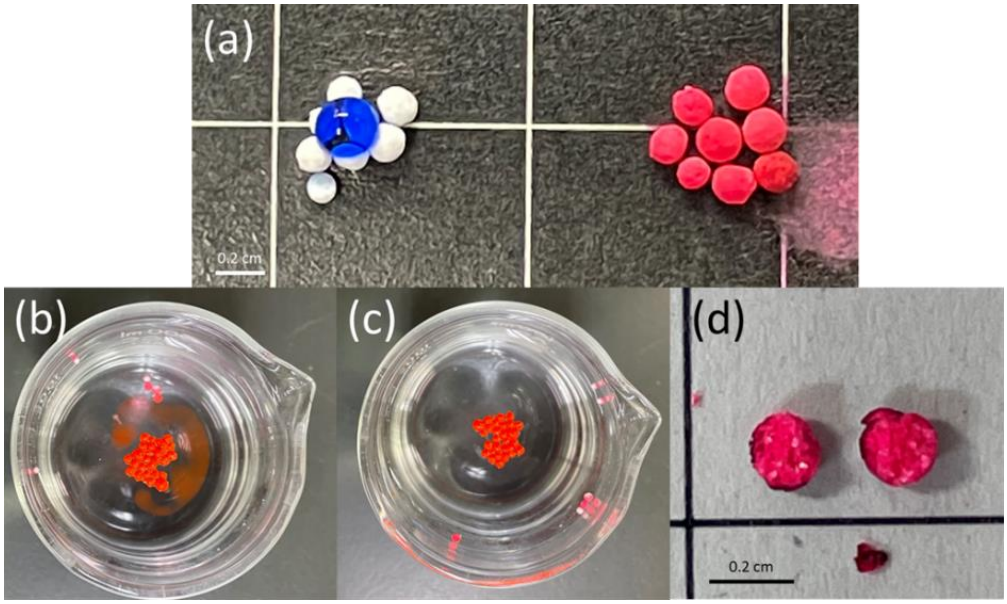

Fig.5-5. Hydrophobicity of pTrim cryogel particles (a) left; aqueous droplet on the particles, right; organic droplet on the particles. The adsorption of organic solvent from water by pTrim cryogel particles (b) 3 sec and (c) 10 sec. (d) appearance cross section of the particle after adsorption organic solvent.

cryogel particles were thus shown to have a potential to be applied as separation material because of their substance permeability function with the internal through monolithic porous structure.

4.1.4. Surface Modification by Stabilized Oil-in-water Emulsion

Based on the characteristics of pTrim cryogel and its fundamental properties, the possibility to recover the oil-in-water emulsion from the aqueous solution. Typically, the oil-in-water emulsion can be formed by dispersing and stirring a small amount of oil in water. The formed oil-in-water emulsion is unstable in long-term and becomes a two-phase system which is thermodynamically stable state. However, via adsorption of surfactant on the interface, the emulsion is stabilized and exists long-term in heterogeneous system. It is difficult to remove organic solvent from the stabilized emulsion because the emulsion does not spontaneously cause phase separation. Herein, the separation of stabilized oil-in-water emulsion with surfactant was performed by using pTrim cryogel particles as shown in **Fig.5-6**. The emulsions were observed in bulk-scale

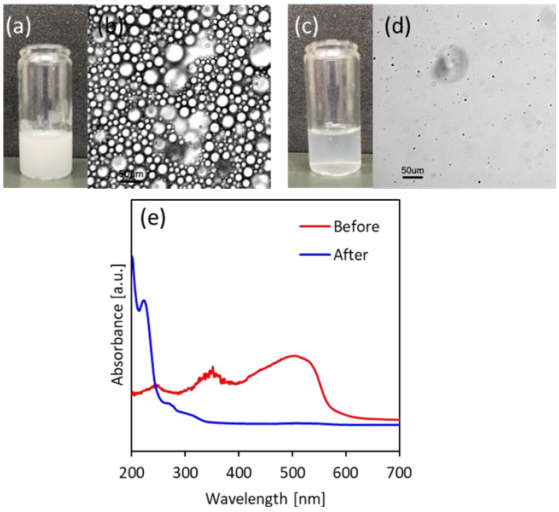

Fig.5-6. Separation of stabilized emulsion by using pTrim cryogel particles. Before separation of (a) photograph of the emulsion in bulk scale and (b) optical microscope image, and after separation of (c) photograph of the emulsion in bulk scale and (d) optical microscope image. (e) UV-vis spectra of emulsion.

image and optical microscope image before separation, and in bulk-scale image and optical one after separation **(Fig.5-6 (a)-(d))**. From bulk-scale images **(Fig.5-6 (c)** and **(d))**, the solution was deeply cloudy in white before the addition of the cryogel particles while the solution became transparent after that. The color change of these solutions indicates that the organic solvent was dispersed and became heterogeneous system as a colloidal state (before the addition of cryogel particles) and then the colloid was removed (after the particle addition). As shown in **Fig.5-6 (b)** and **(c)**, the states of solution were observed by using an optical microscope, the emulsions with several μ-meter scales were dispersed in the solution (before the particle addition), and then there was no colloidal emulsion (after the particle addition). It is possible that the slight turbidity of the solution after the particle addition could be caused by dispersed microemulsions that could not be observed with optical microscope. Subsequently, the separation property of pTrim cryogel particles was evaluated from UV-Vis spectra of the emulsion in which the organic phase was dyed with probe **(Fig.5-6 (e))**. In the spectrum before the particle addition, the characteristic absorbance peak derived from the dye dissolved in the organic phase was detected. On the contrary, there was no absorbance peak in the spectra in the supernatant after the particle addition. The separation was induced simply by adding the cryogel

particles with macroporous and hydrophobic nature through the interaction between the hydrophobicity of pTrim and the organic solvent as colloidal state dispersed in the solution. As a result, the separation of stabilized oil-in-water emulsion with surfactant has been demonstrated.

4.2. Lipid Impregnation Method [Organic/Aqueous Solution]

4.2.1. Observation of Phospholipid-Impregnated the Particles

The structure of the phospholipid-impregnated PPPs (DPPC-PPPs) was observed by scanning electron microscopy (SEM), and the distribution of phosphorus atoms in DPPC-PPPs was clarified by elemental mapping using EDX (**Fig.5-7**). SEM observations were performed for the surface and cross-sections (**Fig.5-7a**). The overall morphology of DPPC-PPPs was spherical with a sphere diameter of approximately 200 μm (**Fig.5-7b**). On the surface and in the cross section, rough pores (diameter of approximately 20 μm) were homogeneously distributed. The pores could be constructed by the cross linking of DVB during *in situ* W/O/W emulsion polymerization (Gokmen *et al* 2012; Sitoh *et al.,* 2006; Li *et al.,* 2014; Kitabayashi *et al*; 2013; Matushita *et al.,* 2011). The large specific surface area of PPPs was utilized for the deposition of DPPC molecules. Considering that numerous pores were distributed from the surface to the inside of the particles, it is expected that mass transfer (or molecular diffusion) from the outside to the inside was promoted. Notably, the surface and cross-sectional structures of bare PPPs (without phospholipid impregnation) were almost the same as those of the DPPC-PPPs. It is suggested that the phospholipid impregnation of PPPs has a negligible influence on the material structure itself.

The surface and cross section of the DPPC-PPPs were analyzed by elemental mapping using EDX (**Figs.5-7d** and **5-7e**). The results indicated that phosphorus, derived from phospholipids, was distributed on the surface and cross section of PPPs, revealing that phospholipid molecules diffused into the inner pores of PPPs during the impregnation process, and were successfully deposited onto the PPPs after solvent evaporation. It has been reported that amphiphiles, that is, trioctylamine and polyoxyethylene-type nonionic surfactants, were successfully impregnated on polystyrene–DVB porous resin (Saitoh *et al.,* 2012; Shiomori *et al.,* 2005. It is suggested that the hydrophobic framework of the polymer could be suitable for the impregnation of hydrophobic molecules.

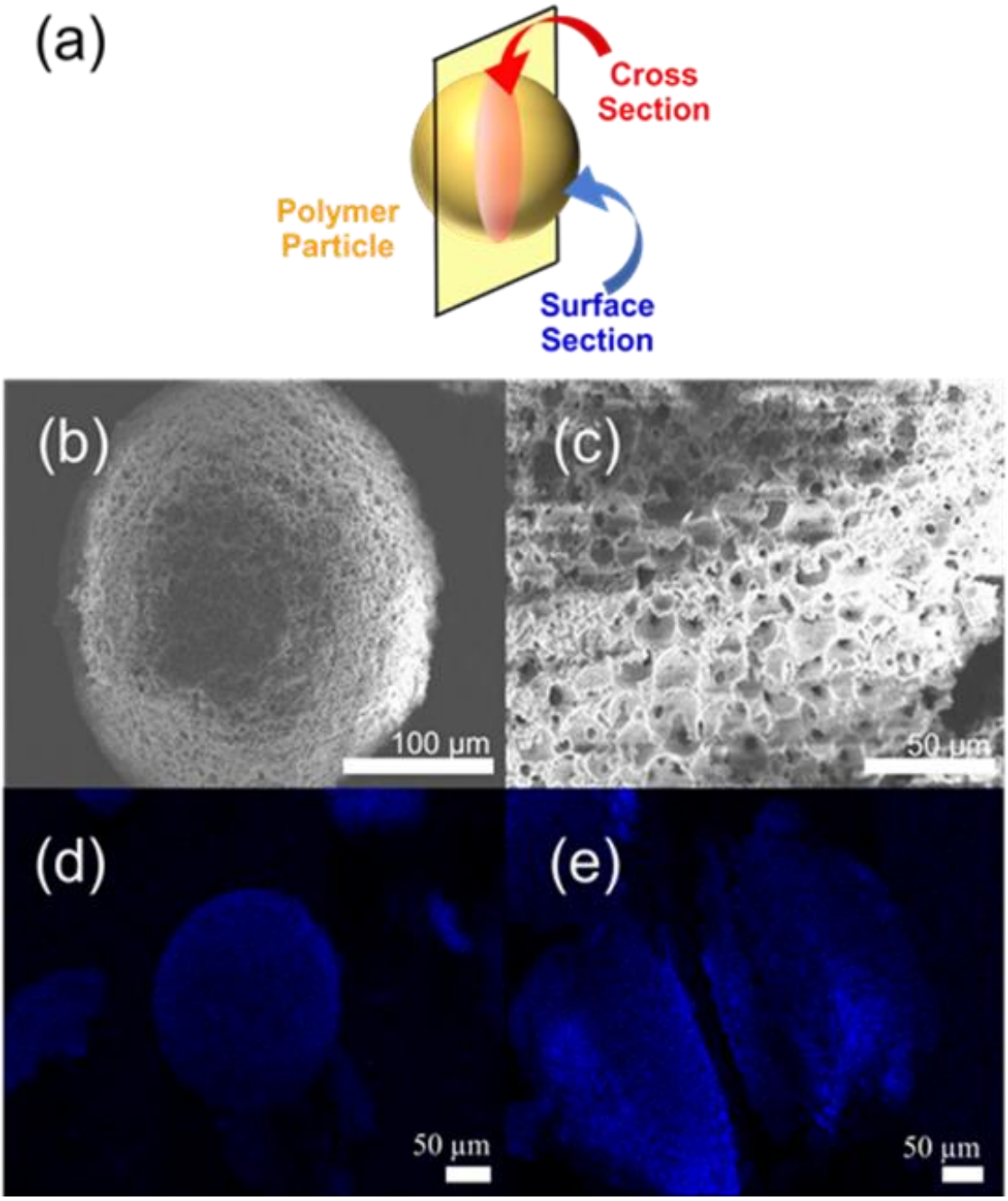

Figure 5-7 SEM-EDX analyses of DPPC impregnated on porous polymer particles. (a) Illustration of DPPC-PPPs and morphological observation by SEM images DPPC impregnated on PPP. (b) Surface section image and (c) cross section image. The distribution of phosphorus element derived from DPPC in (d) surface section and in (e) cross section were confirmed by the element mapping using EDX.

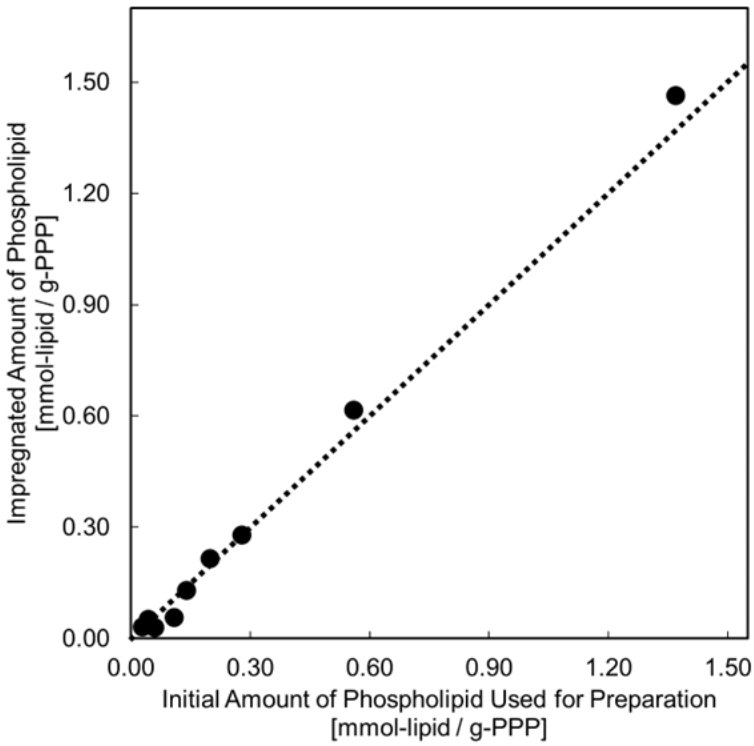

Figure 5-8 Relationship between initial amounts of phospholipid used for preparation and impregnated amount of phospholipid.

To determine the amount of phospholipid deposited on the PPPs, ICP emission spectroscopy measurements were performed. As a pre-treatment, DPPC-PPPs were heated and oxidatively decomposed to obtain an aqueous solution. According to Equation 1, the impregnated amount of phospholipid was calculated. **Figure 5-8** shows the relationship between the amount of applied phospholipids and the amount of impregnated phospholipid per g-PPPs. With an increasing the amount of phospholipids used for preparation, the impregnated amount of phospholipids increased. A significant amount of phospholipid was deposited on PPPs because of the large specific surface area of PPPs. In addition, the polymer matrix of polyDVB (PDVB) was not tightly packed, and the hydrophobic interactions between the PDVB framework of PPPs and the hydrocarbon chains of phospholipids could be a main factor in the coating of phospholipids in PPPs.

4.2.2. Evaluation of the Membrane Properties

The phospholipids impregnated into PPPs formed self-assembled membrane structures, which were investigated using a conventional fluorescence spectroscopy method. The fluorescence probe Laurdan was anchored at the phospholipid membrane and was generally used for membrane characterization at various temperatures, which resulted in the phase transition behavior of membranes. The Laurdan fluorescence emission peaks were red-shifted as the phospholipid membrane environment changed from a non-polar to a polar environment (Okamoto *et al.,* 2017; Suga *et al.,* 2016). The membrane properties of DPPC-PPPs in response to temperature were evaluated (**Fig.5-9**). Laurdan in DPPC liposomes (T_m = 41 °C) showed a sharp peak at around 440 nm at temperatures below the T_m of DPPC, in which the liposome membrane was confirmed as the gel phase (ordered phase). Furthermore, the spectrum drastically changed at temperatures above the T_m, where the fluorescence intensity at 440 nm decreased and shifted to 490 nm. This confirmed that the liposome membrane on the surface was in the liquid-crystalline phase (disordered phase).

In **Fig.5-9 b**, Laurdan in DPPC-PPPs showed a peak at 440 nm at a temperature below T_m; in the case above the temperature of the T_m, the intensity of the peak at 440 nm was decreased and appeared at 420 nm and 490 nm, where the iso-emission point was observed at 465 nm. These results suggest that the DPPC-PPPs were covered with the phospholipid membrane, and their membrane properties were similar to those of DPPC liposomes at temperatures below T_m. In contrast, at temperatures above T_m, the phospholipid membrane on DPPC-PPPs displayed a disordered state similar to that of DPPC liposomes; however, the obtained GP_{340} values were slightly different (**Fig.5-9 c**). The iso-emissive point in the spectra of DPPC-PPPs revealed the temperature-dependent phase transition of the phospholipid membranes deposited on the PPPs. In addition, **Figure 5-9d** showed the reversibility of ordered/disordered states of the coated phospholipid membrane on PPPs. The reversibility changes in phospholipid membrane on PPPs was confirmed by controlling the temperature cycles which was cooling and heating cycles between 30 °C and 50 °C, and calculated GP_{340} values. Hence, it was found that the phospholipid membrane coated on PPPs with similar physical properties as those of liposomal membranes, which have ability of reversibly change the ordered/disordered

state of the membrane depending on the temperature change. It was confirmed that DPPC-PPPs have a lipid membrane in an ordered state at temperatures below 35 °C, which could be essential for chiral selective adsorption of L-amino acids (Ishigami *et al.,* 2015; Hiramure *et al.,* 2018; Ishigami *et al.,* 2015).

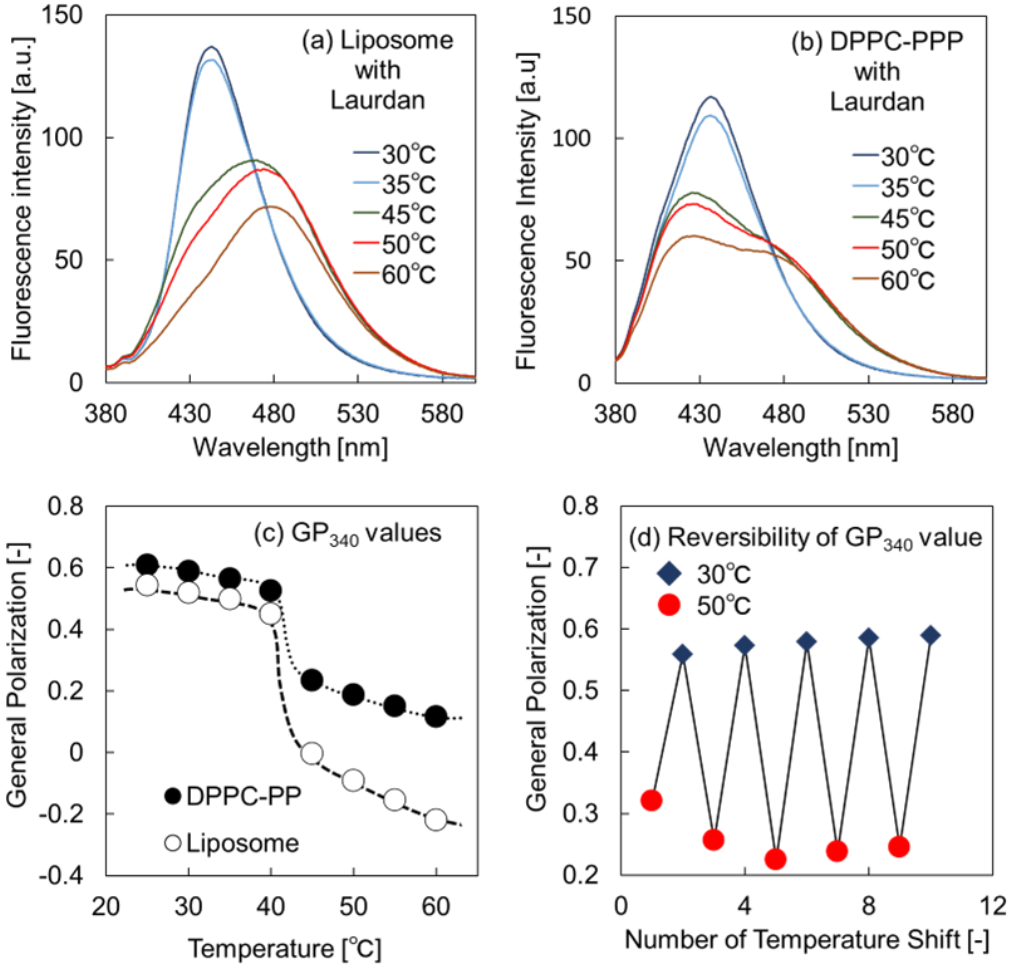

Figure 5-9 Temperature dependence of Laurdan spectra in (a) liposome suspension, and in (b) DPPC-PPPs suspension. (c) GP_{340} values calculated based on Eq. (2), and (d) reversibility of DPPC-PPPs GP_{340} value. All experiments were performed with DPPC-PPPs of 0.14 mmol-lipid/g-PPP. For liposome experiments, the concentrations of DPPC and Laurdan were 100 μM and 1 μM, respectively.

4.3. Comparison of Modification Methods by Lipid Membrane

Two case studies to modify the polymer surface by lipid membrane are shown in the previous chapters based on the general classification shown in **Fig.5-1**. As shown in **Fig.5-10**, the modification methods for porous polymer particles by lipid membrane are summarized as a general classification of three categories: (1) vesicle fusion method (delivery of amphiphiles-on-vesicle), (2) O/W emulsion method (delivery of amphiphiles-on-emulsion), and (3) lipid impregnation method (delivery of amphiphiles-in-solvent and washout of the excess). In vesicle fusion method, the phospholipids or amphiphiles that formulate the bilayer membrane of vesicle are used for the coating after the vesicle delivery and then, the surface of polymer material can be modified after the vesicle fusion. As shown in **Fig.5-1(1-a)**, vesicles are first injected into an aqueous solution dispersing the polymer material, as shown in **Fig.5-1(1-b)**, the dispersed vesicles are approaching on polymer surface and, then, as shown in **Fig.5-1(1-c)**, the vesicles are ruptured their membrane onto surface of polymer, resulting that the lipid membrane are coated on the polymer surface. In O/W emulsion method, the surfactants or appropriate amphiphiles that are utilized for the stabilization of the emulsions are utilized for the modifiers of the polymer surface. Basic strategy of this method is similar with that of the above vesicle fusion method, where the lipid molecules or amphiphiles are accumulated on the interface of oil-(bulk)water phases when the emulsion dispersed in a bulk aqueous solution as shown in **Fig.5-1(2-a)**. The O/W emulsions dispersed in bulk aqueous solution are delivered and contacted with the surface of polymer materials to adsorb oil phase from the emulsion as shown in **Fig.5-1(2-b)**. During adsorption of the oil, the lipid molecules are transferred from the emulsion onto the polymer surface, resulting that the solid-liquid interface can be modified with lipid molecules and the lipid membrane of the accumulated lipids can be formulated as shown in **Fig.5-1(2-c)**. The final strategy can be called as “lipid impregnation method”, where the lipids are efficiently transferred into the internal parts of the materials because of the porosity (high diffusivity) of the polymer particles. As shown in **Fig.5-1(3-a)**, the porous polymer particles are prepared as carrier and substrate which the lipid molecules are delivered, and a lipid membrane are finally formed. As shown in **Fig.5-1(3-b)**, for the impregnation to the porous polymer particles, the particles are mixed with the solvent solubilizing the target lipid molecules. Subsequently,

the solvent is removed and dried with rotary evaporator as shown in **Fig.5-1(1-c)**. The lipid molecules used for the impregnation are entirely transferred onto all the surface of the porous polymer particles because of solvent. After the solvent evaporation, the lipid molecules are accumulated on the surface of the polymer wall. When the impregnated porous polymer particles are hydrated, the lipid membrane spontaneously form the membrane structure on the polymer wall. These methodologies for modification polymer surface with lipid membrane are useful technique for the functionalization of the polymer. Since each method has advantage/disadvantage, it is necessary to select the most appropriate method depending on the purpose and experiment condition, considering the characters of polymer materials and the amphiphilic molecules.

Based on the obtained results and previous findings, the minimal characters of advantages and disadvantages of these methodologies for modification surface of the polymer materials were summarized in **Table 5-2**. In vesicle fusion method, the lipid bilayer on the surface of the polymer materials can clearly be aligned as bilayer membrane formulation. Since the step of rupture of vesicles to the substrate, the lipid membrane is coated with certain orientation (i.e, inner leaflet and outer leaflet). As the disadvantage of the vesicle fusion method, the kinds of lipid molecules are limited for utilization. When vesicles are utilized, the membrane must have “soft properties”, that is, it must exist as l_d and l_o phase that can be easily rupture. While the experimental procedure is simple, the oil that is used for the dispersed phase in the emulsion could become contaminants, which could be retained inside the substrate in the case of O/W emulsion. In the case of the lipid impregnation method, since the lipid molecules are dispersed in solvent, the lipid molecules are entirely transferred to the internal region of the polymer particles because of the large porosity of the polymer particles and, together, high diffusible nature of the lipid molecules inside the particles. So, the lipid molecules are efficiently utilized for the modification of the polymer particles.

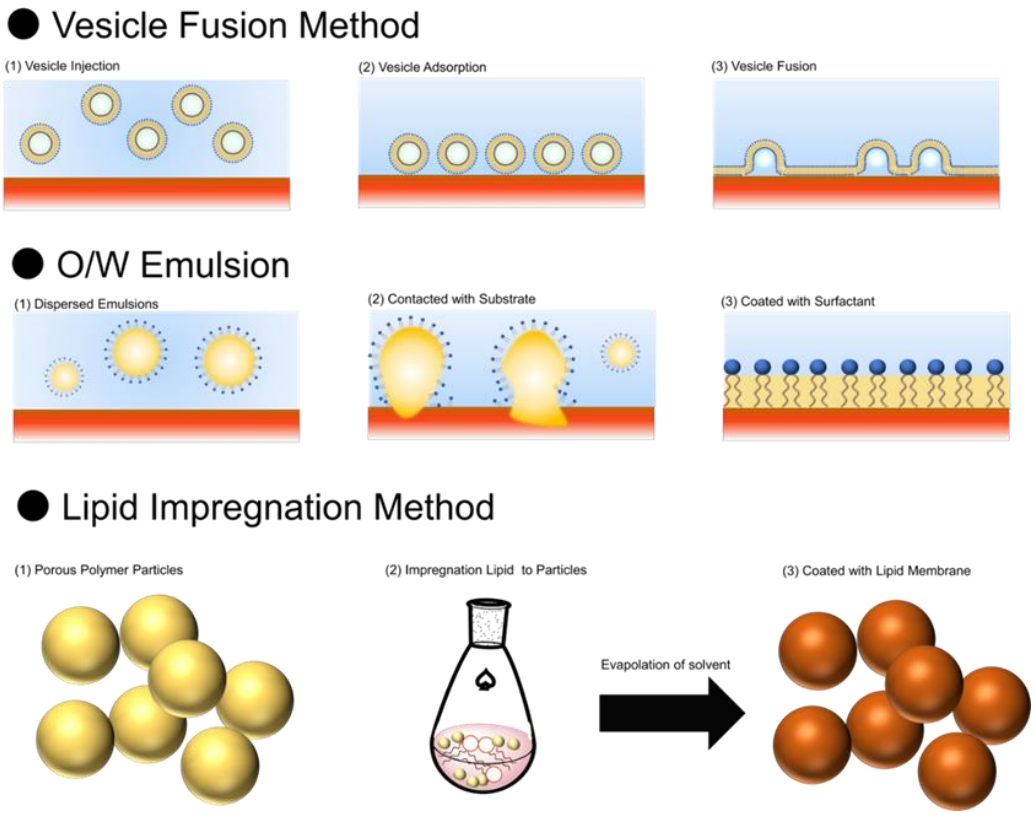

Figure 5-10. Schematic illustration of polymer surface modification method by lipid membrane. (a) Vesicle fusion method, Oil-in-water emulsion method, and (c) lipid impregnation method.

Table 5-2. List of comparison method for modification polymer with lipid

Method	State of lipid	Image	Advantage	Disadvantage
Vesicle Fusion	Vesicles	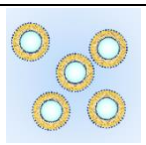	Alignment of Membrane	Limited variety of lipids
O/W Emulsion	Emulsions	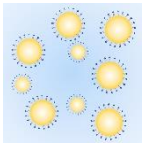	Simple operation	Oil contamination on substrate
Impregnation	Dispersed molecules	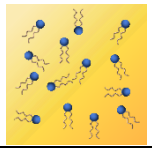	Modification entire pores	Large consumption of phospholipid

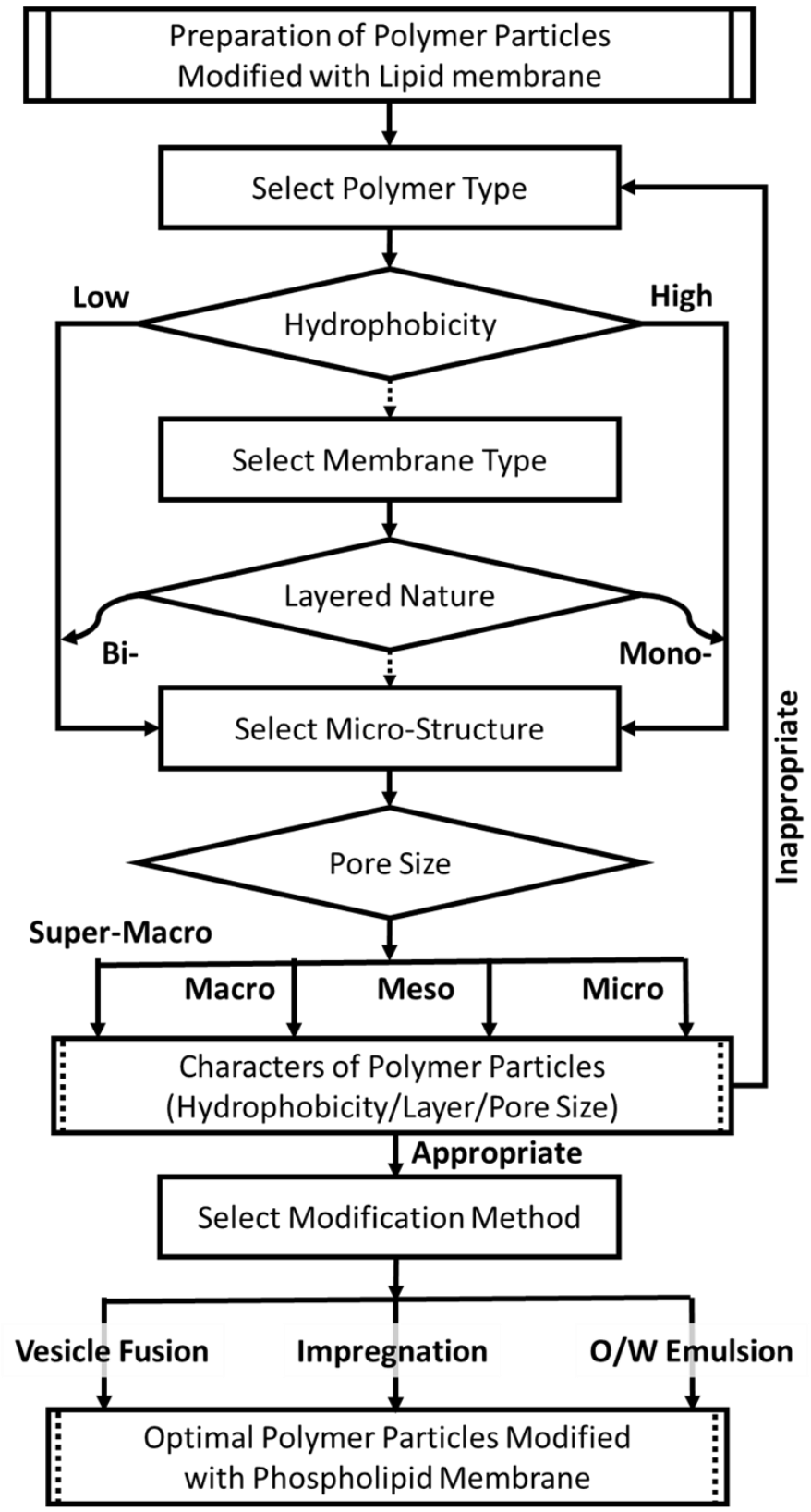

Scheme 5-1. Proposed method to modify polymer surface by lipid membrane.

5. Summary

The methods to modify the surface of the polymer particles with the amphiphiles (i.e. phospholipids) were classified, especially, focusing on (a) O/W emulsion method and (b) lipid impregnation method. In the case of "O/W Emulsion Method", the pTrim based cryogel particles were prepared by adopting our developed method; iLF cryo-method. The particle properties, such as (i) D_v, (ii) ρ, (iii) C_v, (iv) σ_{bulk}, and (v) size distribution of pore size, were characterized by using optical microscope and SEM. The cryogel particle was thus found to have monolithic supermacroporous structure. Subsequently, the hydrophobicity of cryogel particles was tested by placing aqueous and organic droplets on the particles. While the aqueous droplet was held on the particle by repelling, the organic droplet was immediately adsorbed into the particle due to the hydrophobic surface of the particles. Furthermore, it was found that the adsorbed organic solvent was diffused into entire the particle by observation cross-section of the cryogel particle. The separation of stabilized oil-in-water emulsion by using cryogel particles was performed. As a result, the efficient removal of stabilized oil-in-water emulsion has been demonstrated. This cryogel particle materials can be applied for the separation of oil phase in emulsion state and, at the same time, the efficient delivery of amphiphile onto the polymer surface. Based on the **Scheme 5-1**, modification method for polymer surface with lipid membrane is comprehensibly classified.

Chapter 6

Recognition of L-Amino Acid by L-Phospholipid Membrane Loaded on Porous Polymer Particles

1. Introduction

Porous polymer particles (PPPs) are attracting great scientific and technological attention in many fields, owing to their superior physical and chemical properties (Wang *et al*;2017; Saba *et al*; 2015; Hou *et al.,* 2003). Furthermore, the polymer structure and inner morphology can be controlled by polymerization methods and conditions (Yoshizawa *et al.,* 1995). During the *in-situ* emulsion polymerization method, hydrophobic monomers disperse from a continuous aqueous phase and form a layer of oil phase, while PPPs with internal spherical pores are prepared by water-in-oil-in-water (W/O/W) emulsion polymerization (Inda *et al.,* 2017). The PPPs have a large specific surface area originating from numerous pores existing at the surface and inner section. Owing to these advantages, PPPs are applicable in various fields, such as separation, purification, and catalyst support (Gokmen *et al.,* 2016). They are also suitable for separation media or packing materials in chromatography (Causon *et al.,* 2010). Although such porous materials have been utilized for bioseparation, the hydrophobic nature of the polymer could lead to unexpected interactions with biomolecules (Zhai *et al.,* 2012). Therefore, surface modification is one of the most important strategies to increase the surface function of PPPs (Saitoh *et al.,* 2005).

Self-assembled lipid membranes are self-organized materials consisting of amphiphilic molecules, wherein their highly ordered interface is enriched with functional groups such as choline, phosphate, and carbonyl. Furthermore, they feature dynamic properties such as phase transitions. Since the membrane properties can be controlled by the molecular composition and by tuning environmental conditions, especially temperature, self-assembled membranes have been utilized as a platform for molecular recognition and conversion (Walde *et al.,* 2014, Serrano *et al.,* 2018; Ishigami *et al.,* 2015;

Zhou *et al.,* 2018; Hirose *et al.,* 2019; Chen *et al.,* 2019; Tsuchiya *et al.,* Okamoto *et al.,* 2017). For the fundamental interactions of biological molecules, such as amino acids, sugars, nucleic acids, and proteins in biological systems, molecular chirality plays a key role (Chen *et al.,* 2020; Wagner *et al.,* 2017; Verkujil *et al.,* 2011; Skolnick *et al.,* 2019). Hence, chiral separation is one of the most important processes in the production of pharmaceuticals and drugs (Scriba *et al.,* 2016). In most cases, only one enantiomer is effective, but the other is inactive or even toxic (Smith *et al.,* 2009; Czerwinska *et al.,* 2020). Interestingly, the chiral lipids and their self-assemblies can be a chiral selector in molecular separation process (Hu *et al.,* 2021; Martin *et al.,* 2021; Penny *et al.,* 2018).

In our previous reports, liposomes were used for chiral recognition of small molecules (Ishigami *et al.,* 2015; Okamoto *et al.,* 2017; however, there were some problems, such as the instability of liposomes that makes the recovery and reuse difficult, toward the practical use of self-assembled membranes. Furthermore, the outer leaflet of the liposomes could be utilized for interaction with chiral molecules, while the inner leaflet is utilized as a scaffold to maintain the liposome structure. To overcome this problem, a self-assembled lipid membrane–polymer composite will be beneficial. Phospholipid membranes can be immobilized on a solid support Suga *et al.,* 2015; Kurniawan *et al.,* 2018; Dolstra *et al.,* 2019) and on a polymer matrix (Hiramure *et al.,* 2018), where the substrate (e.g*.,* glass, mica, hydrogel matrix) would help to maintain the structure of the self-assembled membrane. To increase the available surface in dispersion, a material with a high specific surface area is desired.

In this chapter, the chiral selective adsorption of L-amino acid was performed using PPPs coated with a self-assembled membrane of 1,2-dipalmitoyl-*sn*-glycero-3-phosphocholine (DPPC (L-phospholipid)). Herein, a self-assembled membrane in a highly ordered state (gel phase) was deposited on PPPs, which could enhance the chiral adsorption of L-tryptophan (L-Trp) (Ishigami *et al.,* 2015; Hiramure *et al.,* 2018; Ishigami *et al.,* 2015). By employing the impregnation method, DPPC molecules were loaded onto PPPs. Mapping images of energy dispersive X-ray (EDX) analysis revealed a homogeneous distribution of the impregnated DPPC molecules on the surface and within the framework of PPPs. The membrane properties of DPPC-PPPs were characterized from the fluorescence spectra of 6-lauroyl-2-dimethylamino naphthalene (Laurdan),

which confirmed the ordered state of DPPC membranes in DPPC-PPPs, and corresponded to the chiral selective adsorption of L-Trp. The chiral selectivity depended on temperature, revealing the high enantioselectivity of amino acid adsorption by DPPC-PPPs at temperatures below the phase transition temperature of DPPC.

2. Materials and Methods

2.1. Materials

1,2-Dipalmitoyl-sn-glycero-3-phosphorylcholine (DPPC) was purchased from Avanti Polar Lipids, Inc. (Alabaster, AL, USA). Monomeric divinylbenzene (DVB) was purchased from Wako Pure Chemical Industries, Ltd. (Osaka, Japan). The DVB was washed with a 10 wt% NaOH aqueous solution to remove the polymerization inhibitor. 6-Lauroyl-2-dimethylaminonaphthalene (Laurdan) and other chemicals were also purchased from Wako Pure Chemical Industries, Ltd. (Osaka, Japan) and were used as received.

2.2. Preparation of PPPs Coated with Phospholipid

Briefly, porous polymer particles (PPPs) were prepared from a water-in-oil-in-water (W/O/W) emulsion by *in situ* polymerization (Inda *et al.,* 2017). The DVB monomer dissolved in the oil phase forms the polymer framework. The obtained PPPs and DPPC dissolved in chloroform and methanol solution (volume ratio of 2:1) were mixed in a round-bottom flask and dried using a rotary evaporator under vacuum to remove the solvent mixture. This procedure was repeated three times, and the phospholipid was impregnated in PPPs and kept under a high vacuum for at least 3 h to obtain DPPC-coated PPPs (DPPC-PPPs).

2.3. Temperature-dependent Chiral Adsorption of L-Amino Acid

The chiral adsorption behavior of amino acids (L- and D-Trp) by DPPC-PPPs was evaluated at different temperatures. The DPPC-PPPs and PPPs were added to L- and D-Trp aqueous solutions at 30 °C and 45 °C, and incubated for 70 h. Subsequently, the solid particles and the adsorbed amino acids were removed by ultrafiltration with the 50,000 Da of molecular weight cutoff (USY-5; Toyo Roshi Kaisha, Ltd., Tokyo, Japan). The

concentrations of the initial (C_{ini}) and filtered (C_{flt}) amino acids were measured by UV absorbance at a wavelength of 278 nm using a UV spectrophotometer (UV-1200, Shimadzu, Kyoto, Japan). The adsorbed amount of amino acid molecules per DPPC molecule coated on PPP (q) was calculated using the following Eq.6-3.

$$q = \left(C_{ini} - C_{flt}\right) \cdot V / (E_{DPPC} \cdot W_{PPP}) \qquad \text{Eq.6-3}$$

From the q values of L-Trp and D-Trp, the enantio excess of adsorption was calculated using the following Eq.6-4.

$$Enantio\ Excess\ [\%] = \frac{q_{L-AA} - q_{D-AA}}{q_{L-AA} + q_{D-AA}} \times 100 \qquad \text{Eq.6-4}$$

where $q_{\text{L-AA}}$ and $q_{\text{D-AA}}$ represent the q values of L-Trp and D-Trp, respectively, on DPPC-PPPs.

2.4. Fluorescence Spectra of Tryptophan

The fluorescence emission peaks of Trp are relevant to its surroundings (microenvironments). A shift in the maximum fluorescence peak can be attributed to the hydrophobicity of the solvent (Umakoshi *et al.,* 2012; Zahid *et al.,* 2013; Suga *et al.,* 2016). The fluorescence spectrum of the L-Trp-adsorbed DPPC-PPPs was measured using a fluorescence spectrophotometer (FP-8500, JASCO, Tokyo, Japan) at an excitation wavelength of 280 nm. Before the measurements, the adsorption of L-Trp on DPPC-PPPs was performed at 30 °C, and then DPPC-PPPs was washed with distilled water to remove unadsorbed L-Trp.

2.5. Time Course of Amino Acid Adsorption

To evaluate the adsorption behavior, the time course of the adsorption of chiral amino acids on DPPC-PPPs was measured. DPPC-PPPs and PPPs were incubated in L- or D-Trp solution at 30 °C, and the absorbance was measured using a UV spectrometer at each time point. The adsorption amount of amino acids per lipid molecule coated on PPPs (C_{ads}) was calculated using the Eq.6-3. The DPPC-PPPs with adsorbed amino acids

were washed with distilled water and dried using the same procedure.

2.6. Optical Resolution of L-/D-Tryptophan

DPPC-PPPs were applied into racemic solution of L-/D-Trp (total Trp conc. 1.0 mM), and then incubated for 70 h at 30 °C. Subsequently, the solid particles and the adsorbed amino acids were removed by ultrafiltration. The supernatant was analyzed by using a chiral column chromatography (Waters 1500 HPLC System, Waters, Milford, MA, USA), equipped with CHIRALPAK ZWIX(+) (3 mm-ϕ × 150 mm, particle size: 3 μm) (DAICEL, Osaka, Japan). Mobile phase was methanol/water (98/2 volume ratio), including 50 mM formic acid and 25 mM diethylamine, flow rate was 0.5mL/min, and Trp was detected by UV at wavelength of 254 nm. The retention time of D- and L-Trp was 4.8 min and 6.3 min, respectively. The concentrations of L- and D-Trp were determined by peak area.

3. Results and Discussion

3.1 Typical Dependence of Chiral Selective Adsorption of L-/D-Trp

Prior to the research using the DPPC-PPPs, the chiral recognition function of the DPPC membrane was explained here. It is known that the DPPC liposome bilayer membranes have ordered structures owing to molecular alignment and can also be characterized as gradient polarity layers at nano-meter scale. It has already been reported that the Trp dissolved in the aqueous phase was partitioned to the liposome membranes by mixing them for 48 hours (Ishigami *et al.,* 2015), where the yield of L-Trp recovery, calculated by its partitioning behavior from the aqueous phase to the phospholipid phase,

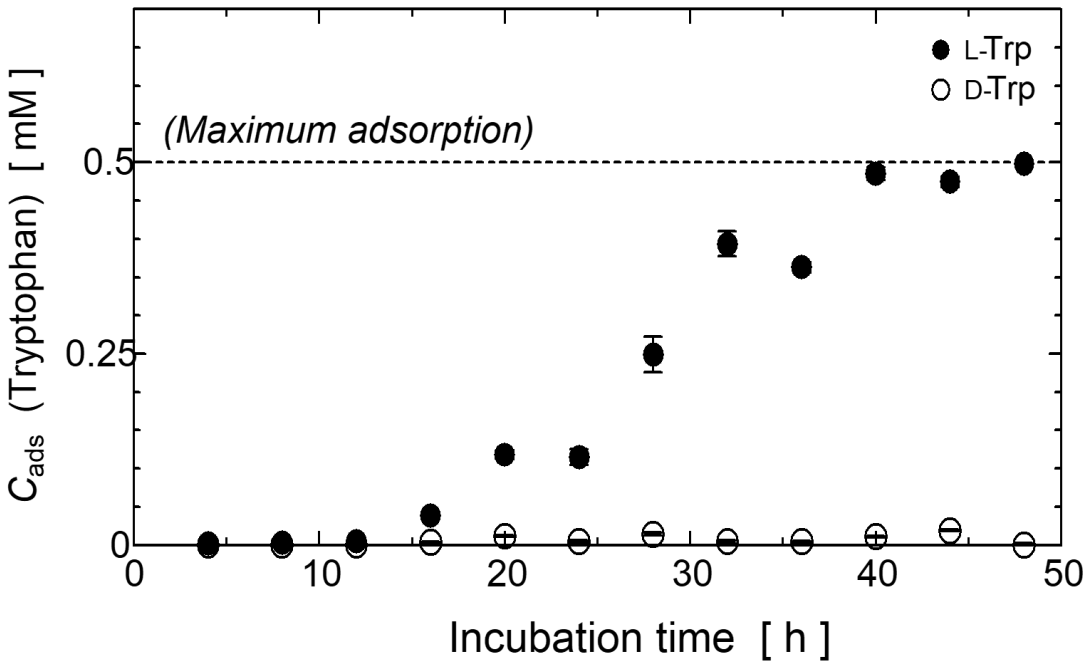

Fig. 6-1. Time course of adsorbed concentration (C_{ads}) of L or D-forms of amino acids. C_{ads} of L-Trp (filled) and D-Trp (open). (Ishigami *et al.,* 2015)

was found to be high, while that of D-Trp was extremely low. As a result, the chiral selectivity in the liposome system showed an extremely high value (~10^4) as compared with other solvent extraction systems. It is thought that the liposome membrane could provide a suitable environment for the partitioning of the hydrophilic Trp, where some interactions (i.e. electrostatic interaction, and hydrogen bond) neighboring to the chiral carbon of the lipid molecules could be related to its chiral recognition. **Figure 6-1** shows the time course for the adsorption of Trp on DPPC liposomes. The adsorbed amounts of L-Trp gradually increased after 16-hour incubation and reached to be an equilibrium after 48 hours, where almost all of the amino acids adsorbed on DPPC liposomes. On the other hand, negligible amounts of D-Trp adsorbed on the DPPC liposomes even at 48 hours. As a result, extremely high chiral selectivity in the Trp adsorption on the DPPC liposome was observed at the final stage of the adsorption process, while such behaviors were not found in the solvent-water system modified with DPPC. This result was also implying that the binding of L-amino acids on the liposome structure can be very weak at the initial stage of adsorption, considering the previous findings on the adsorption in supported lipid bilayer (Sarangi, *et al.,* 2012). This is because the amino acids preferably exist in the

aqueous phase rather than in liposome membranes, judging from the negative values of Log*P*. It is thought that the membrane property could be varied after the accumulation of amino acids on the membranes at the initial stage: such varied membrane properties could recruit the additional L-Trp partitioned to the membrane at the latter step.

3.2. Chiral Selective Adsorption of Amino Acid on the Coated PPP

DPPC-PPPs were incubated with amino acid enantiomers in aqueous solutions, wherein L-Trp and D-Trp were treated at 30 °C (below phase transition temperature (T_m) of DPPC) and 45 °C (above the T_m of DPPC). **Figure 6-2a** shows the chiral adsorption behavior of amino acids for DPPC-PPPs at different temperatures. DPPC-PPPs adsorbed L-Trp at 30 °C, whereas the adsorbed amount decreased at 45 °C. In contrast, D-Trp was not adsorbed on DPPC-PPP, regardless of the incubation temperature. Furthermore, the bare PPPs, without the impregnated phospholipids, did not adsorb Trp regardless of the incubation temperature. Herein, the view from chiral selectivity, DPPC-PPP at 30 °C of enantio excess is remarkably high, whereas DPPC-PPPs at 45 °C did not show chiral selectivity. These results indicate that the chiral adsorption ability of DPPC-PPPs was affected by the temperature. The difference in adsorption ability could be due to the change in the ordered state in the phospholipid membrane (Ishigami *et al.,* 2015; Ishigami *et al.,* 2015. The phospholipid impregnated PPPs possess self-organized membranes with a higher molecular ordering at 30 ℃; however, the phospholipid molecular ordering could be reduced at 45 ℃ due to the phase transition. It is thus assumed that DPPC-PPPs have the ability to selectively adsorb amino acids at temperatures below the T_m of DPPC. In previous reports, the key factors in chiral adsorption by phospholipid membranes have been suggested to be multiple interactions such as electrostatic, hydrophobic, and hydrogen bond interactions, which synergistically contribute to the adsorption of enantiomer (Ishigami *et al.,* 2015; Okamoto *et al.,* 2017; Suga *et al.,* 2017).

Adsorbed L-Trp on DPPC-PPPs was furthermore analyzed based on fluorescence spectroscopy. The fluorescence emission peak position of Trp was highly influenced by the polarity of its microenvironment such as hydrogen bonding and other non-covalent interactions. Generally, a blue shift of Trp was observed in a lower dielectric environment (Ghisaidoobe *et al.,* 2014. The fluorescence spectrum of L-Trp adsorbed on DPPC-PPPs

was used for comparison (**Fig.6-2 b**). The maximum fluorescence peak of L-Trp (*aq.*) was detected at 352 nm, whereas the adsorbed L-Trp was at 329 nm. Therefore, it was revealed that the L-Trp adsorbed on DPPC-PPPs was located in hydrophobic environment. Such blue shifts were usually observed by an intrinsic Trp of protein, and by a Trp in a transmembrane segment. The adsorbed L-Trp could be migrated into the hydrophobic sites of DPPC-PPPs, such as PDVB framework (ε ~ 2 (Fu *et al.,* 2001).) and acrylchain region of lipid membrane (ε < 6 (Cevc *et al.,* 1990)).

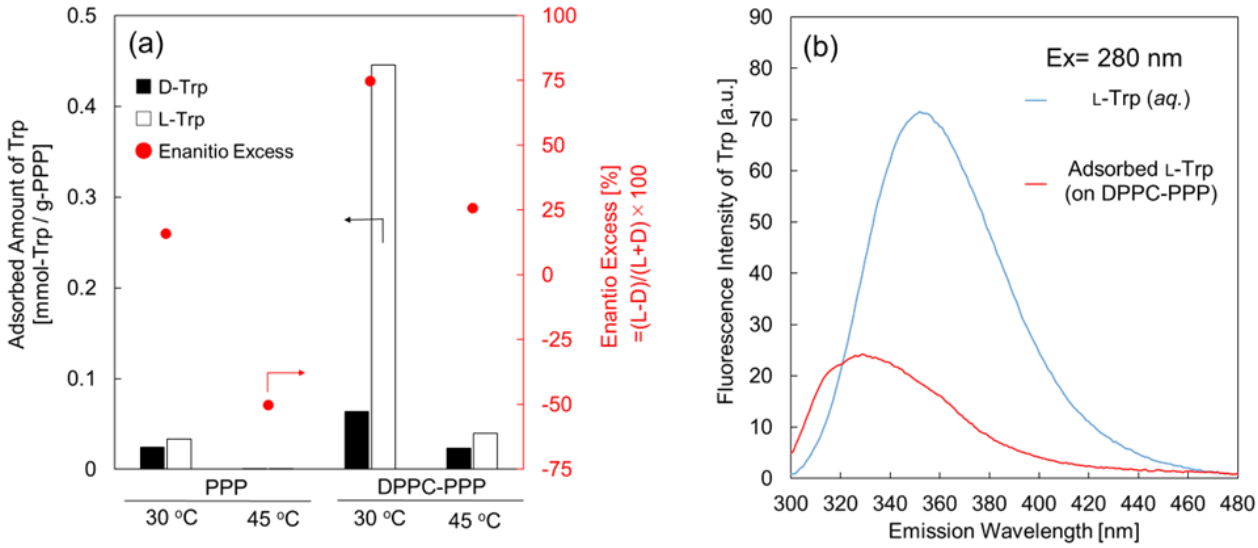

Figure 6-2 (a) Temperature dependence of L- and D-Trp adsorption by PPPs and by DPPC-PPPs. All samples were incubated 70 h at 30 °C and 45 °C, the initial concentration of Trp and DPPC-PPPs were 0.5 mM and 1.0 g/mL, respectively. Enatio excess (e.e.) values were calculated based on Eq. (4). (b) Fluorescence emission spectra of L-Trp in aqueous solution (*blue line*) and in DPPC-PPPs suspension (red line). L-Trp and DPPC-PPPs were preliminary incubated at 30 °C, and unadsorbed L-Trp was removed before measurement. All experiments were performed with DPPC-PPPs of 0.14 mmol-lipid/g-PPP.

In DPPC liposome system, the Trp adsorbed onto DPPC liposome did not display blue-shifted fluorescence, suggesting the binding of L-Trp at the hydrophilic-hydrophobic interface region. Hence, the DPPC molecule could play dual roles: a chiral selective interaction with L-Trp by the lipid head group, and a compartment for the adsorbed L-Trp by the lipid tail. In contrast in DPPC-PPP system, the adsorbed Trp

displayed blue-shifted fluorescence, suggesting more hydrophobic surrounding of the Trp adsorbed in DPPC-PPPs. Because DPPC molecules were impregnated to PPPs via hydrophobic interaction, the hydrophobic tail region of the DPPC and PPP could be smoothly connected that Trp can bind onto the surface of DPPC-PPPs, and enantioselectively, adsorbed Trp can diffuse into the inner part of PPPs.

3.3. Time Course Adsorption and Optical Resolution

To investigate the adsorption behaviors of L- and D-Trp by DPPC-PPPs, the time course of Trp adsorption was examined for fresh DPPC-PPPs and reused DPPC-PPPs (**Fig.6-3)**. DPPC-PPP started the adsorption of L- and D-Trp at approximately 16 h. Subsequently, L-Trp adsorption gradually continued, whereas D-Trp adsorption almost reached a plateau at 30 h. In the L-Trp adsorption by DPPC-PPPs, the lag time exists in the incubation time range of 21–31 h and 39–53 h. According to previous reports, the membrane property was inalterable during lag-phase (t <16h), and then the membrane property was gradually altered together with the L-Trp adsorption (Ishigami *et al.,* 2015; Hiramure *et al.,* 2018. This suggests that the adsorbed L-Trp can disturb the tightly packed DPPC membrane. Considering the blue-shift of Trp fluorescence (**Fig.6-4b**), it is assumed that 1) L-Trp in aqueous phase interacts with the DPPC membrane on DPPC-PPPs, 2) L-Trp starts adsorption into DPPC membrane after lag-phase, 3) adsorbed Trp diffuses into the inner part (hydrophobic environment) of DPPC-PPPs. Although this adsorption pathway is plausible, the first step could be regarded as rate-limiting step because the membrane of DPPC-PPPs could be tightly packed as well as DPPC liposome (**Fig.6-3**).

After the first-round L-Trp adsorption, the DPPC-PPPs were washed with distilled water, dried under vacuum, and then incubated with L-Trp and D-Trp. Reused DPPC-PPP with L-Trp exhibited a lag time of several hours, and the adsorption continued until 80 h, while the second-round D-Trp adsorption amount by reused DPPC-PPPs was approximately the same value as the first-round D-Trp adsorption amount. It is hypothesized that the chiral selective adsorption of amino acids by DPPC-PPPs involved several steps. First, both L- and D-Trp were adsorbed on the surface of the DPPC-PPPs. Then, only L-Trp was dispersed into the inner part of the DPPC-PPPs over time. Hence, the kinetics of adsorption of L-Trp was higher than that of D-Trp. The impregnated DPPC

could act as a chiral selector when the surface-adsorbed Trp was distributed into the inner section of the particles. Overall, the reused DPPC-PPPs displayed a superior ability for L-Trp adsorption compared with fresh DPPC-PPPs. These results suggest that the deposition of DPPC membranes onto PPPs was necessary for the chiral selective adsorption of L-amino acids, which could perform chiral selectivity as well as free-suspended phospholipid liposomes in water.

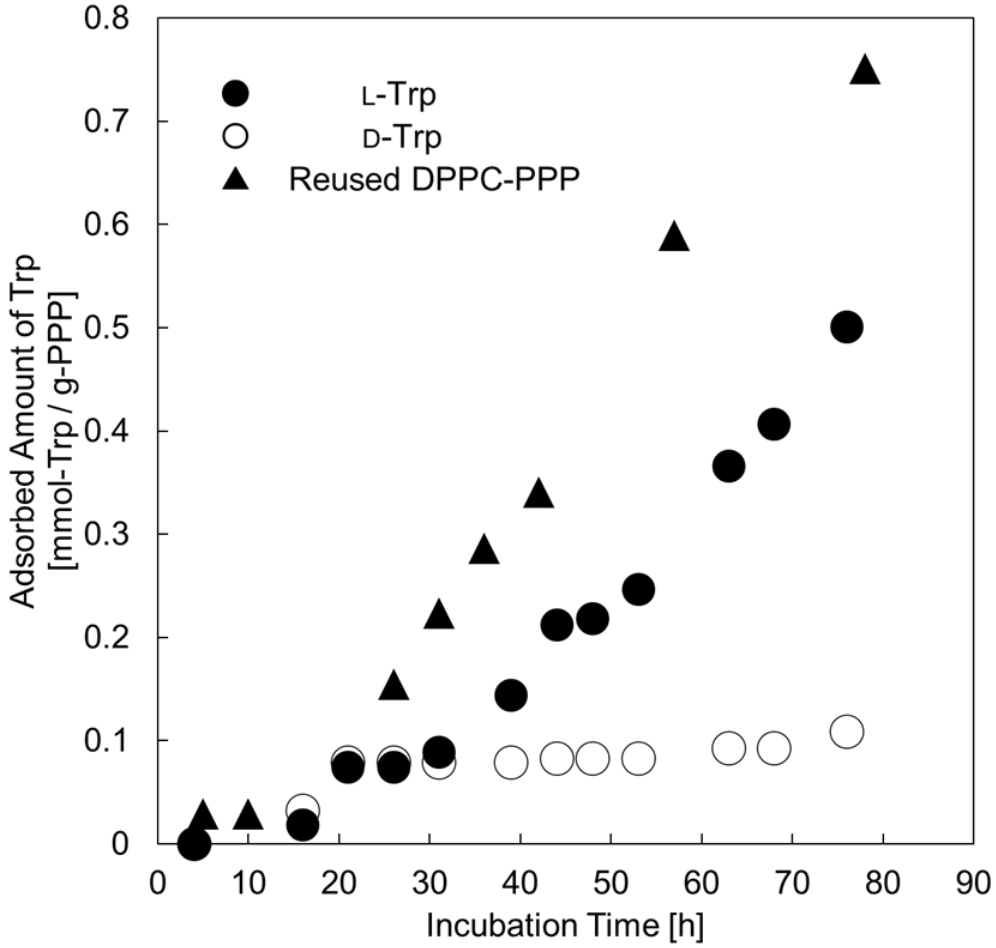

Figure 6-3 Time course of L- and D-Trp adsorption on DPPC-PPPs, and on reused DPPC-PPPs. (●) DPPC-PPPs with L-Trp, (○) DPPC-PPPs with D-Trp, and (▲) reused DPPC-PPPs with L-Trp. Adsorption experiments were carried out at 30 °C. All experiments were performed with DPPPC-PPPs of 0.14 mmol-lipid/g-PPP.

The L-Trp selective adsorption by DPPC-PPPs was evaluated in racemic solution.

As shown in **Fig.6-4**, DPPC-PPPs preferentially adsorbed L-Trp, then the supernatant enriched with D-Trp. Therefore, the DPPC-PPPs was found that DPPC-PPPs could perform optical resolution of amino acid in racemic solution. The adsorbed ratio of each enantiomer and enantio excess for DPPC-PPPs are summarized in **Table 6-1**. The performance of optical resolution using DPPC-PPPs in enantio excess of D-Trp was >60%. Thus, DPPC-PPPs have the potential of chiral selective adsorption of L-amino acid, which can used as chiral separation materials.

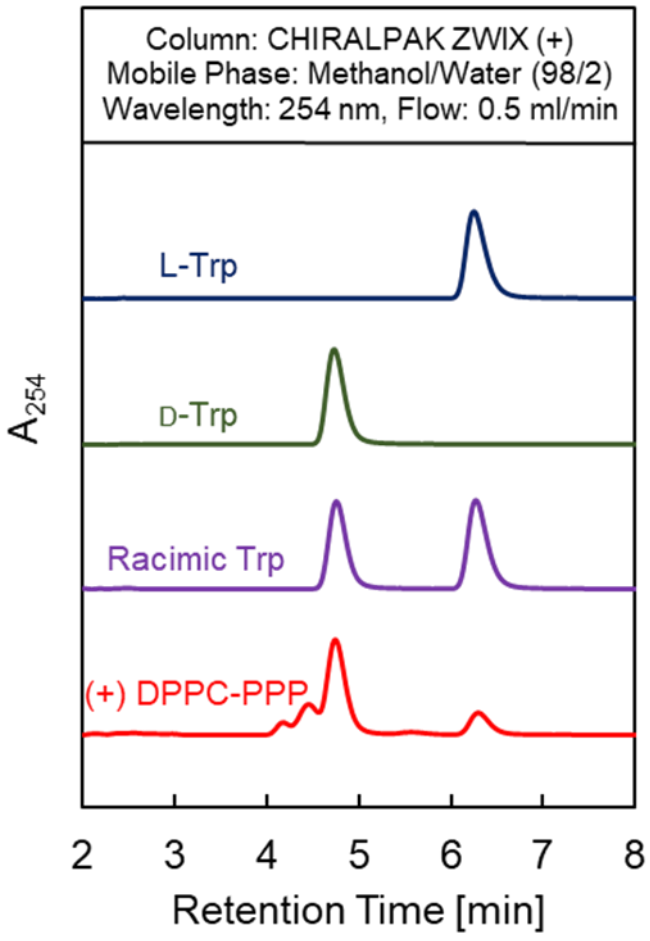

Figure 6-6 Optical resolution of racemic Trp mixture treated by DPPC-PPPs. Unadsorbed Trp was evaluated by HPLC chromatogram. CHIRALPAK ZWIX (+) was used as column, and Trp was detected by UV absorbance at 254 nm. Retention time of D- and L-Trp was 4.8 and 6.3 min, respectively.

4. Summary

In this chapter, prepared porous materials that could perform chiral selective adsorption of amino acids were successfully prepared. L-Phospholipid-coated porous polymer particles (DPPC-PPPs) were characterized by EDX and ICP, revealing the successful deposition of DPPC molecules at the surface and inner sections of PPPs. The physicochemical membrane properties of DPPC-PPPs were investigated by Laurdan and revealed that DPPC-PPPs could possess well-ordered membranes at the temperatures below T_m of DPPC similar to conventional DPPC liposomes. It was demonstrated that DPPC-PPPs had a chiral adsorption ability for L-Trp, where a higher amount of L-Trp was adsorbed at temperatures below the T_m of DPPC, while the adsorption decreased at temperatures above T_m. Thus, it was proved that the phospholipid membrane, particularly the state of the membrane, could play a crucial role in chiral selective adsorption. Phospholipid-membrane-coated porous polymer particles are expected to be applied in chiral separation devices, such as chiral columns. Consequently, the modification method for polymer surface with phospholipid membrane via impregnation method was revealed that the modified lipid membrane on polymer surface have membrane properties and function similar to liposome membrane.

Chapter 7

Bio-separation by Lipid Membrane Coated Cryogel Particle

1. Introduction

Cryogel are attractive materials with unique porous structure and sponge-like mechanical properties (Shirbin *et al.,* 2016). Through polymer of the cryogel composed with biocompatible (Bolgen *et al.,* 2010), it can be utilized for aqueous media such as bio-separation material (Senta *et al.,* 2014), organ-mimic material (Lilandra *et al.,* 2021)*.,* bio-scaffold (Ankur *et al.,* 2015). Furthermore, the physicochemical properties of cryogel is able to manipulate with modification such as coating, composing, blending (Damania *et al.,* 2018; Selin *et al.,* 2019; Liaila *et al.,* 2021). The modification of materials to be functionalized have the potential to create that innovative material have some possibility to breakthrough. Here, focusing on "separation", the principles are represented as rate-governed separation (i.e, centrifugation, chromatography) (Cambiella *et al.,* 2006; Eiji *et al.,* 2005) and equilibrium separation (i.e, adsorption, crystallization, extraction) (Xinyi *et al.,* 2018; Ivan *et al.,* 2022; Wu *et al.,* 2019) and both of the principles are practically utilized. Although the number of more improved techniques with the principle are developed, there are still remained inevitable problem which realize both high-selectivity and high-efficiency. When the high-selectivity is required for drugs such as chiral molecules (Xiaoju *et al.,* 2020) and biomolecules such as exosomes (Justyna *et al.,* 2013), the efficiency is abandoned. In contrast, the high-efficiency is required such as large-scale separation, the selectivity such as sensitive operation is abandoned. For the breakthrough of the relationship, it is required that comprehensive design from the macroscopic material properties to microscopic properties at molecular level.

Here, for the manipulation of microscopic properties, life and biological systems have the key point. These systems are understood to be complex and hierarchical systems. In living organisms, various biological reactions such as enzymatic reactions and immune responses are known to be induced at the molecular level. Even in a biological environment with complex molecular intermingling, biological macromolecules correctly recognize the target molecules and control competing biochemical reactions and their

pathways (complex concurrent reactions). Substances and byproducts involved in reactions are appropriately supplied in "advanced separation" (≒ molecular identification) and "advanced reactions" (≒molecular transformation and metabolism), and are also separated and discharged as waste products. In this way, "molecular unit operations" and "molecular unit reactions" on the micro- and meso-scale constitute a complex system that interacts across hierarchical levels, triggering responses at the cell, tissue, and organ levels, which are higher levels, and ultimately maintains homeostatic physiological functions. Although a vast amount of data has been accumulated, the approach of existing research is considered to be limited to the "science of life and living systems.

Hence, in this chapter the sophisticated separation material with high-selectivity and high-efficiency is developed by combining sponge-like material which have a large specific surface area and elastic mechanical properties and soft material which self-assembled ordered at molecular level. As shown in **Figure 7-1**, the concept of this chapter was designed the separation materials through macroscopic to microscopic. To separation for biomolecules, the lipid membrane modified at interface of cryogel particles were used. The lipid membrane was mechanically perturbed by compression of the particles and the membrane properties were induced to change that revealed from analysis of the fluorescence behaviors. Subsequently, the separation properties via mechanical compression as driven-force were revealed.

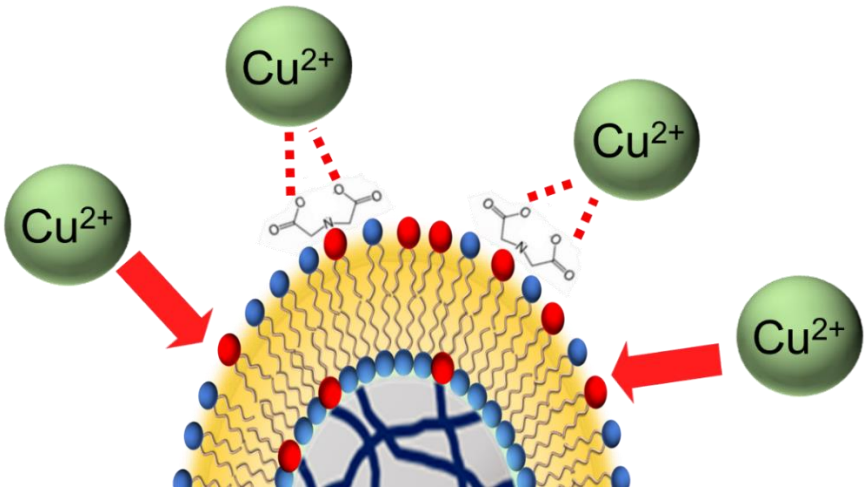

Figure 7-1. Conceptual illustration of chapter 7.

2. Materials and Methods

2.1. Materials

1,2-Dipalmitoyl-*sn*-glycero-3-phosphorylcholine (DPPC) (Aldrich) and 1,2-dioleoyl-*sn*-glycero-3-phosphocholine (DOPC) were purchased from Avanti Polar Lipid Inc.(Alabaster, AL), and were used as received. Hexadecilbromide, *d*iethyliminodiacetate, triethylamine, 6-dodecanoyl-2-dimethylaminonaphthalene (Laurdan), and dimethylpolysiloxane were purchased from Sigma Aldrich (St. louis, MO, USA). Acrylamide (AAm), *N,N'*-methylenebisacrylamide (MBA), ammonium persulfate (APS), *N,N,N',N'*-tetramethlethylenediamine (TEMED), liquid paraffine, ethanol, methanol, chloroform, tetrahydrofuran (THF), n-hexane, acetonitrile, and cupper (II) sulfate were purchased from Wako Pure Chemical (Osaka, Japan) and were used without further purification.

2.2. Preparation of Lipid Membrane Coated Cryogel Particles

Briefly, cryogel particles was prepared via iLF cryo-method, reported our previous works. For modification of cryogel particles with phospholipid membrane, the impregnation method was adopted. Dissolved phospholipid with methanol and cryogel particles were mixed in round-bottom flask and evaporated the solvent by rotary evaporator. Then, lipid impregnated cryogel particles was dried under pressure. The dried lipid coated cryogel particles were hydrated in ultra-pure water at 60 ºC. After that, the dispersed lipid molecules (did not coated) were removed by ultracentrifugation.

2.3. Analysis of Steady-state Laurdan Spectra

Fluorescence probe, Laurdan located near the interfacial region within lipid membrane, is sensitive to the polarity around them, which allows the membrane polarity to be determined (Watanabe *et al.,* 2018). The fluorescence spectrum of Laurdan in the DPPC lipid membrane coated cryogel particles, DPPC liposome, and non-coated cryogel particles were recorded with excitation wavelength of 340 nm, at appropriate emission wavelengths from 400 to 600 nm at difference temperature at 25-60 ºC, and the general polarization (GP_{340}) for each emission wavelength is as follows the **Eq. 7-1**.

$$GP_{340} = \frac{(I_{440}-I_{490})}{(I_{440}+I_{490})} \qquad \text{Eq. 7-1.}$$

Where I_{440} and I_{490} are the emission intensities of Laurdan at 440 and 490 nm, respectively.

2.4. Time-resolved Emission Spectrum (TRES) Measurement

Time-resolved fluorescence measurements were all performed using the time-resolved emission spectroscopy (Delta flex, Horiba). For the excitation of the samples, a diode laser with a light source of 378 nm was used. Emission decays were obtained from 400-540 nm in 10 nm steps with 64-picosecond resolution.

2.5. Compression of Lipid Membrane Coated Cryogel Particles

The lipid membrane coated cryogel particles were mechanically compressed and their macroscopic shape was deformed in the 1cm × 1cm cuvette. To compression the particles, the PDMS stamp was manufactured as syringe.

2.6. Synthesis of HIDA

The chemical structures for synthesis of HIDA were as shown in **Figure 7-2**. The synthesis was reacted according to **Figure 7-2 (e)**. Diethyl iminodiacetate (1.7g), bromohexadecane (07ml), and triethylamine (1.33ml) were added into three-pronged flask. After that, the THF: Acetronitrile = 1:1 was also added as solvent. The precursor was reacted for 48h at 80 ° under reflux by nitrogen gas. After reacted, HIDA was extracted with water-chloroform. The product of HIDA was confirmed by using fast atom bombardment mass spectra (JMS-700, JEOL, Tokyo, Japan) in the negative ion mode with 3-nitrobenzyl alcohol as the matrix and xenon gas to confirm HIDA molecule. As shown in **Figure 7-2 (f)**, the mass spectrum of HIDA molecule was measured. A peak derived from the molecular weight of HIDA was detected.

2.7. Adsorption Cu (II) by Lipid Membrane Coated Cryogel Particles

The synthesized HIDA and DPPC was coated on cryogel particles via impregnation method. The ratio of HIDA/DPPC = 6:4 were used for coating cryogel particles. The adsorption Cu (II) experiments were performed with 10mM $CuSO_4$ (2ml). The absorbance of Cu (II) were measured at 810 nm by using UV-Vis spectrometer at room temperature. The adsorption Cu (II) concentration of C_{adv} was calculated according to **Eq. 7-2**.

$$C_{adv} = \frac{C_{ini} - C_{flt}}{C_{ini}} \qquad \text{Eq. 7-2.}$$

where C_{ini} and C_{flt} are represented initial concentration and filterer concentration after adsorption.

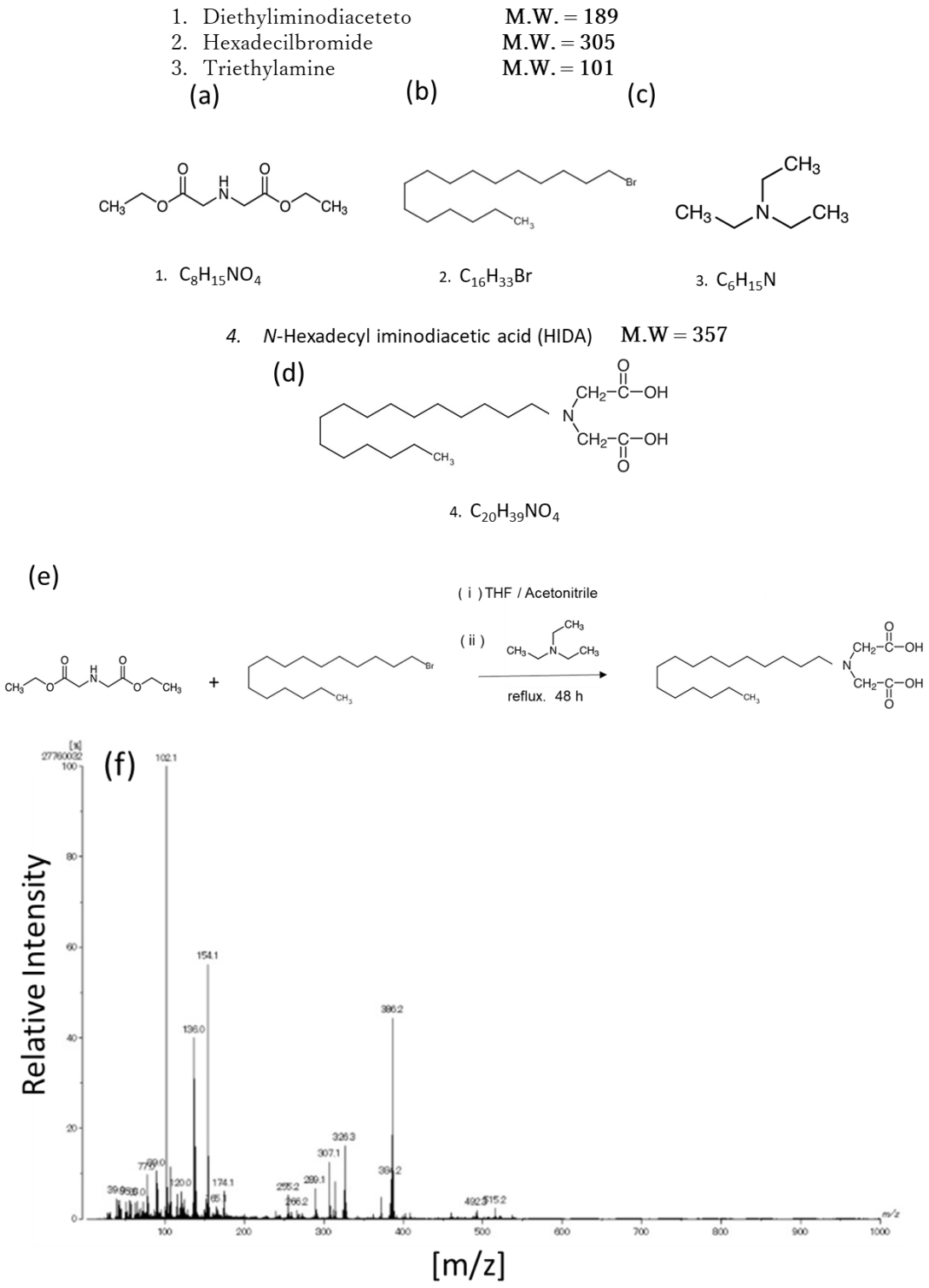

Figure 7-2. Chemical structures using for synthesis of HIDA (a) diethyliminodiacetate, (b) hexadecilbromide, and (c) triethylamine, and (d) HIDA and (e) reaction protocol, and (f) mass spectra of HIDA molecule.

3. Results and Discussion

3.1 Compression Induced Changes in Membrane Properties

In biological systems, the advanced separation (i.e, molecular recognition) and the advanced reaction (i.e, enzyme reaction and immune responses) are controlled by self-assembly membrane with highly ordered interfaces at the molecular level. Taking "biological systems" as the starting point, for example, by preparing "Bio-Inspired Materials" in which self-assembled molecules are oriented on the surface of a base material, the physical functions (e.g. elasticity) should better be added to solid polymer materials that have been conventionally utilized, where the mechanical and physical stimuli in a macro scale can be used as driving forces to interactively create a "bio-inspired material" that can be used for the development of new materials. By preparing "Bio-Inspired Materials," in which self-assembled molecules are oriented on the surface of the base material, we can create innovative separation materials in which the physical properties of the meso/micro-scale self-assembled interface can be controlled in tandem with the driving force of mechanical and physical stimuli on the macro-scale. The required basic material is a polymer carrier with elasticity and high material processability/manipulability. By combining the "inverse Leidenfrost effect (iLF effect)" and the "cryogelation method," we have developed an original method for preparing sponge-like cryogel particles without using a surfactant, which was essential for existing particle design. Herewith, the iLF-Cryo method is highly versatile, and the possibility of controlling particle size was also investigated by utilizing microfluidic channels. Furthermore, it has a bimodal internal structure, and is suitable for the separation and recovery of various emulsions. The lipid-membrane-modified polymer supports (Bio-Inspired materials) was also prepared and it has been shown that they can be applied to optical resolution of amino acids and mechanochemical separation of high-molecular-weight biomolecules. For the application to bio-separation, the modified material is created by cryogel particles which have shape-memory function with high elasticity and large capacity as a carrier modified their polymer wall by phospholipid membrane. As the strategy for inducing the sophisticated bio-separation, it can be expected to be achieved by manipulating the orientation of the modified lipid membrane by deforming the macroscopic shape of the material.

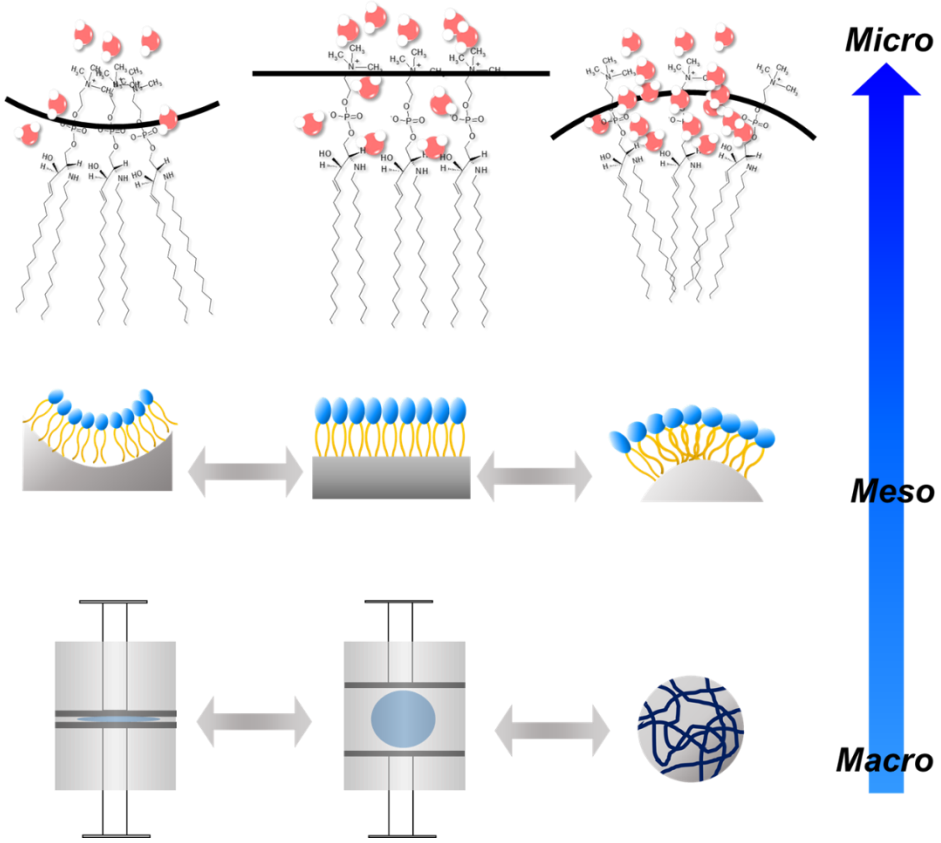

Figure 7-3. Model of sophisticated separation materials with high-performance and high-efficiency.

3.2. Membrane Properties of Coated on Cryogel Particles

The fluorescence probe Laurdan is known to be sensitive to the polarity around itself, which allows the membrane polarity of lipid membrane to be determined. The polar environment of the lipid membrane coated on cryogel particles was characterized as shown in **Fig.7-4**. It was found that the coated lipid membrane on cryogel particles have a temperature dependence of membrane properties that are similar to liposome membrane, whereas unmodified cryogel particles show no temperature dependence **(Figs.7-4 (a), (b),** and **(c))**. The fluorescent spectra of Laurdan on the coated cryogel particles have a peak at 440 nm at 25-45 ºC and the peak was drastically red-shift around at 490 nm from 50

°C **(Fig.7-4(a))**. The fluorescent spectra of liposome system were shown to indicate be same behavior of temperature-dependent manner **(Fig.7-4(b))**. It was indicated that the peak shift of the spectra caused a phase transition from ordered phase (S_o) phase to liquid disordered (l_d) phase by temperature. From the temperature dependence of fluorescence spectra of the coated cryogel particles and liposome membrane, lipid membrane coated on cryogel particles shows similar membrane properties as those of intact liposome membrane. Subsequently, the GP values was calculated based on **Eq.7-1**; it was shown that the GP value of non-coated cryogel particles was kept same upon the temperature change, whereas the coated cryogel particles have significantly decreased above 50 °C similarly in the case of intact liposome membrane (above 45 °C). At the difference of temperature points for changing temperature between the lipid coated particles and liposome, it can be considered that the phase transition temperature (T_m) of the coated lipid membrane was slightly increased because the lipid membrane supported on cryogel particles as hydrophilic substrate and be stable.

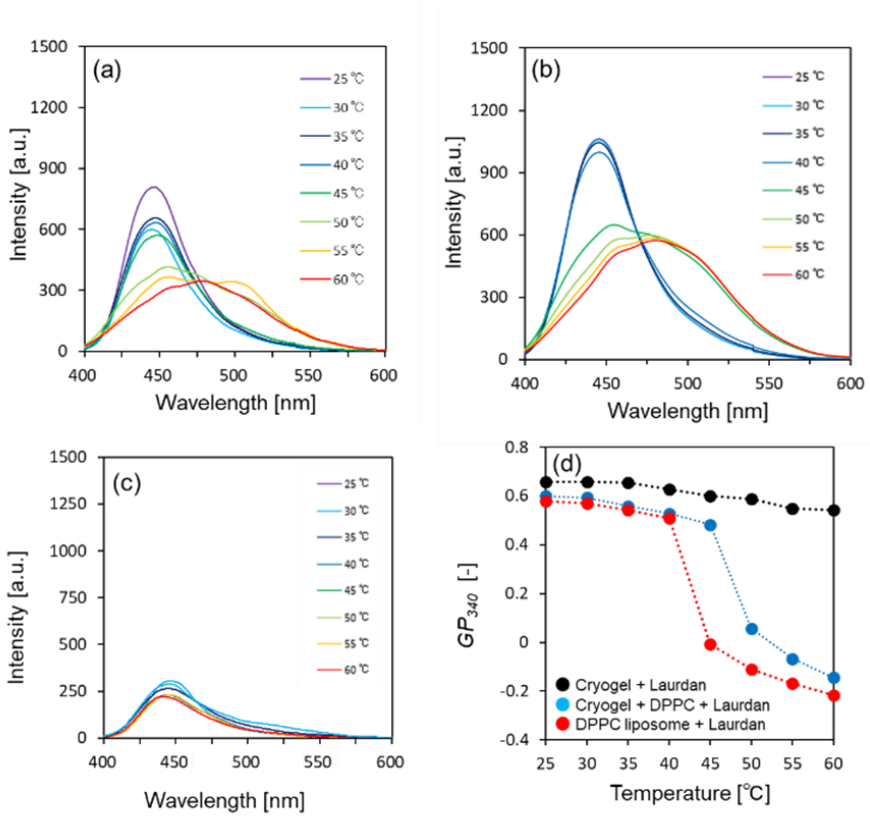

Figure 7-4. Steady-state spectra of Laurdan (a) DPPC coated cryogel, (b) DPPC-liposome (c) non-coated cryogel, and (d) GP values.

3.3. Effect of Compression for Distribution of τ and λ

Typically, the lipid membrane depended on composition of lipid kinds is behaved as rigid soft-material at below T_m, whereas become tender behavior above T_m. For example T_m of DPPC membrane is 41°C, and DOPC is -17 °C. Interestingly, the phase states of lipid membrane (i.e, l_d, l_o, and s_o) are affected in response to environmental changes such as pressure, solvent, salt concentration not only for temperature. Here, the change of the phase states of the lipid membrane could also be induced via mechanical compression. Since the curvature of the lipid membrane could be varied to become negative or positive, it is expected that the phase transition of lipid membrane could be induced among the different phases that depend on the curvature. In order to characterize the phase states of lipid membrane, the fluorescent spectra analysis of Laurdan is useful to know the polarity of the membrane interface (Justyne *et al.,* 2013). The fluorescence probe, Laurdan, in microenvironment of phospholipid bilayer membrane is known to have several emission peaks, such as 440 nm and 490 nm, that depend on the hydrophobic environment around itself. From the relative intensity of the fluorescence peaks, the polarity of lipid membrane was identified as GP_{340} at the conventional steady-state measurement mode. Recently, a new method to analyze the Laurdan fluorescence at kinetical measurement mode has been reported (Watanabe *et al.,* 2018a, 2018b); the method can be called as time-resolved fluorescent emission spectra analysis (TRES). It has been reported that the kinetic behaviors of the Laurdan fluorescence can herewith be analyzed as the fluorescence lifetime (τ) and peak position (λ) and these analyzed parameters are varied in dependent manner on the microenvironment of the phospholipid membrane. Thus, the membrane properties of phospholipid membrane coated on cryogel particles via lipid implementation method were comprehensively analyzed by the TRES, as shown in **Fig.7-5**. At the shorter lifetime (τ), the values of τ and λ for phospholipid coated bimodal cryogel particles were not significantly changed regardless of the lipid composition that differs in the phase state before and during compression. On the contrary, at the longer lifetime, the τ was shifted to be slightly shorter for DPPC-membrane coated on the cryogel. Subsequently, for the shorter lifetime, the τ value for lipid coated monomodal cryogel particles was slightly shifted to shorter as compared with the states that the longer lifetime was not significantly changed. As shown in **Fig.7-6,** the plots for fluorescence intensity

along with both τ vs. λ axis could be visually displayed to know the induced change of the membrane properties via mechanical perturbation. As summarized in **Fig.7-6**, in the DOPC system above T_m, both τ values for longer lifetime and shorter lifetime were not changed regardless of the type of cryogel particles when they are compared before compression and during compression. Furthermore, in DPPC system above T_m, they are not also changed. Interestingly, the τ value was shifted to shorter one for both type of cryogel particles below T_m. For the bimodal cryogel particles, the lifetime, τ, became longer, whereas it became the shorter for the monomodal cryogel particles. It was thus found that, among possible phase states of the phospholipid membrane, only s_o state could be affected by the mechanical compression of the cryogel and, among the porous structures of cryogel particles, the membrane properties on the bimodal particles could be affected in the longer lifetime of the TRES analysis while those of monomodal particles were not affected in the shorter lifetime. It is hypothesized that the change of membrane properties at *micro-*/*meso*-scale could be regulated via macroscopic mechanical perturbation because of the change of the variation of the curvature at both *micro-*/*meso*- and macro-scopic viewpoints, especially in the case of the "rigid lipid-states" and the "porous properties of the cryogel particle".

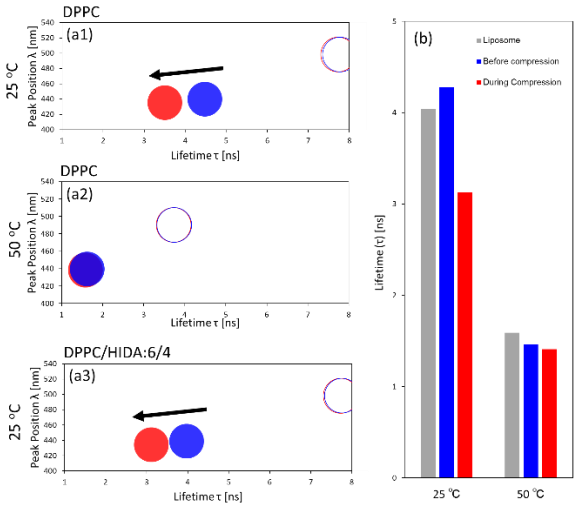

Figure 7-5. Membrane fluorescence map of Laurdan. The filled and open plots indicated as used carrier material; monomodal and bimodal porous cryogel particles, respectively, and the colored as blue and red represented as the before compression state and during one.

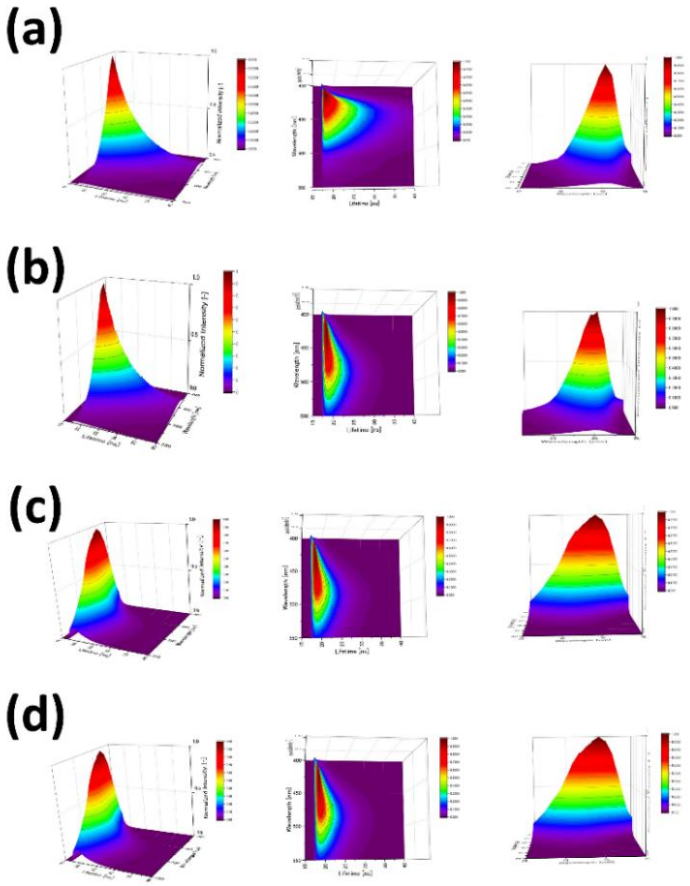

Figure 7-6. The plots of intensity vs. τ vs. λ for DPPC coated on monomodal cryogel particles. (a) the before compression and (b) during compression at 25 ºC, and (c) the before compression and (d) during compression at 50 ºC.

3.4. Metal-affinity of Lipid Membrane Modified Polymer Particles

In order to achieve the sophisticated separation that has high performance with high-selectivity and high-efficiency, it is a key point that the core material must hierarchically be designed from macroscopic to microscopic viewpoint. Herewith, the ordered alignment of the phospholipid molecules at the self-assembled membrane at "molecular level" could be deformed via the mechanical perturbation after the macroscopic compression of the supported carrier material. It is herewith indicated that the membrane properties have a potential to be changed by mechanical force expect other eternal force (i.e, temperature, pH, solvent, concentration of salt).

By inducing the membrane properties change from other external forces, except for

mechanical perturbation, as driven-force, the effects of the external forces on the target molecules cannot be ignored, where it could also affect the membrane properties and, therefore, the critical understanding of the molecular mechanism, resulting in the specific application especially in the case of “bio-inspired” separation. Therefore, the designed material is expected to widely utilize for application to bio-separation, analysis of biological event, and bio-sensor with the different aspect of typical material.

As shown in **Fig.7-7**, the adsorption behavior of cupper via the lipid membrane coated on cryogel particles. From the absorbance spectra of cupper, the concentration in bulk solution was decreased 3 hours after the addition of the cupper solution into the aqueous solution suspending the cryogel particles modified with phospholipid membrane. As a result, it was revealed that the lipid membrane coated on the cryogel particles have the potential of metal affinity. The metal affinity function of the particles was caused by the composition of membrane on the cryogel particle. Here, the HIDA molecules were performed as metal affinity ligand because have the imidazole functional group at head of itself.

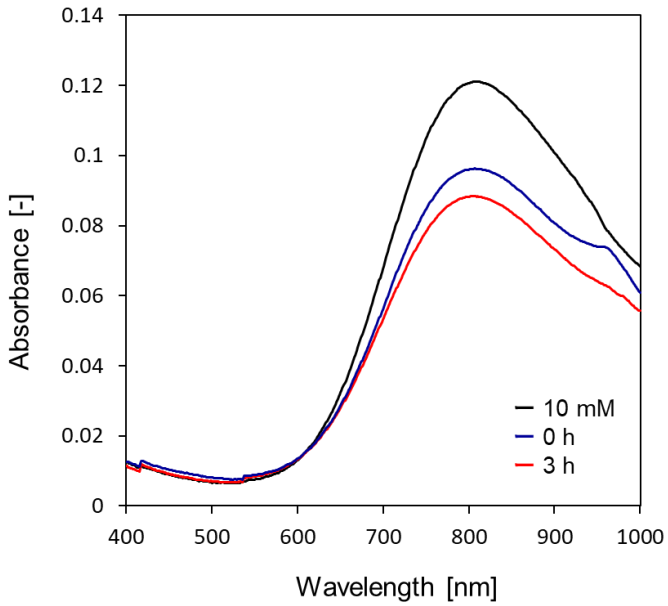

Figure 7-7. Adsorption behavior of cupper by using lipid membrane coated cryogel particles.

3.5. Model of Sophisticated Bioseparation

The overall design for separation material at macro/meso/micro scale is essential to establish the sophisticated bioseparation. As shown in **Fig.7-8**, the schematic illustration of sophisticated bioseparation model by phospholipid membrane modified polymer particles are described. In macroscopic scale, the core material designed that cryogel particles have sponge-like mechanical properties with high porosity. Since cryogel particle drastically deforms and restores its shape at macro scale by mechanical force at state of released and compressed, the deformation ratio can be evaluate from the ΔA by microscope image. According to the macroscopic deformation, the lipid membrane modified on the surface of polymer particles can be affected, at meso scale, membrane properties because membrane curvatures are changed. The change of membrane properties can be revealed by the fluorescence analysis technique (i.e, steady-state spectra and TRES). Focusing on TRES analysis for state of compression and release, the state of lipid membrane can be controlled as S_o-like and l_d-like on the polymer surface. Subsequently, the change of membrane properties can be implied that the interactions between lipid membrane and target molecules (i.e, metals, biomolecules, drug molecules), at micro scale, can be expected to control. Since the membrane curvature is changed as positive, neutral, and negative, the orientation of lipid molecules can be attributed by microshape of polymer surface. Hence, the adsorption/desorption properties by mechanical stimuli for phospholipid membrane modified polymer particles can be expected to manipulate.

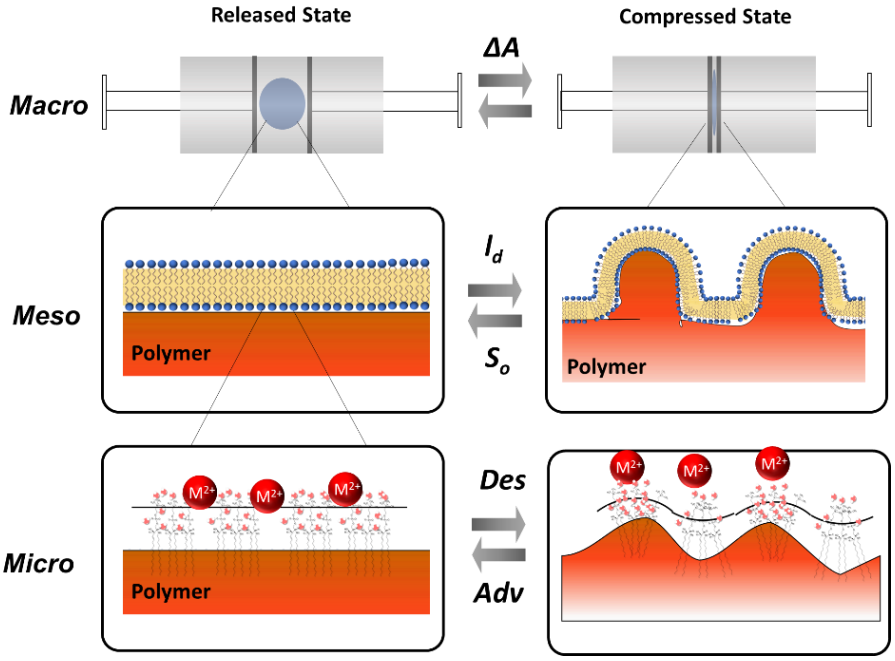

Figure 7-8. Schematic illustration of sophisticated separation by phospholipid membrane modified polymer particles.

4. Summary

In this chapter, a case study of the sophisticated bio-separation has been demonstrated that the lipid membrane coated on cryogel particles adsorbed metal ion from aqueous solution. This work was described following there three points; (i) preparation of lipid membrane coated cryogel particles, (ii) TRES investigation of the changing membrane properties coated on cryogel particles via mechanical compression, and (iii) characterization of metal affinity properties by using affinity-ligand lipid coated cryogel particles. Firstly, the lipid membrane coated cryogel particles were prepared by adopting lipid impregnation method, as described on chapter 5, revealing the formation of lipid membrane on the cryogel particles by characterization of temperature dependence steady-state fluorescence analysis. Since the Laurdan fluorescence behavior was similar with that of liposome, the supported lipid membrane on cryogel particles were shown to have similar membrane properties with liposome membrane. Subsequently, for TRES investigation, the changing membrane properties by mechanical compression were comprehensibly characterized from the relevance fluorescent intensity, at distinct conditions that differ in λ and τ. It was therefore found that the variation of the lipid membrane with rigid state (i.e, S_o) was induced by the changing membrane property under the mechanical compression. Interestingly, the behavior of changing membrane property was also related with porous structure of the carrier cryogel particles. Finally, the separation of metal ion was achieved by using metal-affinity ligand lipid coated cryogel particles. Hence, the affinity-ligand lipid coated cryogel particles could have a potential to applicate for separation device such as chromatography.

Chapter 8

General Conclusion

The cone materials for the sophisticated bioseparation was established in order to realize high-performance separation material with high-selectivity and high-efficiency. To develop the material, it is essential to comprehensively design the material from macroscopic scale and microscopic scale. From the macroscopic viewpoint, it was focused on substrate material which have elasticity and porous structure for modification self-assembly molecules such as lipid membrane. Subsequently, from the microscopic viewpoint, the lipid membrane which is highly-ordered by self-assembly was selected as the modified of the polymer particle because it has potentials which can manipulate their properties via mechanical stimuli. By employing these elastic porous substrate and lipid membrane, the possibility to develop a sophisticated bioprocess that could induce a breakthrough in conventional bioprocess was investigated.

In Chapter 2, the preparation method for sponge-like elastic cryogel particles with porous structure was established. For preparation of cryogel particles, the process was described as two steps; 1) preparation of frozen particles by using inverse Leidenfrost effect and 2) cryo-polymerization under frozen temperature. According to the characterization of prepared cryogel particles, it was found that the monolithic supermacroporous structure was observed by using SEM. Furthermore, the swelling degree and the porosity of cryogel particles with HEMA (monomer) and MBA (cross-linker) could be controlled by ratio of monomer/cross-linker. The cryogel particles were confirmed to poses elasticity and shape-memory function, resembling those of a sponge. Notably, the shape deformation ratio of the cryogel particles reached 93.4 %, while exhibiting good reversibility features. Overall, the method proposed herein is prospected to provide an auspicious platform for the design and preparation of various polymer materials with sponge-like mechanical properties. In particular, the cryogel particles obtained here are attractive for the design of mechanical stimuli-responsive materials, such as biosensors with added bio-separation/purification functionalities.

In Chapter 3, the versatility of preparation method was revealed by demonstrated

to preparation with adopting different type of precursor (i.e. hydrophobic monomer, hydrophilic monomer, and natural polymer). As the notably point, the preparation method for polymer particles, was designed without “surfactant” in whole the process. All type of prepared cryogel particles via the method were systematically and comprehensively characterized. The particle size, sphericity, porosity, and elasticity were characterized as the physical properties of cryogel particles. It was revealed that all type of cryogel particles have high sphericity (> 92 %) with large porosity (> 74 %). As the result of mechanical properties, there are some slight difference in detail characteristic. The type of hydrophobic cryogel particles with using HEMA, NIPA, AAm for precursor show the shape-memory function; deformation and restoration of the shape by mechanical compression. Nevertheless, type of pTrim did not have shape-memory function. In the case of agarose type, it takes time for restoration of shape. Totally, this preparation method was found to be versatile and could possibly be beneficial for the “*tailor-made*” because of no-limitation caused by detergents for emulsion formation.

In Chapter 4, the hierarchical porous structure of cryogel particles was controlled aspect of size (i.e. supermacropores, and macropores) and shape (i.e. directional pores and open-pores). It was expected that controlled porous structure was optimized for separation material. As a whole, morphologies of cryogel particles were revealed from SEM images and MIP analysis. For the monomodal porous cryogel particles, it has monolithic supermacroporous structure on surface side and directional porous structure was distributed from surface to interior of the particles. For the bimodal porous cryogel particles, it was found that monolithic supermacroporous structure with microporous structure as open-pore shape formed on the polymer wall and directional porous structure was also distributed with the macropores on the polymer wall. Subsequently, the performance of cryogel particles was confirmed from macroscopic diffusion test and kinetics of swelling degree. It was found that bimodal porous cryogel particles could be beneficial for the mass transfer to the entire the particle through the pores and could have ultrafast swelling ability. Therefore, the porous designed cryogel particles have potential to application to separation carrier with those porous properties.

In Chapter 5, the polymer surface modification method with lipid membrane was systematically and comprehensively designed and suggested. The method was

categorized as (1) vesicle fusion method, (2) O/W emulsion method, and (3) impregnation method. Based on **Scheme 5-1**, it can be designed the optimal polymer particles modified with phospholipid membrane. Beforehand, the hydrophobic cryogel particles were characterized with focusing on particle properties such as D_v, ρ, Cv, σ_{bulk}, and size distribution of pore size. Furthermore, the hydrophobicity of cryogel particles was tested by placing aqueous and organic droplet on the particles. While the aqueous droplet was held on the particle by repelling force, the organic droplet was immediately adsorbed into the particle due to the hydrophobic polymer surface. It was found that the adsorbed organic solvent was diffused into entire the particle by observation cross-section of the cryogel particles. As the case study, it was demonstrated that the separation of O/W emulsions stabilized with surfactant were accomplished by using hydrophobic cryogel particles. It can be indicated that the surfactant using for emulsion stabilization distributed and modified on the polymer surface through the separation process.

In Chapter 6, the utility of impregnation method was demonstrated by impregnation lipid molecules with solvent in porous polymer particles and evaporated the solvent. It was compared the functions with lipid membrane modified with the particles and liposome membrane. The hydrophobic polymer particles modified with phospholipid membrane were performed the chiral recognition of amino acid above T_m and below T_m of phospholipid membrane. As the result, the modified lipoid membrane on polymer surface was accomplished chiral recognition below T_m similar as liposome membrane system. Aspect of analysis of UV-spectra for the particles after chiral adsorption, it could be implied that the adsorbed amino acid was diffused into hydrophobic region of lipid membrane. For the practical application, the chiral separation of amino acid by using lipid modified polymer particles were performed under racemic solution. It was found that the modified polymer particles preferentially adsorbed L- amino acid. Thus, it has potential of chiral selective adsorption of amino acid which can used as optical resolution materials. Since the modified lipid membrane have a molecular recognition function same as liposome membrane, the utility of impregnation method was revealed.

In Chapter 7, the whole designed the material at molecular scale to at bulk scale was investigated the physicochemical properties of the modified lipid membrane. Consequently, the changing membrane properties was induced by mechanical

compression of cryogel particles. As the macroscopic view, the sponge-like cryogel particles were drastically changed their shape by mechanical compression. According to the shape deformation, the modified lipid on polymer surface could be caused the membrane curvature at meso scale. Thus, the orientation of molecules with highly-ordered and self-assembly by mechanical stimuli as microscopic scale at molecular level have potentially attributed to change the various kinds of interactions.

In summary, it is expected that the sophisticated bioseparation can be designed based on two schemes for polymer particles and for their modification with lipid membrane by the interactions of target molecules on lipid membrane are controlled by mechanical compression of cryogel particles.

Nomenclatures

A	= area of the particle after compression	[μm^2]
A_o	= area of area of the particle before compression	[μm^2]
C_{ini}	= initial concentration of amino acid	[mM]
C_{flt}	= filtered concentration of amino acid	[mM]
C_P	= phosphorus concentration	[mM]
C_v	= coefficient of variation	[-]
d_0	= needle's interior diameter	[μm]
D_v	= The mean diameter of the particles	[μm]
D	= pore diameter of porous polymer particle	[μm]
e.e.	= Enantiomer excess	[%]
E_{DPPC}	= entrapped amount of DPPC in PPP	[mol]
g	= gravitational force	[g・cm/s^2]
I	= Intensity of fluorescence	[-]
Log P	= partition coefficient	[-]
M_w	= molecular weight of phosphorus	[g/mol]
P	= mercury pressure	[psia]
q	= adsorbed amount of amino acid per DPPC molecule	[-]
R	= Maximum diameter of cryogel particle	[μm]
r	= Minimum diameter of cryogel particle	[μm]
S	= Sphericity of cryogel particle	[%]
T_m	= Phase transition temperature	[^{o}C]
$V_{cylinder}$	= Volume of particles in gradual cylinder	[cm^3]

V_d	= Volume of precursor droplet	[µl]
V_s	= Volume of solution	[µl]
W	= Weight	[g]
ρ	= density of solution	[g/ml]
ρ_{bulk}	= tapped bulk density	[g/ml]
σ	= surface tension	[mN/m]
γ	= surface tension of mercury	[mN/m]
θ	= contact angle of liquid mercury	[-]
τ	= fluorescence lifetime	[s]
λ	= peak position	[nm]
ε	= relative dielectric constant	[-]
φ	= porosity of cryogel particle	[-]

List of Abbreviations

AA	Amino acid
AAm	Acrylamide
AES	Atomic emission spectroscopy
APS	Ammonium persulfate
BPO	Benzoyl peroxide
CCD	Charge-coupled device
CCB	Coomassie brilliant blue G-250
DMSO	Dimethyl sulfoxide
DNA	Deoxyribonucleic acid
DOPC	1,2-Dioleoyl-*sn*-glycero-3-phosphocholine
DPPC	1,2-Dipalmitoyl-*sn*-glycero-3-phosphocholine
DVB	Divinylbenzene
EDMAB	Ethyl-4-dimethylaminobenzoate
EDX	Energy dispersed X-ray
GP_{340}	General polarization calculated at exciting light at 340 nm
HEMA	2-Hydroxyethylmethacrylate
His	Histidine
HIDA	*N*-Hexadecyl iminodiacetic acid
ICP	Inductively coupled plasma
iLF	inversed Leidenfrost effect
KPS	Potassium persulfate
Laurdan	6-Lauroyl-2-dimethylamino naphthalene

l_d	Liquid disordered phase
l_o	Liquid ordered phase
MBA	*N, N'*-Methylenebisacrylamide
MIP	Mercury intrusion porosimeter
NIPA	*N*-Isopropylacrylamide
O/W	Oil-in-water
AA	Amino acid
PIPS	Polymerization induced phase separation
PPP	Porous polymer particle
RNA	Ribonucleic acid
SD	Swelling degree
SEM	Scanning electronic microscope
S_o	Solid ordered phase
TEMED	*N,N,N′,N′*-tetramethylethylenediamine
THF	Tetrahydrofuran
TIPS	Temperature induced phase separation
T_m	Phase transition temperature
TRES	Time-resolved emission spectra
Trim	Trimethylolpropane trimethacrylate
Trp	Tryptophan
UV-Vis	Ultraviolet-visible
W/O/W	Water-in-oil-in-water

References

Abdulrazzaq Hadi, A.; Abdulkhabeer Ali, A. Chemical Demulsification Techniques in Oil Refineries: A Review. *Mater. Today Proc*, **2022**, *53*, 58–64.

Abshirini, M; Saha, Mrinal. Synthesis and Characterization of Hierarchical Porous Structure of Hierarchical Porous Structure of Polydimethylsiloxane (PDMS) Sheets via Two-step Phase Separation Method, *Mat.Des*, **2021**, *212*, 110194.

Ammann, S.; Ammann, A.; Ravotti, R.; Fischer, L. J.; Stamatiou, A.; Worlitschek, J. Effective Separation of Awater in Oil Emulsion from a Direct Contact Latent Heat Storage System. *Energies*, **2018**, *11*, 2264.

Andaç, M.; Baydemir, G.; Yavuz, H.; Denizli, A. Molecularly Imprinted Composite Cryogel for Albumin Depletion from Human Serum. *J. Mol. Recognit*. **2012**, *25*, 555–563.

Arrieta, J.; Sevilla, A. On the Flow Separation Mechanism in the Inverse Leidenfrost Regime, *J. Fluid Mech*, **2020**, *897*, 1-18.

Aydoğan, C.; Andaç, M.; Bayram, E.; Say, R.; Denizli, A. Molecularly Imprinted Cryogel for L-Glutamic Acid Separation. *Biotechnol. Prog*, **2012**, *28*, 459–466.

Baimenov, A.; Montagnaro, F.; Inglezakis, V. J.; Balsamo, M. Experimental and Modeling Studies of Sr^{2+} and Cs^{+} Adsorption on Cryogels and Comparison to Commercial Adsorbents. *Ind. Eng. Chem. Res*, **2022**, *61*, 8204–8219.

Bao, S.; Wu, D.; Su, T.; Wu, Q.; Wang, Q. Microgels Formed by Enzyme-Mediated Polymerization in Reverse Micelles with Tunable Activity and High Stability. *RSC Adv*, **2015**, *5*, 44342–44345.

Batchuluun, S.; Matsune, H.; Shiomori, K.; Bayanjargal, O.; Baasankhuu, T. Preparation of Polystyrene Microcapsules Containing Saline Water Droplets via Solvent Evaporation Method and Their Structural Distribution Analysis by Machine Learning. *J. Chem. Eng. Japan*, **2021**, *54*, 517–524.

Béduer, A.; Braschler, T.; Peric, O.; Fantner, G. E.; Mosser, S.; Fraering, P. C.; Benchérif, S.; Mooney, D. J.; Renaud, P. A Compressible Scaffold for Minimally Invasive Delivery of Large Intact Neuronal Networks. *Adv. Healthc. Mater*, **2015**, *4*, 301–312.

Bencherif, S. A.; Sands, R. W.; Bhatta, D.; Arany, P.; Verbeke, C. S.; Edwards, D. A.; Mooney, D. J. Injectable Preformed Scaffolds with Shape-Memory Properties. *Proc. Natl. Acad. Sci. U. S. A*, **2012**, *109*, 19590–1959.

Bereli, N.; Ertürk, G.; Tümer, M. A.; Say, R.; Denizli, A. Oriented Immobilized Anti-

HIgG via Fc Fragment-Imprinted PHEMA Cryogel for IgG Purification. *Biomed. Chromatogr*, **2013**, *27*, 599–607.

Cambiella, A.; Benito, J. M.; Pazos, C.; Coca, J. Centrifugal Separation Efficiency in the Treatment of Waste Emulsified Oils. *Chem. Eng. Res. Des*, **2006**, *84*, 69–76.

Causon, T. J.; Shellie, R. A.; Hilder, E. F. Kinetic Performance Appraisal of Poly(Styrene-*co*-Divinylbenzene) Monolithic High-Performance Liquid Chromatography Columns for Biomolecule Analysis. *Journal of Chromatography A*, **2010**, *1217*, 3765–3769.

Cevc, G. Membrane Electrostatics. *Biochimica et Biophysica Acta (BBA) - Reviews on Biomembranes*, **1990**, *1031*, 311–382.

Chen Y.; Ma W. The origin of biological homochirality along with the origin of life. *PLOS Computational Biology*, **2020**, *16* (1), e1007592.

Chen, K.; Sheng, Y.; Wang, J.; Wang, W. Chirality-Dependent Adsorption between Amphipathic Peptide and POPC Membrane. *International Journal of Molecular SciencesI*, **2019**, *20*, 4760.

Chen, W.; Wang, T.; Dou, Z.; Xie, X. Self-Driven Pretreatment and Room-Temperature Storage of Water Samples for Virus Detection Using Enhanced Porous Superabsorbent Polymer Beads. *Environ. Sci. Technol*, **2021**, *55*, 14059–14068.

Chen, X.; Sui, W.; Ren, D.; Ding, Y.; Zhu, X.; Chen, Z. Synthesis of Hydrophobic Polymeric Cryogels with Supermacroporous Structure. *Macromol. Mater. Eng*, **2016**, *301*, 659–664.

Corradini, R.; Sforza, S.; Tedeschi, T.; Marchelli, R. Chirality as a Tool in Nucleic Acid Recognition: Principles and Relevance in Biotechnology and in Medicinal Chemistry. *Chirality*, **2007**, *19*, 269–294.

Czerwinska, J.; Parkin, M. C.; Cilibrizzi, A.; George, C.; Kicman, A. T.; Dargan, P. I.; Abbate, V. Pharmacokinetics of Mephedrone Enantiomers in Whole Blood after a Controlled Intranasal Administration to Healthy Human Volunteers. *Pharmaceuticals*, **2021**, *14*, 5.

Dhamecha, D.; Le, D.; Movsas, R.; Gonsalves, A.; Menon, J. U. Porous Polymeric Microspheres With Controllable Pore Diameters for Tissue Engineered Lung Tumor Model Development. *Front. Bioeng. Biotechnol*, **2020**, *8*, 1–16.

Do Nascimento, D. F.; Avendaño, J. A.; Mehl, A.; Moura, M. J. B.; Carvalho, M. S.; Duncanson, W. J. Flow of Tunable Elastic Microcapsules through Constrictions. *Sci. Rep*, **2017**, *7*, 1–7.

Dolstra, C. C.; Rinker, T.; Sankhagowit, S.; Deng, S.; Ting, C.; Dang, A. T.; Kuhl, T. L.; Sasaki, D. Y. Mechanism of Acid-Triggered Cargo Release from Lipid

Bilayer-Coated Mesoporous Silica Particles. *Langmuir* **2019**, *35*, 10276–10285.

Doshi, B.; Sillanpää, M.; Kalliola, S. A Review of Bio-Based Materials for Oil Spill Treatment. *Water Res*, **2018**, *135*, 262–277.

Eivgi, O.; Blum, S. A. Real-Time Polymer Viscosity–Catalytic Activity Relationships on the Microscale. *J. Am. Chem. Soc.* **2022**, *144*, 13574– 13585.

Erber, M.; Lee, G. Production and Characterization of Rapidly Dissolving Cryopellets. *J. Pharm. Sci*, **2015**, *104*, 1668–1676.

Fu, G.-D.; Shang, Z.; Hong, L.; Kang, E.-T.; Neoh, K.-G. Nanoporous, Ultralow-Dielectric- Constant Fluoropolymer Films from Agglomerated and Crosslinked Hollow Nanospheres of Poly(Pentafluorostyrene)-Block-Poly(Divinylbenzene). *Advanced Materials*, **2005**, *17*, 2622–2626.

Gauthier, A.; Lajoinie, G.; Snoeijer, J. H.; van der Meer, D. Inverse Leidenfrost Drop Manipulation Using Menisci. *Soft Matter*, **2020**, *16*, 4043–4048.

Ghisaidoobe, A. B. T.; Chung, S. J. Intrinsic Tryptophan Fluorescence in the Detection and Analysis of Proteins: A Focus on Förster Resonance Energy Transfer Techniques. *International Journal of Molecular Sciences*, **2014**, *15*, 22518–22538.

Gokmen, M. T.; Du Prez, F. E. Porous Polymer Particles—A Comprehensive Guide to Synthesis, Characterization, Functionalization and Applications. *Progress in Polymer Science*, **2012**, *37*, 365–405.

Goodarzi, F.; Zendehboudi, S. A Comprehensive Review on Emulsions and Emulsion Stability in Chemical and Energy Industries. *Can. J. Chem. Eng*, **2019**, *97*, 281–309.

Grundy, L. S.; Lee, V. E.; Li, N.; Sosa, C.; Mulhearn, W. D.; Liu, R.; Register, R. A.; Nikoubashman, A.; Prud'Homme, R. K.; Panagiotopoulos, A. Z.; Priestley, R. D. Rapid Production of Internally Structured Colloids by Flash Nanoprecipitation of Block Copolymer Blends. *ACS Nano*, **2018**, *12*, 4660–4668.

Guan, X.; Jiang, H.; Ngai, T. Pickering high internal phase emulsions templated super-hydrophobic–oleophilic elastic foams for highly efficient oil/water separation. *ACS Appl. Polym. Mater.* **2020**, *2*, 5664– 5673.

Guastaferro, M.; Baldino, L.; Reverchon, E.; Cardea, S. Production of Porous Agarose-Based Structures: Freeze-Drying vs. Supercritical CO_2 Drying. *Gels*, **2021**, *7*, 198.

Guo, F.; Wang, Y.; Chen, M.; Wang, C.; Kuang, S.; Pan, Q.; Ren, D.; Chen, Z. Lotus-Root-like Supermacroporous Cryogels with Superphilicity for Rapid Separation of Oil-in-Water Emulsions. *ACS Appl. Polym. Mater*, **2019**, *1*, 2273–2281.

Han, S.; Feng, Y.; Zhang, F.; Yang, C.; Yao, Z.; Zhao, W.; Qiu, F.; Yang, L.; Yao, Y.;

Zhuang, X.; Feng, X. Metal-Phosphide-Containing Porous Carbons Derived from an Ionic-Polymer Framework and Applied as Highly Efficient Electrochemical Catalysts for Water Splitting. *Adv. Funct. Mater*, **2015**, *25*, 3899–3906.

Han, S.; Choi, J.; Seo, Y. P.; Park, I. J.; Choi, H. J.; Seo, Y. High-Performance Magnetorheological Suspensions of Pickering-Emulsion-Polymerized Polystyrene/Fe_3O_4 Particles with Enhanced Stability. *Langmuir*, **2018**, *34*, 2807– 2814.

Hashmi, S. M.; Dufresne, E. R. Mechanical Properties of Individual Microgel Particles through the Deswelling Transition. *Soft Matter*, **2009**, *5*, 3682–3688.

Hiramure, Y.; Suga, K.; Umakoshi, H.; Matsumoto, J.; Shiomori, K. Preparation and Characterization of Poly-N-Isopropylacrylamide Cryogels Containing Liposomes and Their Adsorption Properties of Tryptophan. *Solvent Extr. Res. Dev*, **2018**, *25*, 37–46.

Hirose, M.; Sugisaki, S.; Suga, K.; Umakoshi, H. Detection of L-Proline-Catalyzed Michael Addition Reaction in Model Biomembrane *J. Chem.* **2019**, No. 4926438.

Hixon, K. R.; Lu, T.; Sell, S. A. A Comprehensive Review of Cryogels and Their Roles in Tissue Engineering Applications. *Acta Biomater*, **2017**, *62*, 29–41.

Hou, Q.; Grijpma, D. W.; Feijen, J. Porous Polymeric Structures for Tissue Engineering Prepared by a Coagulation, Compression Moulding and Salt Leaching Technique. *Biomaterials*, **2003**, *24*, 1937–1947.

Hu, J.; Cochrane, W. G.; Jones, A. X.; Blackmond, D. G.; Paegel, B. M. Chiral Lipid Bilayers Are Enantioselectively Permeable. *Nat. Chem.* **2021**, 1–6.

Hussain, M.Regulation of Drug Release by Tuning Surface Textures of Biodegradable Polymer Microparticles. *ACS Appl. Mater. Interfaces* **2017**, *9*, 14391– 14400

Inda, N. I.; Fukumaru, M.; Sana, T.; Kiyoyama, S.; Takei, T.; Yoshida, M.; Nakajima, A.; Shiomori, K. Characteristics and Mechanism of Cu(II) Extraction with Polymeric Particles with Interconnected Spherical Pores Impregnated with LIX84-I. *Journal of Chemical Engineering of Japan*, **2017**, *50*, 102–110.

Ishigami, T.; Suga, K.; Umakoshi, H. Chiral Recognition of L-Amino Acids on Liposomes Prepared with l-Phospholipid. *ACS Appl. Mater. Interfaces*,**2015**, *7*, 21065–21072.

Izza, N.; Watanabe, N.; Okamoto, Y.; Suga, K.; Wibisono, Y.; Kajimura, N.; Mitsuoka, K.; Umakoshi, H. Dependence of the Core-Shell Structure on the Lipid Composition of Nanostructured Lipid Carriers: Implications for Drug Carrier Design. *ACS Appl. Nano Mater*, **2022**, *5*, 9958–9969.

Jensen, B. E. B.; Dávila, I.; Zelikin, A. N. Poly(vinyl alcohol) Physical Hydrogels: Matrix-Mediated Drug Delivery Using Spontaneously Eroding Substrate. *J. Phys. Chem. B*, **2016**, *120*, 5916– 5926

Juan, L. T.; Lin, S. H.; Wong, C. W.; Jeng, U. S.; Huang, C. F.; Hsu, S. H. Functionalized Cellulose Nanofibers as Crosslinkers to Produce Chitosan Self-Healing Hydrogel and Shape Memory Cryogel. *ACS Appl. Mater. Interfaces*, **2022**, *14*, 36353–36365.

Kartal, F.; Denizli, A. Molecularly Imprinted Cryogel Beads for Cholesterol Removal from Milk Samples. *Colloids Surfaces B Biointerfaces*, **2020**, *190*, 110860.

Kirsebom, H.; Rata, G.; Topgaard, D.; Mattiasson, B.; Galaev, I. Y. Mechanism of Cryopolymerization: Diffusion-Controlled Polymerization in a Nonfrozen Microphase. An NMR Study. *Macromolecules*, **2009**, *42*, 5208–5214.

Kirsebom, H.; Topgaard, D.; Galaev, I. Y.; Mattiasson, B. Modulating the Porosity of Cryogels by Influencing the Nonfrozen Liquid Phase through the Addition of Inert Solutes. *Langmuir*, **2010**, *26*, 16129–16133.

Kitabayashi, T.; Sana, T.; Kiyoyama, S.; Takei, T.; Yoshida, M.; Shiomori, K. Extraction Properties of Nickel (II) with Polymeric Particles with Interconnected Spherical Pores Impregnating with LIX84-I. *Solvent Extraction Research and Development, Japan*, **2013**, *20*, 137–147.

Kızılbey, K. Optimization of rutin-loaded PLGA nanoparticles synthesized by single-emulsion solvent evaporation method. *ACS Omega*, **2019**, *4*, 555– 562.

Kulkarni, P. S.; Patel, S. U.; Chase, G. G. Layered Hydrophilic/Hydrophobic Fiber Media for Water-in-Oil Coalescence. *Sep. Purif. Technol*, **2012**, *85*, 157–164.

Kumar, A.; Mishra, R.; Reinwald, Y.; Bhat, S. Cryogels: Freezing Unveiled by Thawing. *Mater. Today*, **2010**, *13*, 42–44.

Kumar, A.; Srivastava, A. Cell Separation Using Cryogel-Based Affinity Chromatography. *Nat. Protoc*, **2010**, *5*, 1737–1747.

Kumar, R.; Das, A. K. Numerical Study of Boiling of Liquid Nitrogen at Solid and Liquid Contact Planes. *Int. J. Heat Mass Transf*, **2022**, *183*, 122075.

Kumari, J.; Kumar, A. Development of Polymer Based Cryogel Matrix for Transportation and Storage of Mammalian *Cells. Sci. Rep*, **2017**, *7*, 1–13.

Kurniawan, J.; Ventrici de Souza, J. F.; Dang, A. T.; Liu, G.; Kuhl, T. L. Preparation and Characterization of Solid-Supported Lipid Bilayers Formed by Langmuir–Blodgett Deposition: A Tutorial. *Langmuir*, **2018**, *34*, 15622–15639.

Li, Z.; Liu, H.; Zeng, L.; Liu, H.; Yang, S.; Wang, Y. Preparation of High Internal

Water-Phase Double Emulsions Stabilized by a Single Anionic Surfactant for Fabricating Interconnecting Porous Polymer Microspheres. *Langmuir*, **2014**, *30*, 12154–12163.

Lin, W.; Mu, C.; Liu, F.; Cheng, Q.; Li, H.; Wu, B.; Zhang, G. Collagen Cryogel Cross-Linked by Dialdehyde Starch. *Macromol. Mater. Eng*, **2010**, *295*, 100–107.

Lotierzo, A.; Bon, S. A. F. A Mechanistic Investigation of Pickering Emulsion Polymerization. *Polym. Chem*, **2017**, *8*, 5100–5111.

Luo, C.; Okubo, T.; Nangrejo, M.; Edirisinghe, M. Preparation of Polymeric Nanoparticles by Novel Electrospray, *Nanoprecipitation. Polym. Int*, **2015**, *64*, 183–187.

Luz, I.; Toy, L.; Rabie, F.; Lail, M.; Soukri, M. Synthesis of Soluble Metal Organic Framework Composites for Mixed Matrix Membranes. *ACS Appl. Mater. Interfaces*, **2019**, *11*, 15638–15645.

Matsumoto, R.; Hasegawa, K. Self-Propelled Leidenfrost Droplets on a Heated Glycerol Pool. *Sci. Rep*, **2021**, *11*, 1–7.

Matsushita, A.; Sana, T.; Kiyoyama, S.; Yoshida, M.; Shiomori, K. Preparation of Microcapsules Containing PC-88A with Interconnected Spherical Pores and Their Extraction Properties for Zn (II). *Solvent Extraction Research and Development, Japan*, **2011**, *18*, 123–135.

McClements, D. J.; Jafari, S. M. Improving Emulsion Formation, Stability and Performance Using Mixed Emulsifiers: A Review. Adv. *Colloid Interface Sci*, **2018**, *251*, 55–79.

Memic, A.; Colombani, T.; Eggermont, L. J.; Rezaeeyazdi, M.; Steingold, J.; Rogers, Z. J.; Navare, K. J.; Mohammed, H. S.; Bencherif, S. A. Latest Advances in Cryogel Technology for Biomedical Applications. *Adv. Ther*, **2019**, *2*, 1–45.

Merakchi, A.; Bettayeb, S.; Drouiche, N.; Adour, L.; Lounici, H. Cross-Linking and Modification of Sodium Alginate Biopolymer for Dye Removal in Aqueous Solution. *Polym. Bull*, **2019**, *76*, 3535–3554.

Mi, H. Y.; Jing, X.; Liu, Y.; Li, L.; Li, H.; Peng, X. F.; Zhou, H. Highly Durable Superhydrophobic Polymer Foams Fabricated by Extrusion and Supercritical CO_2 Foaming for Selective Oil Absorption. *ACS Appl. Mater. Interfaces*, **2019**, *11*, 7479–7487.

Milakin, K. A.; Trchová, M.; Acharya, U.; Breitenbach, S.; Unterweger, C.; Hodan, J.; Hromádková, J.; Pfleger, J.; Stejskal, J.; Bober, P. Effect of Initial Freezing Temperature and Comonomer Concentration on the Properties of Poly(Aniline-*co*-*m*-Phenylenediamine) Cryogels Supported by Poly(Vinyl Alcohol). *Colloid Polym.*

Sci, **2020,** *298*, 293–301.

Mohamed, M. G.; El-Mahdy, A. F. M.; Kotp, M. G.; Kuo, S. W. Advances in Porous Organic Polymers: Syntheses, Structures, and Diverse Applications. *Mater. Adv.* **2022**, *3*, 707–733.

Nayak, A.; Jain, S. K.; Pandey, R. S. Controlling Release of Metformin HCl through Incorporation into Stomach Specific Floating Alginate Beads. *Mol. Pharm*, **2011**, *8*, 2273–2281.

Nguyen, T. T.; Miyauchi, M.; Rahmatika, A. M.; Cao, K. L. A.; Tanabe, E.; Ogi, T. Enhanced Protein Adsorption Capacity of Macroporous Pectin Particles with High Specific Surface Area and an Interconnected Pore Network. *ACS Appl. Mater. Interfaces*, **2022**, *14*, 14435– 14446.

Okamoto, Y.; Kishi, Y.; Suga, K.; Umakoshi, H. Induction of Chiral Recognition with Lipid Nanodomains Produced by Polymerization. *Biomacromolecules*, **2017**, *18*, 1180–1188.

Pacheco-Vázquez, F.; Ledesma-Alonso, R.; Palacio-Rangel, J. L.; Moreau, F. Triple Leidenfrost Effect: Preventing Coalescence of Drops on a Hot Plate, *Phys. Rev. Lett*, **2021**, *127*, 204501.

Pandey, R.; Lu, Y.; Osman, E.; Saxena, S.; Zhang, Z.; Qian, S.; Pollinzi, A.; Smieja, M.; Li, Y.; Soleymani, L.; Hoare, T. DNAzyme-Immobilizing Microgel Magnetic Beads Enable Rapid, Specific, Culture-Free, and Wash-Free Electrochemical Quantification of Bacteria in Untreated Urine, *ACS Sensors*, **2022**, *7*, 985–994.

Penny, W. M.; Palmer, C. P. Sphingomyelin Ability to Act as Chiral Selector Using Nanodisc Electrokinetic Chromatography. *Chemistry and Physics of Lipids*, **2018**, *214*, 11–14.

Perçin, I.; Yavuz, H.; Aksöz, E.; Denizli, A. Mannose-Specific Lectin Isolation from Canavalia Ensiformis Seeds by PHEMA-Based Cryogel. *Biotechnol. Prog*, **2012**, *28*, 756–761.

Pfaunmiller, E. L.; Paulemond, M. L.; Dupper, C. M.; Hage, D. S. Affinity Monolith Chromatography: A Review of Principles and Recent Analytical Applications. *Anal. Bioanal. Chem*, **2013**, *405*, 2133–2145.

Plieva, F. M.; Galaev, I. Y.; Noppe, W.; Mattiasson, B. Cryogel Applications in Microbiology. *Trends Microbiol*, **2008**, *16*, 543–551.

Plieva, F.; Huiting, X.; Galaev, I. Y.; Bergenståhl, B.; Mattiasson, B. Macroporous Elastic Polyacrylamide Gels Prepared at Subzero Temperatures: Control of Porous Structure. *J. Mater. Chem*, **2006**, *16*, 4065–4073.

Pourali, M.; Kröger, M.; Vermant, J.; Anderson, P. D.; Jaensson, N. O. Drag on a

Spherical Particle at the Air-Liquid Interface: Interplay between Compressibility, Marangoni Flow, and Surface Viscosities. *Phys. Fluids*, **2021**, *33*, 062103.

Qian, Z.; Feng, H.; Yang, W.; Bi, S. Theoretical Investigation of Water Exchange on the Nanometer-Sized Polyoxocation $AlO_4Al_{12}(OH)_{24}(H\ 2O)_{12}^{7+}$ (Keggin-Al_{13}) in Aqueous Solution. *J. Am. Chem. Soc*, **2008**, *130*, 14402–14403.

Rabieizadeh, M.; Kashefimofrad, S. M.; Naeimpoor, F. Monolithic Molecularly Imprinted Cryogel for Lysozyme Recognition. *J. Sep. Sci*, **2014**, *37*, 2983–2990.

Saba, S. A.; Mousavi, M. P. S.; Bühlmann, P.; Hillmyer, M. A. Hierarchically Porous Polymer Monoliths by Combining Controlled Macro- and Microphase Separation. *J. Am. Chem. Soc*, **2015**, *137*, 8896–8899.

Saeed, A.; Maya, F.; Xiao, D. J.; Najam-ul-Haq, M.; Svec, F.; Britt, D. K. Growth of a Highly Porous Coordination Polymer on a Macroporous Polymer Monolith Support for Enhanced Immobilized Metal Ion Affinity Chromatographic Enrichment of Phosphopeptides. *Adv. Funct. Mater*, **2014**, *24*, 5790–5797.

Sahiner, N. Super Macroporous Poly(*N*-Isopropyl Acrylamide) Cryogel for Separation Purpose. Polym. *Adv. Technol*, **2018**, *29*, 2184–2191.

Saitoh, T.; Nakane, F.; Hiraide, M. Preparation of Trioctylamine-Impregnated Polystyrene–Divinylbenzene Porous Resins for the Collection of Precious Metals from Water. *Reactive and Functional Polymers*, **2007**, *67*, 247–252.

Saitoh, T.; Suzuki, S.; Hiraide, M. Solid Phase Extraction of Some Precious Metals from Hydrochloric Acid to Polystyrene-Divinylbenzene Porous Resin Impregnated with Polyoxyethylene-Type Nonionic Surfactant. *Journal of Chromatography A* **2005**, *1097*, 179–182.

Sanchez, K. M.; Kang, G.; Wu, B.; Kim, J. E. Tryptophan-Lipid Interactions in Membrane Protein Folding Probed by Ultraviolet Resonance Raman and Fluorescence Spectroscopy. *Biophysical Journal*, **2011**, *100*, 2121–2130.

Savina, I. N.; Galaev, I. Y.; Mattiasson, B. Anion-Exchange Supermacroporous Monolithic Matrices with Grafted Polymer Brushes of *N*,*N*-Dimethylaminoethyl-Methacrylate. *J. Chromatogr. A*, **2005**, *1092*, 199–205.

Scriba, G. K. E. Chiral Recognition in Separation Science – an Update. *Journal of Chromatography A*, **2016**, *1467*, 56–78.

Serrano-Luginbühl, S.; Ruiz-Mirazo, K.; Ostaszewski, R.; Gallou, F.; Walde, P. Soft and Dispersed Interface-Rich Aqueous Systems That Promote and Guide Chemical Reactions. *Nature Reviews Chemistry*, **2018**, *2*, 306–327.

Shen, X.; Ye, L. Interfacial Molecular Imprinting in Nanoparticle-Stabilized Emulsions. *Macromolecules*, **2011**, *44*, 5631–5637.

Shi, M.; Das, R.; Arunachalam, S.; Mishra, H. Suppression of Leidenfrost Effect on Superhydrophobic Surfaces. *Phys. Fluids*, **2021**, *33*, 122104.

Shiekh, P. A.; Singh, A.; Kumar, A. Oxygen-Releasing Antioxidant Cryogel Scaffolds with Sustained Oxygen Delivery for Tissue Engineering Applications. *ACS Appl. Mater. Interfaces*, **2018**, *10*, 18458– 18469.

Shiomori, K.; Fujikubo, K.; Kawano, Y.; Hatate, Y.; Kitamura, Y.; Yoshizawa, H. Extraction and Separation of Precious Metals by a Column Packed with Divinylbenzene Homopolymeric Microcapsule Containing Tri-n-octylamine. *Separation Science and Technology*, **2005**, *39*, 1645–1662.

Shiomori, K.; Matsune, H.; Kiyoyama, S.; Takei, T.; Yoshida, M.; Umakoshi, H. Recent Developments of Microcapsules and Polymer Particles for Separation Medium. *J. Phys. Conf. Ser*, **2021**, *1763*, 012011.

Shirbin, S. J.; Karimi, F.; Qiao, G. G. Macroporous Hydrogels Composed Entirely of Synthetic Polypeptides: Biocompatible and Enzyme Biodegradable 3D Cellular Scaffolds. *Biomacromolecules*, **2016**, *17*, 2981– 2991

Skolnick, J.; Zhou, H.; Gao, M. On the Possible Origin of Protein Homochirality, Structure, and Biochemical Function. *PNAS*, **2019**, *116*, 26571–26579.

Smith, S. W. Chiral Toxicology: It's the Same Thing…Only Different. *Toxicological Sciences*, **2009**, *110*, 4–30.

Suga, K.; Hamasaki, A.; Chinzaka, J.; Umakoshi, H. Liposomes Modified with Cardiolipin Can Act as a Platform to Regulate the Potential Flux of NADP+-Dependent Isocitrate Dehydrogenase. *Metabolic Engineering Communications* **2016**, *3*, 8–14.

Suga, K.; Yoshida, T.; Ishii, H.; Okamoto, Y.; Nagao, D.; Konno, M.; Umakoshi, H. Membrane Surface-Enhanced Raman Spectroscopy for Sensitive Detection of Molecular Behavior of Lipid Assemblies. *Anal. Chem.* **2015**, *87*, 4772–4780.

Takei, T.; Yoshida, M.; Yanagi, K.; Hatate, Y.; Shiomori, K.; Kiyoyama, S. Preparation of Acetamiprid-Loaded Polymeric Microcapsules: Influence of Preparation Parameter in Emulsion System on Microcapsule Characteristics. *Polym. Bull*, **2008**, *61*, 119–127.

Tan, B.; Lee, J. Y.; Cooper, A. I. Synthesis of Emulsion-Templated Poly(Acrylamide) Using CO_2-in-Water Emulsions and Poly(Vinyl Acetate)-Based Block Copolymer Surfactants. *Macromolecules*, **2007**, *40*, 1945–1954.

Tedeschi, A.; Auriemma, F.; Ricciardi, R.; Mangiapia, G.; Trifuoggi, M.; Franco, L.; De Rosa, C.; Heenan, R. K.; Paduano, L.; D'Errico, G. A Study of the

Microstructural and Diffusion Properties of Poly(Vinyl Alcohol) Cryogels Containing Surfactant Supramolecular Aggregates. *J. Phys. Chem. B*, **2006**, *110*, 23031–23040.

Tian, Y.; Zhou, J.; He, C.; He, L.; Li, X.; Sui, H. The Formation, Stabilization and Separation of Oil–Water Emulsions: A Review. *Processes*, **2022**, *10*, 738.

Tripathi, A.; Kathuria, N.; Kumar, A. Elastic and Macroporous Agarose-Gelatin Cryogels with Isotropic and Anisotropic Porosity for Tissue Engineering. J. Biomed. *Mater. Res. A*, **2009**, *90*, 680–694.

Tsuchiya, H.; Mizogami, M. The Membrane Interaction of Drugs as One of Mechanisms for Their Enantioselective Effects. *Medical Hypotheses* **2012**, 79, 65–67.

Umakoshi, H.; Nishida, A. Modulation of Yeast Hexokinase on Bio-Inspired Membranes. *Biochemical Engineering Journal* **2012**, *69*, 138–143.

Vivian, J. T.; Callis, P. R. Mechanisms of Tryptophan Fluorescence Shifts in Proteins. *Biophys. J.* **2001**, *80*, 2093-2109.

Wagner, A. J.; Zubarev, D. Yu.; Aspuru-Guzik, A.; Blackmond, D. G. Chiral Sugars Drive Enantioenrichment in Prebiotic Amino Acid Synthesis. *ACS Cent. Sci.* **2017**, *3*, 322–328.

Walde, P.; Umakoshi, H.; Stano, P.; Mavelli, F. Emergent Properties Arising from the Assembly of Amphiphiles. Artificial Vesicle Membranes as Reaction Promoters and Regulators. *Chem. Commun*, **2014**, *50*, 10177–10197.

Wang, C. F.; Huang, H. C.; Chen, L. T. Protonated Melamine Sponge for Effective Oil/Water Separation. *Sci. Rep*, **2015**, *5*, 1–8.

Wang, H.; Qin, Z.; Liu, Y.; Li, X.; Liu, J.; Liu, Y.; Huang, D.; Di, D. Design and Preparation of Porous Polymer Particles with Polydopamine Coating and Selective Enrichment for Biomolecules. *RSC Adv.* **2017**, *7*, 45311–45319.

Wang, J.; Mao, Q. Methodology Based on the PVT Behavior of Polymer for Injection Molding. *Adv. Polym. Technol*, **2012**, *32*, 474–485.

Wang, M.; Hu, J.; Ou, Y.; He, X.; Wang, Y.; Zou, C.; Jiang, Y.; Luo, F.; Lu, D.; Li, Z.; Li, J.; Tan, H. Shape-Recoverable Hyaluronic Acid-Waterborne Polyurethane Hybrid Cryogel Accelerates Hemostasis and Wound Healing. *ACS Appl. Mater. Interfaces*, **2022**, *14*, 17093– 17108.

Watanabe, N.; Goto, Y.; Suga, K.; Nyholm, T. K. M.; Slotte, J. P.; Umakoshi, H. Solvatochromic Modeling of Laurdan for Multiple Polarity Analysis of Dihydrosphingomyelin Bilayer. *Biophys. J.* **2019**, *116*, 874– 883.

Watanabe, N.; Suga, K.; Slotte, J. P.; Nyholm, T. K. M.; Umakoshi, H. Lipid-Surrounding Water Molecules Probed by Time-Resolved Emission Spectra of Laurdan. *Langmuir*, **2019**, *35*, 6762-6770.

Wells, G. G.; Ledesma-Aguilar, R.; McHale, G.; Sefiane, K. A Sublimation Heat Engine. *Nat. Commun,* **2015**, *6*, 1–7.

Wu, D.; Xu, F.; Sun, B.; Fu, R.; He, H.; Matyjaszewski, K. Design and Preparation of Porous Polymers. *Chem. Rev*, **2012**, *112*, 3959–4015.

Wu, Y.; Shi, C.; Wang, G.; Sun, H.; Yin, S. Recent advances in the development and applications of conjugated polymer dots. *J. Mater. Chem. B*, **2022**, *10*, 2995–3015

Xu, Q.; Lee, S.; Cho, Y.; Kim, M. H.; Bouffard, J.; Yoon, J. Polydiacetylene-Based Colorimetric and Fluorescent Chemosensor for the Detection of Carbon Dioxide. *J. Am. Chem. Soc,* **2013**, *135*, 17751– 17754.

Xu, X.; Liu, L.; Geng, H.; Wang, J.; Zhou, J.; Jiang, Y.; Doi, M. Directional Freezing of Binary Colloidal Suspensions: A Model for Size Fractionation of Graphene Oxide. *Soft Matter*, **2019**, *15*, 243–251.

Yang, X.-Y.; Chen, L.-H.; Li, Y.; Rooke, J. C.; Sanchez, C.; Su, B.-L. Hierarchically Porous Materials: Synthesis Strategies and Structure Design. *Chem. Soc. Rev,* **2017**, *46*, 481– 558.

Yoshizawa, H.; Fujikubo, K.; Uemura, Y.; Kawano, Y.; Kondo, K.; Hatate, Y. Preparation of Divinylbenzene Homopolymeric Microcapsules with Highly Porous Membranes by *in Situ* Polymerization with Solvent Evaporation. *Journal of Chemical Engineering of Japan*, **1995**, *28*, 78–84.

Yu, Y.; Chen, H.; Liu, Y.; Craig, V. S. J.; Lai, Z. Selective Separation of Oil and Water with Mesh Membranes by Capillarity, **2016**, *235*, 46–55.

Yuan, Z.; Yuan, X.; Zhao, Y.; Cai, Q.; Wang, Y.; Luo, R.; Yu, S.; Wang, Y.; Han, J.; Ge, L.; Huang, J.; Xiong, C. Injectable GelMA Cryogel Microspheres for Modularized Cell Delivery and Potential Vascularized Bone Regeneration. *Small*, **2021**, *17*, 1–13.

Yun, J.; Dafoe, J. T.; Peterson, E.; Xu, L.; Yao, S. J.; Daugulis, A. J. Rapid Freezing Cryo-Polymerization and Microchannel Liquid-Flow Focusing for Cryogel Beads: Adsorbent Preparation and Characterization of Supermacroporous Bead-Packed Bed. *J. Chromatogr. A*, **2013**, *1284*, 148–154.

Yusof N.N.M., Kobayashi T.: Efficient separation on vanillin operated with permeability performance of hollow fiber membranes embedded vanillin imprinted polymer particles. *Ind. Eng. Chem. Res*, **2013**, *52*, 16951–16957.

Zahid, N. I.; Abou-Zied, O. K.; Hashim, R. Evidence of Basic Medium in the Polar Nanochannels of the Inverse Bicontinuous Cubic Phase of a Guerbet Glycolipid: A Steady-State and Time-Resolved Fluorescence Study. *J. Phys. Chem. C*, **2013**, *117*, 26636–26643.

Zhai, Y.; Zhou, W.; Wei, W.; Qu, J.; Lei, J.; Su, Z.; Ma, G. Functional Gigaporous Polystyrene Microspheres Facilitating Separation of Poly(Ethylene Glycol)–Protein Conjugate. *Analytica Chimica Acta*, **2012**, *712*, 152–161.

Zhan, X. Y.; Lu, D. P.; Lin, D. Q.; Yao, S. J. Preparation and Characterization of Supermacroporous Polyacrylamide Cryogel Beads for Biotechnological Application. *J. Appl. Polym. Sci*, **2013**, *130*, 3082–3089.

Zhao, X.; Guo, B.; Wu, H.; Liang, Y.; Ma, P. X. Injectable Antibacterial Conductive Nanocomposite Cryogels with Rapid Shape Recovery for Noncompressible Hemorrhage and Wound Healing. *Nat. Commun*, **2018**, *9*, 2784.

Zhou, L.; Yue, J.; Fan, Y.; Wang, Y. Self-Assembly and Chiral Recognition of Chiral Cationic Gemini Surfactants. *Langmuir*, **2018**, *34*, 12924–12933.

List of Publications

[Papers]

1. Hayato Takase, Keishi Suga, Hideki Matsune, Hiroshi Umakoshi, Koichiro Shiomori, Preferential Adsorption of L-Tryptophan by L-Phospholipid Coated Porous Polymer Particles, *Colloids Surf. B*, **2022**, 216, 112535.

2. Hayato Takase, Koichiro Shiomori, Yukihiro Okamoto, Nozomi Watanabe, Hideki Matsune, Hiroshi Umakoshi, Micro Sponge Balls: Preparation and Characterization of Sponge-like Cryogel Particles of Poly(2-hydroxyethylmethacrylate) via the Inverse Leidenfrost Effect, *ACS Appl. Polym. Mater*, **2022**, 4, 7081-7089.

3. Hayato Takase, Nozomi Watanabe, Koichiro Shiomori, Yukihiro Okamoto, Hideki Matsune, Hiroshi Umakoshi, Versatility of the Preparation Method for Macroporous Cryogel Particles Utilizing the Inverse Leidenfrost Effect, *ACS Omega*, **2023**, 8, 829-832.

4. Hayato Takase, Nozomi Watanabe, Koichiro Shiomori, Yukihiro Okamoto, Endang Ciptawati, Hideki Matsune, Hiroshi Umakoshi, Preparation of Hydrophobic Monolithic Supermacroporous Cryogel Particles for the Separation of Stabilized Oil-in-water Emulsion, *Colloids Interfaces*, **2023**, 7, 9.

[Related Papers]

1. Hayato Takase, Nozomi Watanabe, Koichiro Shiomori, Yukihiro Okamoto, Hideki Matsune, Hiroshi Umakoshi, Hierarchical Porous Cryogel Particles with Directional and Bimodal Porous Morphologies, *to be submitted*.

2. Hayato Takase, Nozomi Watanabe, Yuya Niwa, Koichiro Shiomori, Yukihiro Okamoto, Hideki Matsune, Hiroshi Umakoshi, Characterization of Mechano-Chemical Response of Lipid Membrane Coated on Cryogel Particles, *to be submitted*.

3. Hayato Takase, Nozomi Watanabe, Koichiro Shiomori, Yukihiro Okamoto, Hideki Matsune, Bong Su Kang, Ho-sup Jung, Hiroshi Umakoshi, Preparation of Sub-micrometer Cryogel Particles with Narrow Size Distribution Using a Microfluidic Device, *in preparation*.

4. Hayato Takase, Nozomi Watanabe, Koichiro Shiomori, Yukihiro Okamoto, Hideki Matsune, Hiroshi Umakoshi, Mechano-Chemical Bioseparation of Macromolecules and Self-Assemblies Using Sponge-like Cryogel Particles Modified with Lipid Membrane, *in preparation*.

5. Hayato Takase, Wataru Ogushi, Hideki Matsune, Koichiro Shiomori, Investigation on Extraction Behaviors of Cu (II) on LIX84-I Impregnated on Porous Polymer Particles, *in preparation*.

6. Hayato Takase, Naoya Gouya, Hideki Matsune, Koichiro Shiomori, Preparation and Characterization of Extractant Coated p(trimethylolpropanetrimethacrylate) Cryogel, *in preparation*.

[Article]

1. Hayato Takase, Preparation and Characterization of the Detergent-free Cryogel Particles with Directional Porous (in Japanese), *Bunri Gijutu*, **2023**, *5*, *in press*.

[International Conference / Symposium]

1. Hayato Takase and Koichiro Shiomori, Preparation of Cryogel Containing Liposomes and Its Adsorption Properties of Tryptophan and Histidine, 6th NUM-UOM Joint Student Conference Ulaanbaatar, Mongolia, October (2017) (Oral).

2. Hayato Takase and Koichiro Shiomori, Chiral Selective Adsorption of Tryptophan by Phospholipid Impregnated Porous Particles, 7th UOM-NUM Joint Student Conference, Miyazaki, Japan, February (2018) (Poster).

3. Hayato Takase, Nozomi Watanabe, Koichiro Shiomori, Yukihiro Okamoto, Hideki Matsune, Hiroshi Umakoshi, Development of the Anisotropic Porous Structure Cryogel Particles by Inverse Leidenfrost Effect, International Symposium on Chemical Engineering, Environment and Biochemistry, Miyazaki, Japan, December (2022) (Oral).

Acknowledgements

The author is deeply grateful to Prof. Dr. Hiroshi Umakoshi (Division of Chemical Engineering, Graduate School of Engineering Science, Osaka University), for his insightful comments, guidance, and warm encouragement throughout this work. The author is thankful to Prof. Dr. Masahiro Taya, Prof. Dr. Takayuki Hirai, Prof. Dr. Norikazu Nishiyama (Division of Chemical Engineering, Graduate School of Engineering Science, Osaka University), and Koichiro Shiomori (Department of Applied Chemistry, University of Miyazaki) for a number of valuable comments and suggestions during the completion of this thesis. The author would like to express my gratitude to Assist. Prof. Dr. Nozomi Watanabe (Division of Chemical Engineering, Graduate School of Engineering Science, Osaka University). The author also would like to express the greatest appreciation to Assoc. Prof. Dr. Yukihiro Okamoto (Division of Chemical Engineering, Graduate School of Engineering Science, Osaka University) for his valuable comments and helpful advises. The author would like to offer one's special thanks to Ms. Keiko Fukumoto for her kind support during this work.

The author is thankful to Prof. Dr. Y. Okano, Prof. Dr. N. Matsubayasi, Prof. Dr. M. Nakano, Prof. T. Mizugaki, Prof. Dr. S. Sakai, and all the staff of Division of Chemical Engineering, Graduate School of Engineering Science, Osaka University for their kind cooperation during my research.

The author wishes to thank Prof. Dr. Ho-Sup Jung (Department of Mechanical and Aerospace Engineering, Seoul National University), Prof. Dr. A. Kumar (Department of Biological Science and Bioengineering, Indian Institute of Technology Kanpur), Prof. Dr. B. Mattiasson (Department of Biotechnology, Lund University), Prof. Dr. P. Walde (Institute for Polymer, ETH, Zurich), Prof. Dr. T. L. Kuhl (Department of Chemical Engineering, U.C. Davis), Prof. Dr. H. Nur (Faculty of Mathematics and Natural Science, Universitas Negeri Malang), Prof. Dr. B. Oyuntestseg, Prof. Dr. O Bayanjargal (Department of Chemistry, National University of Mongolia), and Dr. N. I. Inda (Department of Chemistry, Universitas Tadulako) for their comments and suggestions during this work. The author is grateful for the encouragements given by Assoc. Prof. Dr. K. Suga, Prof. Dr. D. Nagao (Department of Chemical Engineering, Tohoku University), Assoc. Prof. Dr. H. Matsune, Prof. Dr. T. Oshima, Prof. Dr. T. Yui, Assoc. Prof. Dr. K. Sugamoto, Assoc. Prof. T. Uto (Department of Applied Chemistry, University of Miyzaki). The author is thankful to Prof. Dr. H. Ishii (Graduate School of Sciences and Technology for Innovation, Yamaguchi University), Assoc. Prof. Dr. T. Shimanouchi (Graduate School of Environmental and Life Science, Okayama University), Assoc. Prof. Dr. K. Hayashi (National Institute of Technology), Assis Prof. Dr. S. Taguchi (Department of Chemical Engineering and Materials Science, University of Hyogo), Prof. Dr. M. Yoshimoto (Department of Applied Molecular Bioscience, Yamaguchi University), Assoc. Dr. N. Yoshinori (Department of Applied Chemistry, Yamaguchi University), Prof. Dr. M. Yoshida, Prof. Dr. T. Takei, Prof. Dr. T. Tamaki, Prof. Dr. S. Nii, (Department of Chemical Engineering, Kagoshima University).

The author is particularly grateful for the assistance given by N. Yuya and T. Kuroki. Special thanks are given to following colleagues for their experimental collaboration: B. T. Tham, M. Faried, M.S. Chern, A. Ajaikumar, R. Xuehui, T. Samwang, E. Ciptawati, A. Suzuta, L. Weiyu, N. Ito, Y. Nagamura, P. Soontornapaluk, Z. Nicolella, T. Ozawa, Y. Suzaki, K. Hamaguchi, S. Watase N. Kadonishi, N. Fukuda, Y. Fuji, M. Watanabe, L. Junghu, Y. Amatsu, K. Chatani, M. Toshii, K. Miura, N. Yoshioka, K. Watanabe, A. G. Larsen and all the membraer in Bio-Inspired Chemical Engineering Laboratory. The author also would like to show appreciation to Dr. Sana Takashi, Dr. S. Enkzaya, Dr. S. Batchuluun, N. Goya, Y, Natsui, T. Ito, K. Tokuda, W. Ogushi, A. Kuwahata and all the member in the Shiomori laboratory.

The author would like to express deepest appreciation to his parent Chieko Takase, and his brother, Tsubasa Takase, Kosumo Takase, Subaru Takase, for their continuous encouragements and great support throughout this work.

The author gratefully acknowledges the financial support of this work by the fellowship of Next Generation Scholarship and ΣRA scholarship.